Discontinuous approaches for nonlinear dynamic analyses of an ancient masonry tower

Angela Ferrante[1], Dimitri Loverdos[2], Francesco Clementi[1], Gabriele Milani [3], Antonio Formisano[4], Stefano Lenci[1], Vasilis Sarhosis[2]

[1]Department of Civil and Building Engineering, and Architecture, Polytechnic University of Marche, via Brecce Bianche, 60131, Ancona, Italy

Email: a.ferrante@pm.univpm.it, francesco.clementi@univpm.it , s.lenci@univpm.it

[2]School of Civil Engineering, University of Leeds, Leeds, LS2 9JT, Leeds, United Kingdom, Email: v.sarhosis@leeds.ac.uk

[3]Department of Architecture, Built Environment and Construction Engineering ABC, Polytechnic of Milano, Piazza Leonardo da Vinci 32, 20133, Milan, Italy

Email: gabriele.milani@polimi.it

[4]Department of Structures for Engineering and Architecture, University of Naples "Federico II", Piazzale Tecchio 80, 80125 Naples, Italy

Email: antonio.formisano@unina.it

Abstract: The aim of this paper is to present the development of discontinuous approaches to simulate the nonlinear dynamic behaviour of the civic clock tower of Rotella, in the province of Ascoli Piceno (Italy). The study involves the use of the Non-Smooth Contact Dynamics method implemented in the LMGC90© code, where sliding motions are governed by Signorini's impenetrability condition and dry-friction Coulomb's law, and the Discrete Element Method with cohesive and tensional behaviours at the joints in the 3DEC© code. The tower was represented using three different geometric models ranged from the most complex one, including the full geometry and multi-leaf masonry walls, to the simplest one, including the single-leaf walls as a simplification of the real masonry. The numerical results highlighted the modes of failure depending on the shape, size and texture of the masonry and the modalities of progressive damage under dynamic actions. Moreover, both numerical approaches have proven to be capable of simulating large displacements and complete block separations, reproducing complex mechanical behaviours and making predictions on the vulnerability assessment of the historical masonry buildings.

1   Introduction

The nonlinear dynamic behaviour of ancient masonry structures is a main issue of past and recent research [1]. The vulnerability assessment of the masonry structures is essential for the preservation of cultural heritage. Although, the presence of ancient masonry in high-seismicity regions owe to intensify the knowledge of these structures to prevent heavy damages and take part in the retrofitting works.

This is especially true in Italy where the recent seismic sequences (Umbria-Marche 1997–1998, Abruzzo 2009, Emilia-Romagna 2012, Marche-Lazio-Umbria-Abruzzo 2016) produced widespread damages in national territory [2]. In October 2016, two major earthquakes occurred in the Marche region in the Centre of Italy, causing widespread damage, highly affecting historical structures [3]. The epicentre of the second earthquake stroked Norcia, Visso, Arquata del Tronto, Accumoli and Amatrice, and a lot of damages to cultural heritage also occurred in the cities of Tolentino, San Severino, Camerino, and Matelica. This work presents the advanced numerical analyses of the ancient civic clock tower of Rotella, in the province of Ascoli Piceno (AP) in Central Italy, in light of the structural damages caused by the quakes that struck it in 2016, plunging the area into chaos for several months. More specifically, the case study is located in Seismic Zone 2 (ref. PCM Ordinance No.3274/2003), i.e. area with medium seismic hazard where strong earthquakes may occur, as visible in the Italian seismic hazard map in Figure 1.
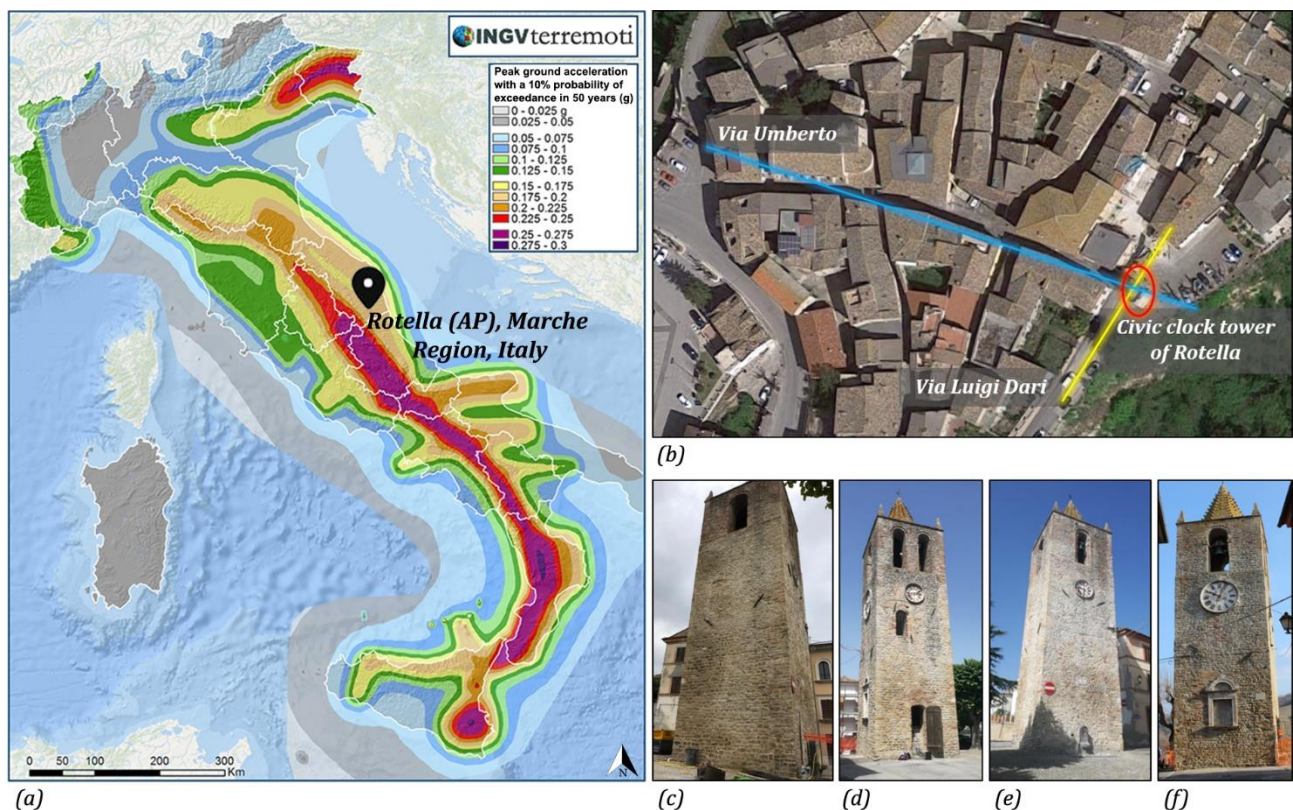
Figure 1 (a, b) Geographical location of the civic clock tower of Rotella (Ascoli Piceno, Italy) on the Italian seismic hazard map (http://www.ingv.it/it/) and views of the (c) South-East façade, (d) South-West façade, (e) North-East façade, (f) North-West façade

The existing ancient masonry tower requires particular attention due to the knowledge of the mechanical proprieties which makes uncertain the development of numerical models.

Moreover, the complexity of the tower's interlocking, made of bricks with various shapes, texture, dimensions and connected by mortar joints, lead to an increase of the computational effort needed.

However, the typical failure mechanisms of the historical towers are determined by the geometry features and can be also estimated by means of simplified approaches which avoid any form of irregularity [4]. In some cases, the preliminary estimation of the expected collapse modes with conventional approaches does not take into consideration the z-component of dynamic input and thus does not investigate the z-displacement of the structure, which affects the outcome for a most realistic prediction.

To properly evaluate the physical consistency and safety of the historical masonry, it is necessary to exploit the considerable wealth of technical-scientific knowledge on the mechanics of materials and structures accumulated over the past centuries, thus arriving at the identification of targeted approaches to be evaluated and verified case by case. Indeed, there are several methods who currently investigate the dynamic response of large-scale masonry structures [5]. The most commonly used is the continuous approach of Finite Element Method (FEM) [6], where a properly homogenised material is introduced in the analyses to reproduce the global behaviour of the considered structure [7]. On the other hand, the discontinuous approach involving Discrete Element Method (DEM) allows the understanding of the global dynamics of a structure by examining the local behaviours [8,9]. DEM is ideally suited for simple structures such as columns and arches [10], but can also be used for the nonlinear dynamic analyses of more complex structures such as churches [11] and towers.

In fact, the ancient masonry structures may be considered as discontinuous structural systems, composed by individual units (e.g. bricks, stones, blocks, etc.), bonded together with or without mortar. Thus, three advanced numerical models are built to adequately represent the behaviour of the investigated real structures. A full 3D detailed discretization is used to provide insight into the modalities of progressive damage and the behaviour of structures under strong dynamic excitations, analysing the influence of the brick fragments of really small element size.

The nonlinear numerical analyses were carried out by means of the Non-Smooth Contact Dynamics (NSCD) method implemented in the LMGC90© code [12,13], and the Discrete Element Method (DEM) implemented in the 3DEC© code [14] released by Itasca. In both software programs, masonry units were represented as an assemblage of distinct rigid blocks which may take any arbitrary geometry. Rigid blocks do not change their geometry as a result of any applied loading and are mainly used when the behaviour of the system is dominated by the mortar joints, assuming the deformation to occur only at the joints. Mortar joints were represented as zero thickness interfaces between the blocks/masonry units. With the application of the external load, large displacements and rotations between blocks, including sliding between blocks, the opening of the cracks and even the complete detachment of the blocks are allowed as the calculations proceed, along with automatic detection of new contacts.

In the NSCD method, the rigid blocks of the structure are undergoing shock laws and Coulomb friction. The tower exhibited a complex dynamic behaviour, because of the geometrical nonlinearity and the non-smooth nature of the contact laws, with a focus on the possible non-smooth nature of the dynamic response, which usually occurs right before or during the collapse with velocity discontinuities.

In DEM models, smooth functions are used to describe the interactions between blocks with velocity continuities and the non-linear behaviour of the mortar assigned to the interfaces corresponds to a Mohr–Coulomb constitutive model, which involve the cohesion, the friction angle and the tensile strength as parameters. The stiffness of the interfaces is represented by two springs in the normal and shear direction, linking the contact stresses with the relative blocks' displacements.

2 Structural characteristics of the Rotella's civic tower

The civic clock tower of Rotella, in the province of Ascoli Piceno (Italy), goes back to the XI century. It was originally known as the bell tower of the Church of Santa Maria della Pietà, which was built before 1099 and renovated in 1430.
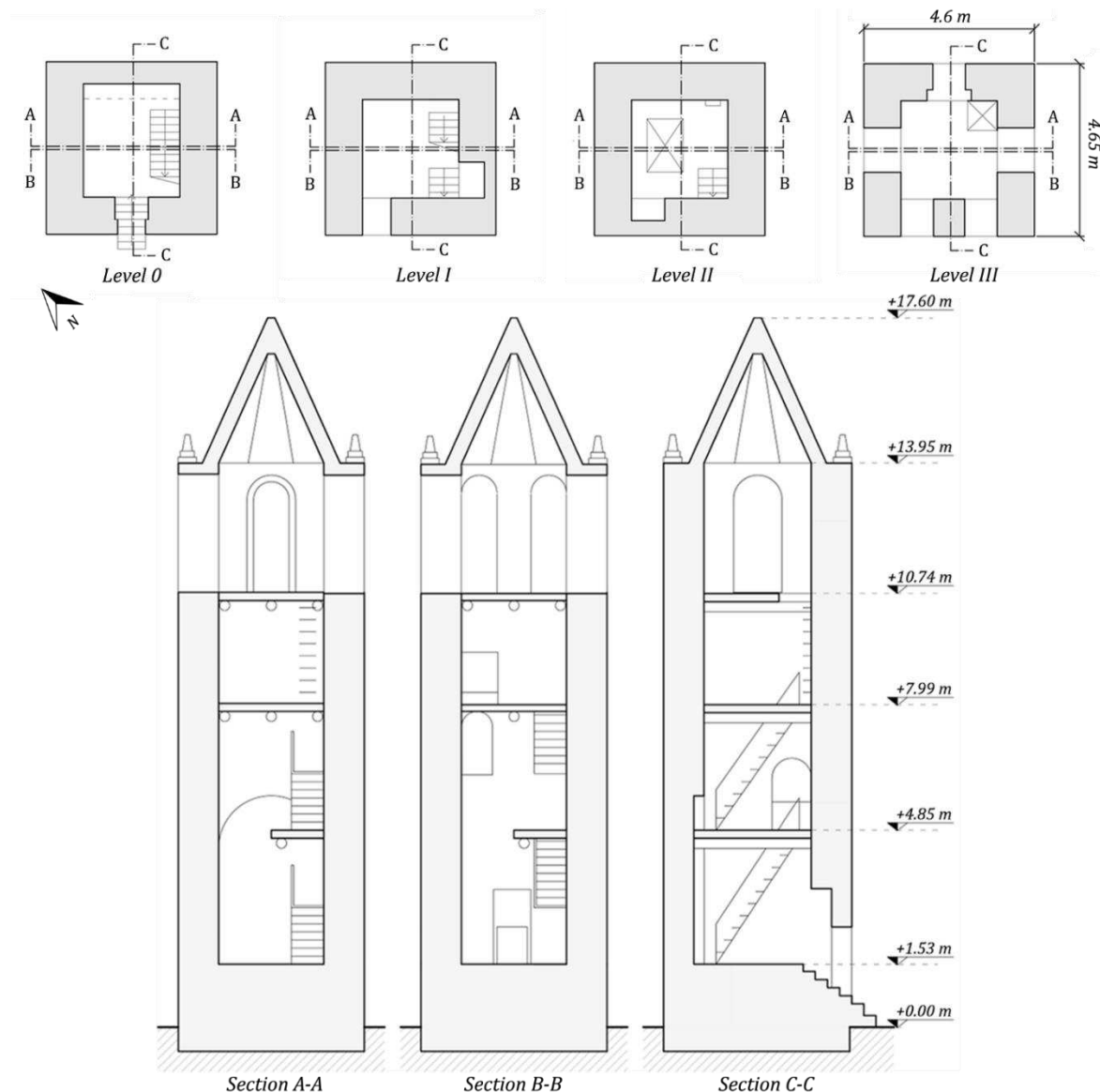
Figure 2 Drawings of plans and cross sections of the civic clock tower of Rotella (Ascoli Piceno, Italy)

In 1755, the church collapsed after landslide movements, due to the erosive actions of the nearby Oste torrent. After this collapse, a small part of the church remained in precarious static condition and therefore was demolished. The bell tower instead proved structurally safe and became the symbol of the municipality of Rotella.
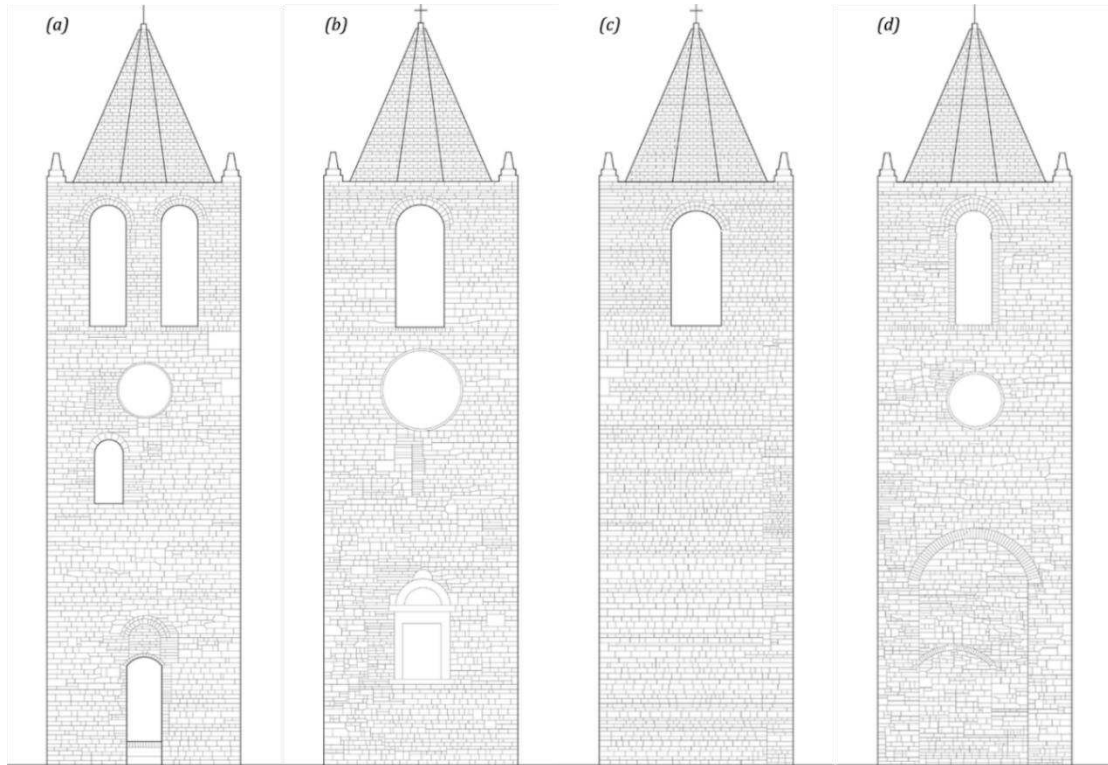
Figure 3 Survey of stones' texture of the (a) South-West façade, (b) North-West façade, (c) South-East façade, (d) North-East façade of the civic clock tower of Rotella (Ascoli Piceno, Italy)
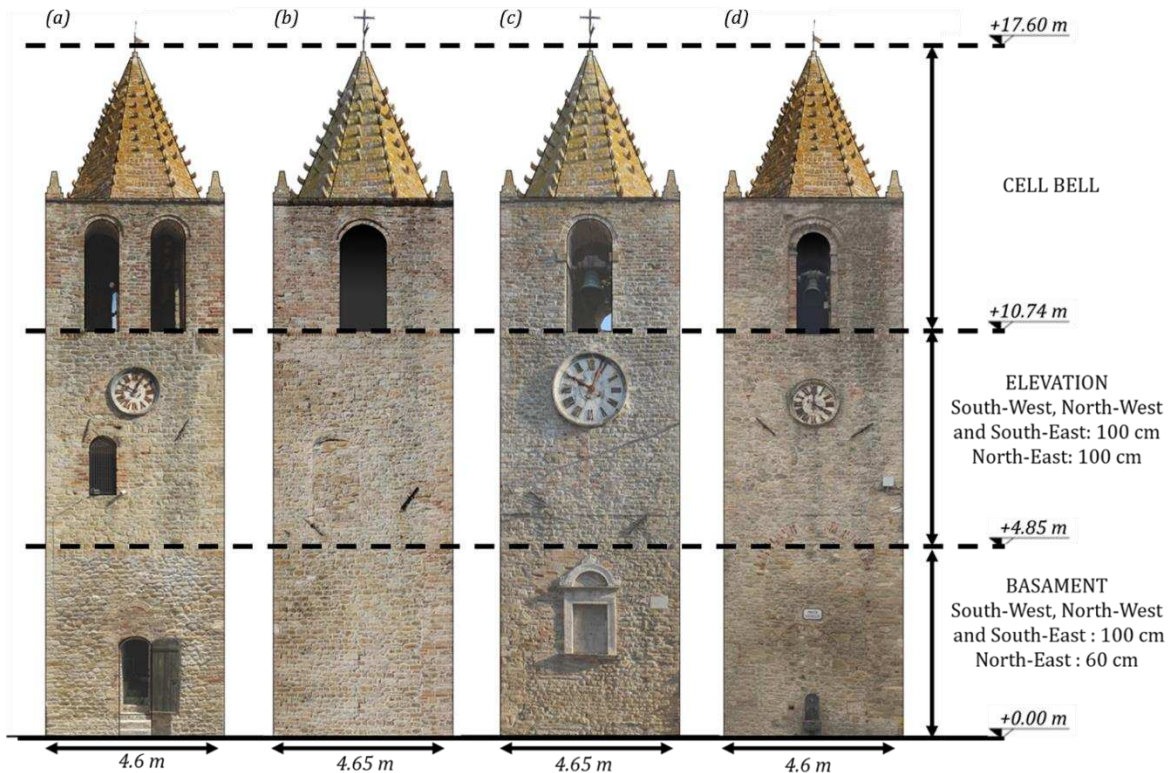
Figure 4 Views of the (a) South-West façade, (b) South-East façade, (c) North-West façade, (d) North-East façade of the civic clock tower of Rotella (Ascoli Piceno, Italy) with the main dimensions of the masonry walls

Recently, the civic clock tower of Rotella suffered significant damages after the Central Italy seismic sequence of 2016. The structural survey carried out in loco, after these destructive events, allowed the observation of significant cracks in the cell bell, in the upper part of the

vertical structure, characterised by the wide arched windows (see Figure 5). Additionally, the main shocks also produced relevant failures of the vertical development of the tower, without total collapse of the masonry structure. The structure is not currently, accessible and under investigation to conduct repair and rehabilitation works.

The civic clock tower of Rotella is composed by a rectangular plan with dimensions equal to 4.60 m x 4.65 m (see Figure 2). The multi-leaf masonry walls are characterised by a thickness equal to 1 m, with the exception of the North-East façade where the first 5 m of the masonry wall from the ground has a thickness of 0.60 m. Furthermore, the tower has a height of about 17.60 m and along its vertical development does not present any relevant variation of geometry, except for the presence of two niches on the South-West and North-West internal sides. The three internal floors are made by wooden tables and it is possible to divide the tower into four fictitious levels, where the separation between the central elevation and the bell cell is visually marked on the outside through a frame of bricks. Additionally, the cell bell has a development of about 6.90 m and presents a single-arched window for the South-West façade and single-arched windows for the other façades, as visible in Figure 3 and Figure 4. The cover of this vertical structure is formed by a masonry cone with a hexagonal base.

(a)　　　　　　　　　　　　　　　　　　　　　*(b)*

(c)
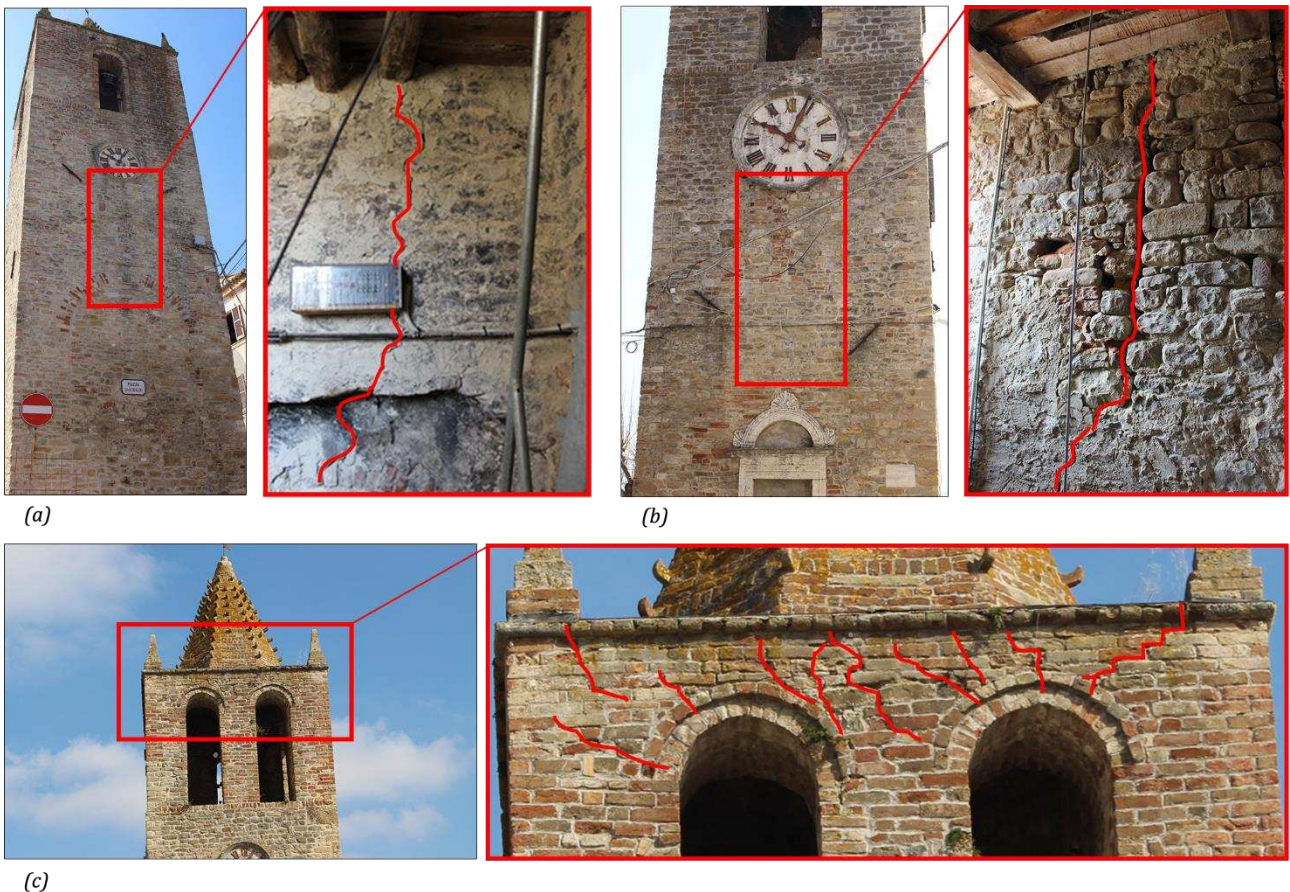
Figure 5 Survey of the crack patterns of the civic clock tower of Rotella (Ascoli Piceno, Italy) after the main shocks of the Central Italy seismic sequence of 2016 on the (a) North-East façade, (b) North-West façade, (c) South-West façade

Finally, the whole civic tower of Rotella has multi-leaf masonry walls characterised by bricks and stones of different sizes, which are irregularly arranged in the panels. Unfortunately, there are no historical documents of the tower that provide more information on how the structure developed over time and on its material properties. Hence, the survey in loco without the use of destructive tests on the masonry was essential for its knowledge.

3 Discontinuous numerical modelling approaches for structural masonry analysis

The discontinuous modelling approaches allow the comprehension of the complex behaviours of masonry structures through the interaction between the distinct elements [15]. Moreover, the laws which define contact between discrete bodies may be described using the smooth and non-smooth contact dynamics. In fact, DEM enables the understanding of the dynamic global behaviour of ancient masonry through the local behaviour, by means of contact points at the interface between blocks. These contact points introduce frictional behaviour of joints, which follow various contacts laws.

Hence, to apply the discrete modelling in this work, two different numerical analysis software based on two different methods were used, namely the LMGC90© open source code, which implements the Non-Smooth Contact Dynamics method, and the 3DEC© commercial code, based on Distinct Element Method. The NSCD method relies on non-smooth (non-differentiable) formulation of bodies dynamics, i.e. of frictional contact laws, involving velocity jumps, i.e. shocks. The 3DEC© is based on smooth (continuous and sufficiently differentiable) contact laws and interaction at contact points, involving relative velocities. Moreover, the NSCD needs to use implicit time integration and contact solvers, whereas the DEM makes use of explicit solution algorithms for the dynamic equation. The NSCD involves inelastic shock laws with restitution coefficient set as a null value. The DEM introduces damping terms with the management of the coefficient of restitution in order to ensure numerical stability of the explicit scheme used.

Nevertheless, the models of both methods consist of a set of polyhedral bodies bonded together by zero thickness interfaces representing mortar joints. At the joints, mechanical interaction between blocks/masonry units is allowed to take place and governed by the appropriate constitutive laws. The motion of masonry units is calculated numerically at each timestep by integrating the Newtonian equations of motion.

The individual elements must necessarily be designed as convex bodies. It is possible though to combine multiple elements to form concave shapes if required, including openings. In the present study, masonry units are assumed as perfectly rigid bodies with six degrees of freedom (three translational and three rotational).

3.1 The Non-Smooth Contact Dynamics method

Included in the family of the discrete element methods presented by P. Cundall [16], the NSCD method differs from the original DEM, as firstly introduced by [17,18], for the implicit scheme used for integrating the time discretized dynamical equation and the non-regularized interactions laws of Signorini unilateral contact and Coulomb dry friction.

The discrete modelling permits the definition of masonry by the interaction between blocks and assumes that the properties of the bodies and their contact points govern the behaviour of the model. Moreover, in the NSCD the contact is supposed to be punctual and not an area of the interfaces, as an additional simplification. Other relevant hypotheses assumed in the NSCD method are that the bodies are rigid, with the strain applied to the contact points, and the contact forces are provided by the strain at the punctual contact, with independent interactions between bodies.

3.1.1 Dynamics of rigid bodies and contact kinematics

The approach of the Non-Smooth Contact Dynamics involves first the contact detection, then the contact problem, i.e. the derivation of the contact forces in local scale, and lastly the individuation of the displacement of bodies in global scale. In fact, the resolution of the local unknowns, due to the interactions, and the global unknowns, due to the bodies, are necessary to compute the multi-contact problem within the NSCD framework. These two sets of unknowns are bound by mapping (see Figure 6).
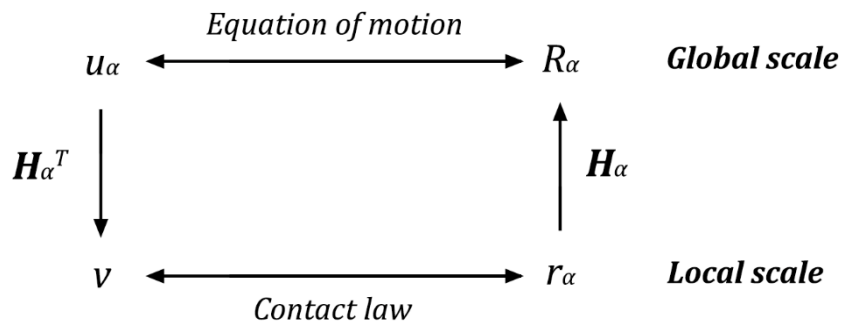
$$u_\alpha \xleftrightarrow{\text{Equation of motion}} R_\alpha \qquad \textbf{\textit{Global scale}}$$

$$\boldsymbol{H_\alpha}^T \Big\downarrow \qquad\qquad\qquad \boldsymbol{H_\alpha} \Big\uparrow$$

$$v \xleftrightarrow[\text{Contact law}]{} r_\alpha \qquad \textbf{\textit{Local scale}}$$

Figure 6 Global and local mapping in the NSCD algorithm

Furthermore, considering two adjacent bodies sufficiently close to be in contact, as schematised in Figure 7, it is possible to define the interaction of the antagonist body A with the candidate body C. The contact force arising at the contact point between the body A and the body C is the force r_α. In fact, the contact is schematised as punctual and in the 3D model it is possible to use a local frame of three vectors. These vectors are characterised by two tangential vectors s_α and t_α and a normal vector n_α from A to C, which introduce the tangential space by means of this convention $s_\alpha \wedge t_\alpha = n_\alpha$. Additionally, it is possible to define the gap g_α as the distance along the normal direction from the body A to the body C. For rigid bodies, this gap is defined positive and there is not interpenetration between the bodies.
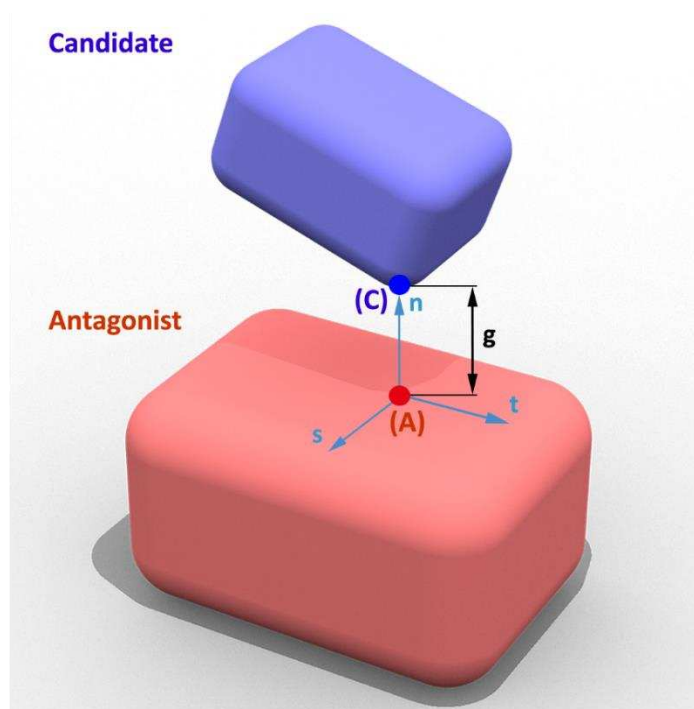

Figure 7 Relation between candidate and antagonist in 3D space

The linear mapping of $\boldsymbol{H}_\alpha$ allows to evaluate the global resultant forces R_α at the contact α related to the local forces r_α, using the equation:

$$R_\alpha = \boldsymbol{H}_\alpha(q)r_\alpha, \tag{1}$$

where $\boldsymbol{H}_\alpha(q)$ is the mapping with the local information and q is the rigid displacement vector of generalised coordinates. Hence, the global resultant contact forces exerted on the bodies is calculated with:

$$R = \Sigma_\alpha R_\alpha. \tag{2}$$

Moreover, the transposed $\boldsymbol{H}^T$ and the velocity of the block can be used to calculate the contact related velocity u_α:

$$u_\alpha = \boldsymbol{H}^T(q)v, \tag{3}$$

where v is the time derivative of q.
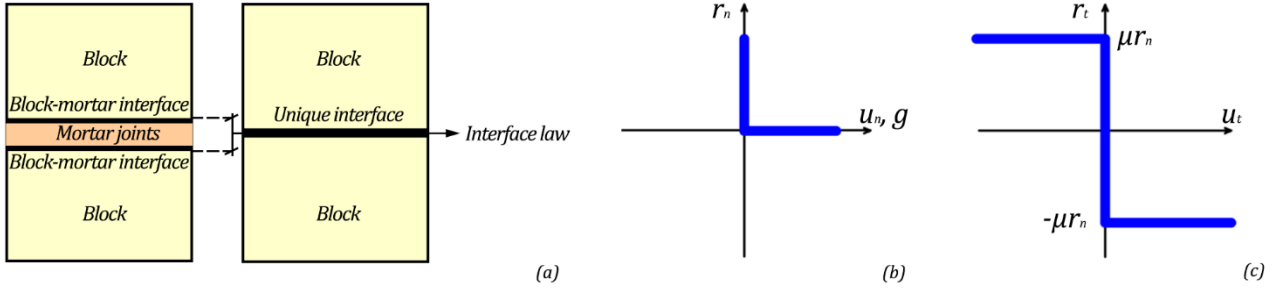
3.1.2   Frictional contact laws

Figure 8 Contact at the interface between blocks (a), Signorini's impenetrability condition (b), and friction Coulomb's law (c)

The reaction force and the relative velocity of the contact are described by the laws of Signorini and Coulomb [17]. More specifically, the impenetrability of the contact between blocks is represented by the Signorini's condition (see Figure 8 (b)), written as:

$$\begin{cases} g \geq 0, \\ r_n \geq 0, \\ g \cdot r_n = 0, \end{cases} \tag{4}$$

where g is the distance between the bodies and r_n is the normal component of the contact force. The same equations can be written for the velocities, considering the normal component u_n, in the following way:

$$\begin{cases} g(t_0) \geq 0 \; at \; initial \; time \; step \; t_0, \\ g(t) \leq 0 \Rightarrow u_n \geq 0, \; r_n \geq 0, \; u_n r_n = 0. \end{cases} \tag{5}$$

Additionally, the dry friction law of Coulomb (see Figure 8 (c)) permits the calculation of the tangential force and the sliding between blocks, using the following system of equations:

$$\begin{cases} \|u_T\| = 0, \|r_T\| < \mu r_n \Rightarrow \|u_T\| = 0 & Sticking, \\ \|r_T\| = \mu r_n \Rightarrow u_T = -k r_T \; k \geq 0, \|u_T\| \neq 0 & Sliding, \end{cases} \tag{6}$$

where μ is the friction coefficient.

3.1.3 Discrete formulation of the dynamical equation

The bodies of the numerical model exhibit dynamics obeying to the following equation of motion:

$$M(q)dv = F(q,v,t)dt + dI, \tag{7}$$

where M is the mass matrix, $F(q,v,t)$ is the vector of internal and external forces of the system, dt is the Lebesgue measure on $\mathbb{R}$, dv is a differential measure of velocity denoting the acceleration measure and dI is a differential measure of the impulse of contact resultant.

It is important to highlight that it is not necessary to manage explicitly the contact events in the time-stepping integration scheme, as in the case of the event-driven scheme. The time subdivision is fixed on intervals $[t_i, t_{i+1}]$ of length h. Consequently, it is possible to deal with a large number of discontinuities during a step. The contact problem is solved over the range of this interval and not point-wise. Thus, the Eq. (7) can be integrated on each time step using the following equation:

$$M(v_{i+1} - v_i) = \int_{t_1}^{t_{i+1}} F(q,v,t)dt + I_{i+1}, \tag{8}$$

The velocity v_{i+1} is the approximation of the right limit at the time t_{i+1},

$$\begin{cases} v_{i+1} = v_i + M^{-1}\int_{t_1}^{t_{i+1}} F(q,v,t)dt + M^{-1}I_{i+1}, \\ v_{free} = v_i + M^{-1}\int_{t_1}^{t_{i+1}} F(q,v,t)dt, \end{cases} \tag{9}$$

where v_{free} is the velocity of the bodies in the absence of contacts. Hence, (9) can be rewritten by means of the Delassus operator $W^{\alpha\beta}$ and the local unknowns in this form:

$$\begin{cases} v_{i+1}^\alpha = v_{loc,free}^\alpha + W^{\alpha\beta} I^\alpha, \\ Contact\ law\ (I^\alpha, v^\alpha) = 0, \end{cases} \tag{10}$$

and $v_{loc,free}^\alpha = H^{T\alpha}(q_m)v_{free} + \sum_{\beta \neq \alpha} W^{\alpha\beta} I^\alpha$. Finally, the Non-Linear Gauss Seidel method allows solvingthe contact problem.

Therefore, between the discrete element methods, there is the NSCD method, which is characterized by three main factors: (i) the non-smooth contact laws are directly integrated in it; (ii) an implicit integration scheme is implemented; and (iii) structural damping is not considered. Furthermore, the NSCD method requires specific simplifications on the building of the model. Firstly, the bodies are assumed to be perfectly rigid and secondly, the contact laws between blocks are determined by the Signorini's impenetrability condition and friction à la Coulomb. Thus, these relations on the contacts involve perfectly plastic impacts, without bounces as a consequence, i.e. a null value of the restitution coefficient in the Newton law. According to it, the main advantage of the limited computational complexity is derived by the simple modelling of the impacts. Afterwards, another relevant benefit due to the perfectly plastic impact is related to the dissipation of energy, which explains the damages to the material and the micro-cracks forming on the stones after collision. Additionally, it supports the numerical integration and its stability from a computational point of view. The dissipated energy of these models is determined by the involvement of the friction and it does not consider the damping effects, which are essential to the continuum models.

3.2 The Discrete Element Method

In the DEM method, initiated by Cundall et al. in [16] and [19,20], the displacement of the blocks is computed with the explicit numerical integration of the Newtonian equations of motion throughout finite and small timesteps.

The DEM code involves the contact detection by means of a common plane between the blocks. Thus, the contact is created when a point of a block gets into the interior of another block. The contact detection algorithm recognizes these cases and provides a unit normal vector, which is the contact normal and defines the plane along where sliding may occur. This unit normal continuously changes direction, as the two blocks move relatively to each other.

Contact exists if the overlap between two blocks is positive. When a face of a rigid block is in contact with the common plane, it is automatically discretized into sub-contacts by triangulating the face. The vertices of the triangles will be the nodes whose translation increments during the actual time-step serve as the basis for the calculation of the forces transmitted between the two contacting blocks.

The basis of the mechanical calculations is the relative velocity v of the sub-contact under question, which is defined as:

$$v_i = v_i^V + v_i^F \, ,$$ (11)

where v_i^V is the velocity of the analysed node and v_i^F is the velocity of the corresponding point of the opposite face on the other block. This latter velocity is calculated with the help of a linear interpolation of the three nodes on the surface of the other block surrounding that opposite point. Then the relative translation vector Δu_i belonging to the sub-contact is calculated as:

$$\Delta u_i = v_i \Delta t \, ,$$ (12)

where v_i is the relative velocity and Δt is the length of the time step. The uniform distributed normal forces belonging to the sub-contact is obtained from the equation:

$$\Delta F_n = -K_n \Delta u_n A_C \, ,$$ (13)

and the uniform distributed shear forces from the relation:

$$\Delta F_{s,i} = -K_s \Delta u_{s,i} A_C \, ,$$ (14)

where K_n and K_s are respectively the normal and shear stiffness of the contact and A_C is the area of the sub-contact. The resultant along the sub-contact area is assigned to the analysed node; and the opposite of the resultant is shared among the three nodes surrounding the coincident point on the opposite face. The same is done for all nodes on the analysed face of the first block. Then the other block is analysed in a similar manner.

Consequently, when two blocks come together, the above-mentioned contact logic is equivalent to two sets of sub-contacts in parallel, each carrying sub-contact forces. The sub-contact forces received in the two steps are summed and halved. The overall interface behaviour is the average of both sets.

3.2.1 Constitutive models for contacts

The mechanical behaviour of contacts in DEM is modelled with the help of contact parameters as friction angle, cohesion, finite tensile strength and stiffness, defined in the normal and shear direction, as schematised in Figure 9 Mechanical representation of contact point between blocks (a), contact constitutive law in tension (b), and in shear (c) (a), relating sub-contact stresses with relative displacements characterizing the sub-contact.

According to literature, e.g. Lemos [21], normal stiffness in masonry modelling may have different physical interpretations. In the case of mortar joints, the normal stiffness can be directly related to mortar thickness and its physical properties. For dry joints, rough and irregular contact surfaces have a finite stiffness against penetration, which is reflected by the contact normal stiffness. In the shear direction, shear stiffness plays a similar role and Coulomb friction sets a limit to the sub-contact shear stress magnitude. In case of model with perfectly rigid blocks, the contact stiffnesses have to represent the block deformability as well.
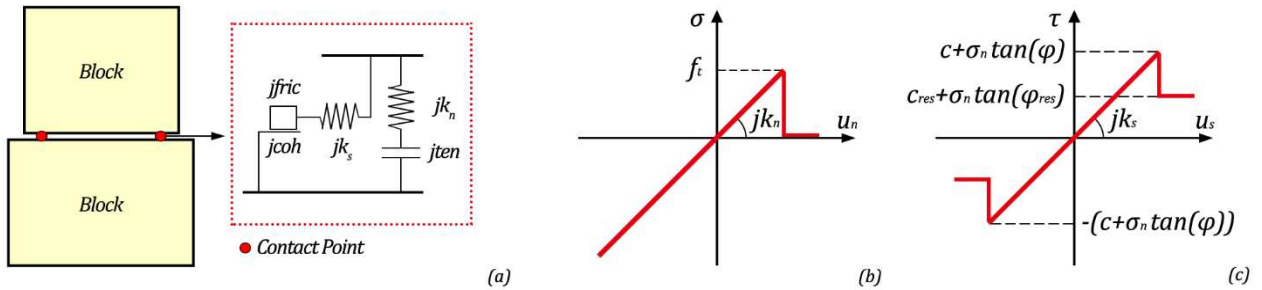

Figure 9 Mechanical representation of contact point between blocks (a), contact constitutive law in tension (b), and in shear (c)

In the elastic range (when contact sliding and separation does not occur), in Figure 9 Mechanical representation of contact point between blocks (a), contact constitutive law in tension (b), and in shear (c) (b) and Figure 9 Mechanical representation of contact point between blocks (a), contact constitutive law in tension (b), and in shear (c) (c), the behaviour of the rigid blocks is governed by the joint normal and shear stiffness (k_n and k_s):

$$\Delta\sigma_n = k_n\Delta u_n \,, \tag{15}$$

$$\Delta\tau_s = k_s\Delta u_s \,, \tag{16}$$

where $\Delta\sigma_n$ and $\Delta\tau_s$ are the normal and the shear force increment (resultant for the sub-contact); k_n and k_s are the joint normal and the joint shear stiffness; Δu_n and Δu_s are the normal and the shear displacement increments belonging to the sub-contact.

The joint constitutive model is the friction law of Coulomb, with both shear and tensile failure. In fact, the force of the joint is controlled by the tensile strength (f_t) in the normal direction with:

$$\sigma_n \leq f_t \,,$$

and the maximum shear force allowed is given by:

$$|\tau_s| \leq c + \sigma_n \tan(\varphi) = \tau_{max} \,, \tag{17}$$

where φ is the frictions' angle.

3.2.2 Solution algorithm for rigid blocks

In the presented model, where the explicit time stepping algorithm is used, the equations of motion for each node of the rigid blocks are:

$$m\frac{d\dot{u}_i}{dt} + \alpha m\dot{u}_i = \sum f_i \,, \tag{18}$$

where u_i is the nodal displacement vector of a node ($i = \{x, y\}$), m is the nodal mass, α is the mass-proportional viscous damping constant. The total nodal force vector $\sum f_i$ is given by a sum of three terms:

$$\sum f_i = f_i^C + f_i^E + f_i^A \,, \tag{19}$$

where f_i^C represents the contact forces, f_i^E is the nodal forces from the internal stresses and f_i^A is the sum of the external applied loads, including gravity.

The explicit scheme applies the central difference method. The dynamic calculation cycle of the performed numerical procedure for rigid blocks is schematised in Figure 10.
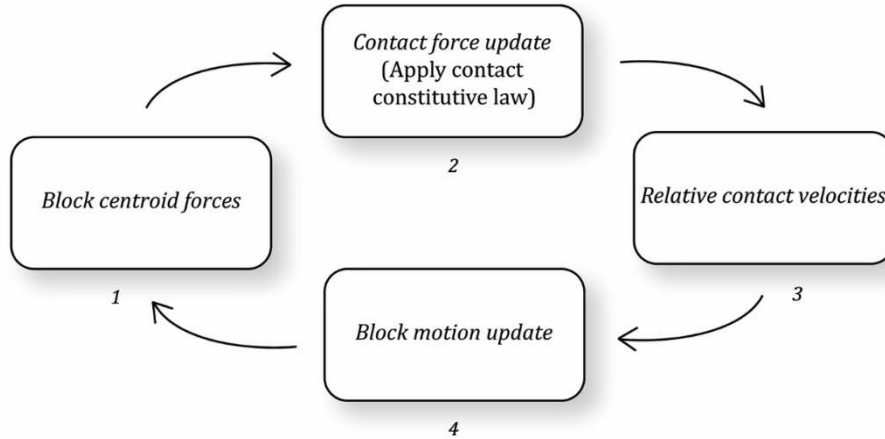

Figure 10 Dynamic calculation cycle for rigid blocks performed in DEM

The central difference method is only conditionally stable. Therefore, to avoid numerical instabilities, a limiting timestep is evaluated for each node by analogy to a simple degree-of-freedom system in the form:

$$\Delta t = 2f_R\sqrt{\frac{m}{K_n}} \,, \tag{20}$$

where m is the nodal mass, K_n is an upper bound of the nodal stiffness, obtained by summing the stiffness of all the elements and contacts connected to the node. With the help of f_R, namely fraction of the critical timestep used in solution, it is possible to decrease the length of the timestep. The simulations in the present paper were done with $f_{ract} = 0.1$, which is equal to the default value in the code.

3.2.3 Mechanical damping

Differently from the NSCD method, damping is applied in 3DEC© to decrease false oscillations originating from the explicit nature of the time integration technique and to reach

the force equilibrium state as quickly as possible. Preliminary experiences gained on test examples showed that shorter computational time was needed to find the equilibrium state when adaptive global damping was used. In the adaptive global damping, the viscous damping forces are used, but the viscosity constant is continuously adjusted in a way that the power dissipated by damping is a given proportion of the rate of change of kinetic energy in the system.

Thus, the adaptive global damping was used for the analyses of the tower, with the default ratio of the damping power and the rate of change of nodal kinetic energy which is equal to 0.5.

4 Development of the numerical models

The survey of the stones texture of the façades of the civic clock tower of Rotella (see Figure 3) is a significant aspect of the modelling with discontinuous approaches. This heavy work permits the designing of extremely detailed geometries of historical masonry structures with their irregularities and vulnerabilities. In fact, the existing configuration of the civic tower, including past retrofitting works, was taken into account during the development of the numerical models.

Thus, to investigate the real dynamical behaviour of the tower, the ancient existing walls of the tower were modelled by multi-leaf rubble masonry including diatons. Three different models of the same tower are presented in this study. All these models use blocks of different dimensions and regular convex shapes. Furthermore, the joints between blocks have thickness equal to zero with the blocks representing both the brick and the mortar combined into one element.

Model 1 is the most complex and accurate in representing the actual geometry of the tower (see Figure 11). It is formed by 31230 blocks, which are extruded from the survey of stones' texture of the tower façades (see Figure 3). Furthermore, the only simplification applied to the geometry of the first model was at the rubble masonry inside the two leave walls. Model 2 uses the same stone' pattern as model 1 to create the single-leaf walls, but without the filling blocks (see Figure 11), and it is composed of 17330 blocks. Model 3 is the simplest as it allows to recreate the genuine tower without the real stone' texture (see Figure 11). It is formed by 1173 blocks with dimensions larger than the actual stones of the masonry tower.
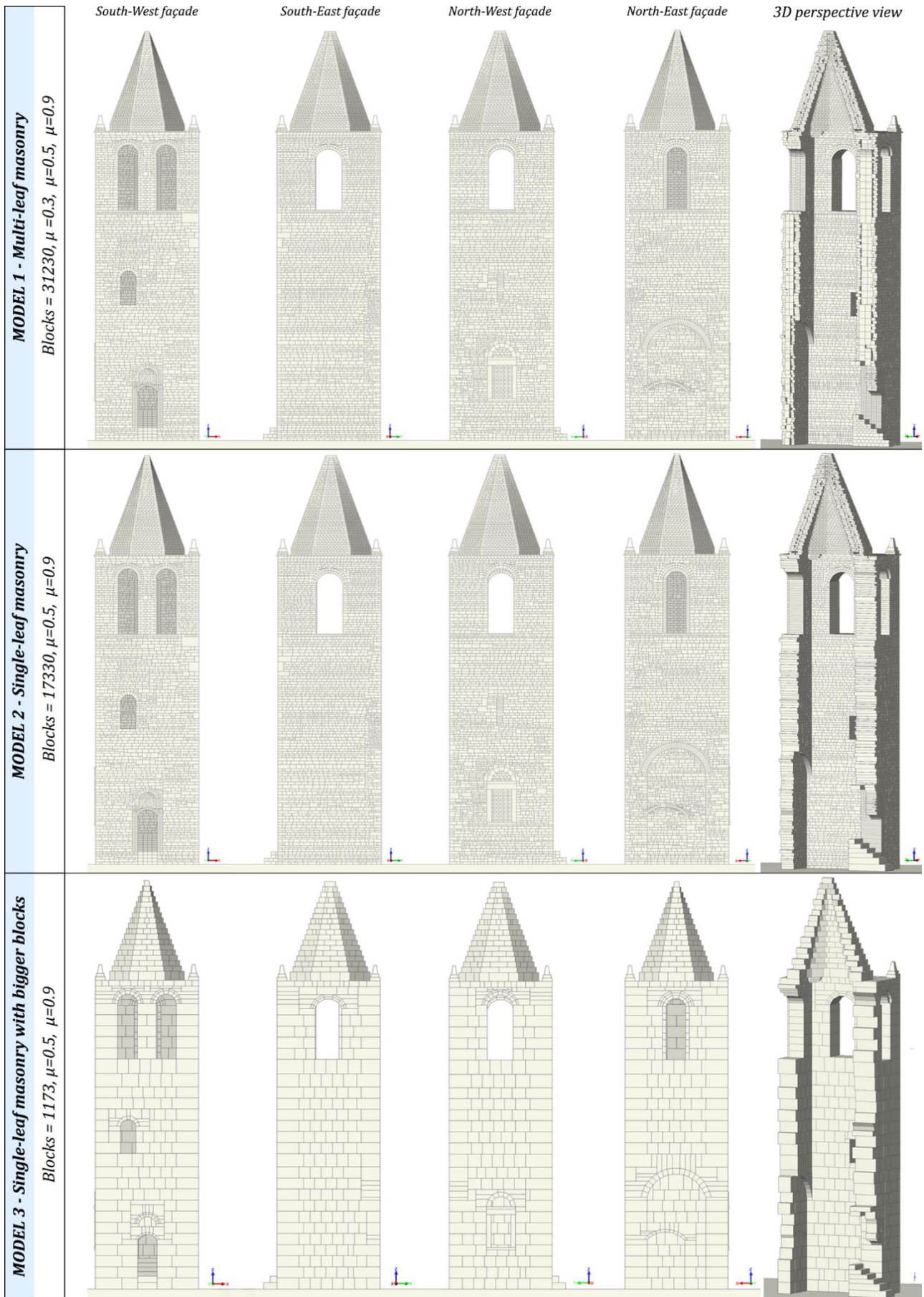
Figure 11 Views of the numerical model 1 with multi-leaf masonry, model 2 with single-leaf masonry and model 3 with single-leaf masonry with bigger blocks of the civic clock tower of Rotella (Ascoli Piceno, Italy)

15

4.1 Geometry

The geometry of the tower and the placement of the individual blocks is fairly complex to create in an automatic way using i.e. a script or the copy function of a CAD software. To represent the position of each block accurately, scaled images of the tower were imported into AutoCAD. These images were used to create a 2D representation of each face of the structure in the form of lines. The 2D lines were extruded to create the 3D geometric model of the main body of the tower.

Importing the geometry of the tower into LMGC90 using the CAD geometry is a straightforward issue. However, the same does not apply to 3DEC. In fact, 3DEC allows the use of CAD files in the form of DXF and STL formats to import and export 3D surfaces and even allows to cut the polyhedrons (3D representation of an object in 3DEC) using a DXF file. The disadvantage of the integrated import command (polyhedron cube) is that it can only create boundaries in two dimensions. A valid alternative is required to create complex geometry in three dimensions.

The approach adopted in here involved the development of a script that translates the 3D geometry in a format compatible to be used in 3DEC. In particular, the output of the script is a text file that uses the polyhedron prism command to represent 3DEC blocks.

4.2 Material properties and boundary conditions

The same mechanical parameters for the tower were used in both codes, with differences related to the adopted methods, as reported in Table 1. Regarding the Non-Smooth Contact Dynamics method, the blocks were modelled as rigid bodies to investigate the influence of the friction between blocks on the structural behaviour. For these purposes, the mass densities were associated with the configurations of the existing masonry and thus they assume definite values equal to 1800 kg/m³ and 1900 kg/m³ for the brick leaves and the internal infill of the masonry respectively, as indicated in the Italian code [22]. The values adopted for mechanical parameters refer to such kind of masonry which is typical for towers located in Central Italy and constituted by clay bricks and disordered bricks with very poor mechanical properties of the joint according to the local technologies used.

The three internal floors and the vertical connection consist of wooden tiles and thus they have been considered in terms of inertial masses and not modelled as rigid bodies.

The mechanical behaviour of the civic clock tower of Rotella is investigated considering the friction coefficient, which is related to the state of conservation of the structure and assumes values affected by the degradation of the mechanical properties of the masonry over time [23]. Since the structure is a heritage building subjected to constrains, it was not possible to conduct semi-invasive experimental tests to determine the mechanical properties of the masonry material. However, it was possible to perform a dynamic identification, which is a fully non-destructive evaluation [24] of the elastic modulus, with the aim of characterizing the structure as much in detail as possible at least in the linear range. In addition, the availability of the modal properties becomes relevant for the present non-linear analyses, because the Italian Code correlates the elastic properties with the inelastic ones, once that masonry texture is known with the typology of blocks and stones used. The dynamic identification was carried out collecting data with ambient vibration tests, a well know technique which consists on the monitoring of vibrations of the building under ambient noises like wind, traffic, etc., in order to

identify the real dynamic behaviour. From these previous investigations and a further calibration, an average value for the Young's modulus was deduced, resulting within the range 1200-1800 N/mm^2 established by Table C8.5.I of the Italian Code [22]. Since the masonry pattern is quite regular and the geometry of the blocks is regular too, the deduced friction angle for the interfaces is close to 27°, according both to [25] and to what stated by the Italian Code [22], with a vanishing cohesion and tensile strength tending to zero. Having no information about the soil mechanical properties, and being impossible to take into account rigorously the soil structure interaction in a DEM approach where soil is modelled with a sufficiently large parallelepiped under the foundation, see the seminal work by De Silva [26], sensitivity analyses on the friction coefficient at the interface between the foundation and the structure were carried out by means of Model 3, in order to have an insight, albeit approximate, on such specific issue. The results obtained are collected in Appendix 1. Similarly, other sensitivity analyses were carried out varying the friction coefficient of the contacts between the blocks of the structure in elevation. The results of such analyses are reported in Appendix 2.

Even though the real value of the friction coefficient between the masonry block units of the tower is variable and quite uncertain, a μ coefficient value equal to 0.9 was finally applied at the interfaces between the masonry blocks and the foundation. Moreover, considering that the performance and quality are worst in rubble masonry of the infill present only in Model 1 and partially in Model 2, it is assumed that the vertical masonry structure is characterised by different friction coefficients (μ) for the different models, as summarized hereafter:

- μ = 0.5, at the contact between the blocks of the internal and external leaf;
- μ = 0.3, at the contact between the blocks of the internal infill of the masonry walls;
- μ = 0.3, at the contact between the blocks belonging to the internal infill of the masonry walls and to internal and external leaf.

In particular, the friction coefficient assumes values equal to μ = 0.3 to reproduce very poor mortar and μ = 0.5 for quite good quality of mortar in the masonry walls.

Moreover, the contact forces are meant to follow a classical Mohr–Coulomb criterion, thus the models require other properties of the joint interface for the analyses implemented to 3DEC code. The following parameters must be assigned: joint normal stiffness equal to 70e9 Pa/m, joint shear stiffness equal to 58e9 Pa/m, joint cohesion equal to 0.1e6 Pa, joint tensile strength equal to 0.1e6 Pa. Indeed, the tensile and cohesion strength, even if small, assume some role in failure, which may influence the displacement capacity.

In absence of specific tests on the existing masonry tower and more detailed information for the walls, such values for the material parameters of the numerical models were adopted from literature [25,27].

Table 1 Mechanical proprieties used for the numerical analyses of the civic clock tower of Rotella (Ascoli Piceno, Italy) in the two different codes

Code		LMGC90	3DEC
Density ρ	[kg/m^3]	1800	1800
Joint Friction inside the structure μ	[-]	0.30, 0.35, 0.40, 0.45, 0.50, 0.55	17°, 19°, 22°, 24°, 27°, 29°
Joint Friction between structure and foundation μ	[-]	0.75, 0.80, 0.85, 0.90	37°, 38°, 40°, 42°
Joint normal stiffness JK$_n$	[Pa/m]	-	70e9
Joint shear stiffness JK$_s$	[Pa/m]	-	58e9
Joint cohesion strength Jcoh	[Pa]	-	0.1e6
Joint tensile strength Jten	[Pa]	-	0.1e6

4.3 Application of Loads

The dynamic behaviour of the civic clock tower of Rotella was firstly investigated under the actions of the gravity loads on the whole system. Afterward, real seismic actions in the three components, i.e. two on horizontal and one on vertical z direction, at the base of the tower were applied. In this study, the nonlinear dynamics analyses of the tower were carried out by means of the three main shocks occurred in the seismic events of Central Italy of 2016. In particular, the three events were introduced by two different sequences of dynamic actions. The first sequence considers the quakes recorded by the station of Ascoli Piceno, which is near the location of the analysed tower. The second sequence includes the strong motion shared by the stations of the epicentres for the three events:

(i) 24th August 2016 Amatrice with $M_L=6.0$ and $M_W=6.0$ (AMT station in Italian Accelerometric Archive (ITACA)),

(ii) 26th October 2016 Campi with $M_L=5.9$ and $M_W=5.9$ (CMI station in ITACA),

(iii) 30th October 2016 Forca Canapine $M_L=6.1$ and $M_W=6.5$ (FCC station in ITACA).

The two different sequences, each one with 41 seconds of total duration, are characterised by sets of 10 seconds for each strong motion and 5 seconds of null velocities in-between the different shocks. Also, a second of null velocities was used at the beginning of the first shock.

The comparison between the characteristics of the seismic actions is reported in Table 2, where [28–30]:

- R_{jb}, is the Joyner-Boore distance, known as the smallest spacing from the site to the surface projection of the rupture surface;
- R_{rup}, is the shortest distance between the site and the rupture surface;
- R_{epi}, is the distance estimated by the geometric swap.

Table 2 Characteristics of main earthquakes recorded in Ascoli Piceno (ASP), Amatrice (AMT), Campi (CMI), Forca Canapine (FCC) stations during the main seismic events of the last few decades in Italy, where * indicates that site classification is not based on a direct Vs,30 measurement

Seismic event	M_L	Depth (km)	Station	Class EC8	R_{jb} [km]	R_{rup} [km]	R_{epi} [km]	Channel NS PGA (cm/s²)	Channel EW PGA (cm/s²)	Channel UD PGA (cm/s²)
24/08/2016	6.0	8.1	ASP	B*	31.35	31.36	37.8	85.73	86.76	38.17
26/10/2016	5.9	7.5	ASP	B*	35.78	35.79	42.9	67.18	-56.72	22.63
30/10/2016	6.1	9.2	ASP	B*	30.18	30.18	44.00	116.91	-117.64	43.52
24/08/2016	6.0	8.1	AMT	B*	1.38	4.62	8.50	368.39	-850.80	391.37
26/10/2016	5.9	7.5	CMI	C*	2.53	7.44	7.10	302.56	-638.31	-468.28
30/10/2016	6.1	9.2	FCC	A*	0	5.55	11.00	843.73	-931.14	893.5

5 Discussion of the numerical results

The results for the different models and methods of the nonlinear dynamic analyses of the civic clock tower of Rotella are presented in graphical form both as displacements against Time Histories (THs) of specific control points and as captures of the evolution of damage for every seismic event applied in sequences.

The first subject of discussion is the comparison of the damages between the numerical models and the real existing structure for the validation of the nonlinear analyses performed. The second and final issue highlights progressive failure mechanisms and provides insight into the dynamic behaviour of the analysed structure, both made possible by the results acquired from the numerical analyses carried out using sequence of the epicentres strong motions.

5.1 Survey of the displacements Time Histories for the nonlinear analyses carried out with the earthquakes recorded in the station of Ascoli Piceno
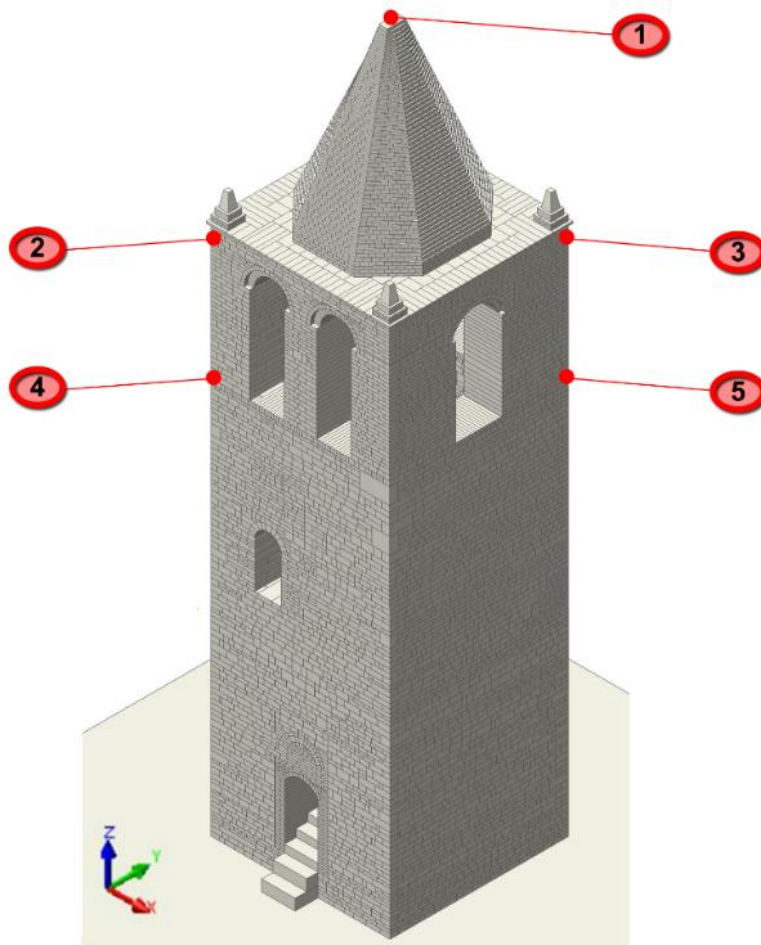

Figure 12 Locations of the control points used for the nonlinear dynamic analyses of the civic clock tower of Rotella (Ascoli Piceno, Italy)

The output results of the control points are expressed in terms of displacements along x, y and z directions for the points shown in Figure 12. These points assume the same coordinates for the three different models. The first point corresponds to the top of the tower. The second and the third point are located at the base of the roof. The fourth and the fifth point are placed at the level of the arched windows base. The control points #2 and #4 belong to the same side of the tower, with the point #2 in higher position than #4 along the vertical development of the cell bell. The points #3 and #5 follow the same disposition along the vertical on the opposite side of the tower. The displacements in the THs graphs are plotted with solid line for the analyses in LMGC90 and dashed line for the analyses in 3DEC.

Firstly, histories of displacements along the THs of the nonlinear analyses performed by means of NSCD method and DEM are examined in view of the earthquakes recorded near the location of the tower, namely Ascoli Piceno station, during the Central Italy seismic events of 2016.
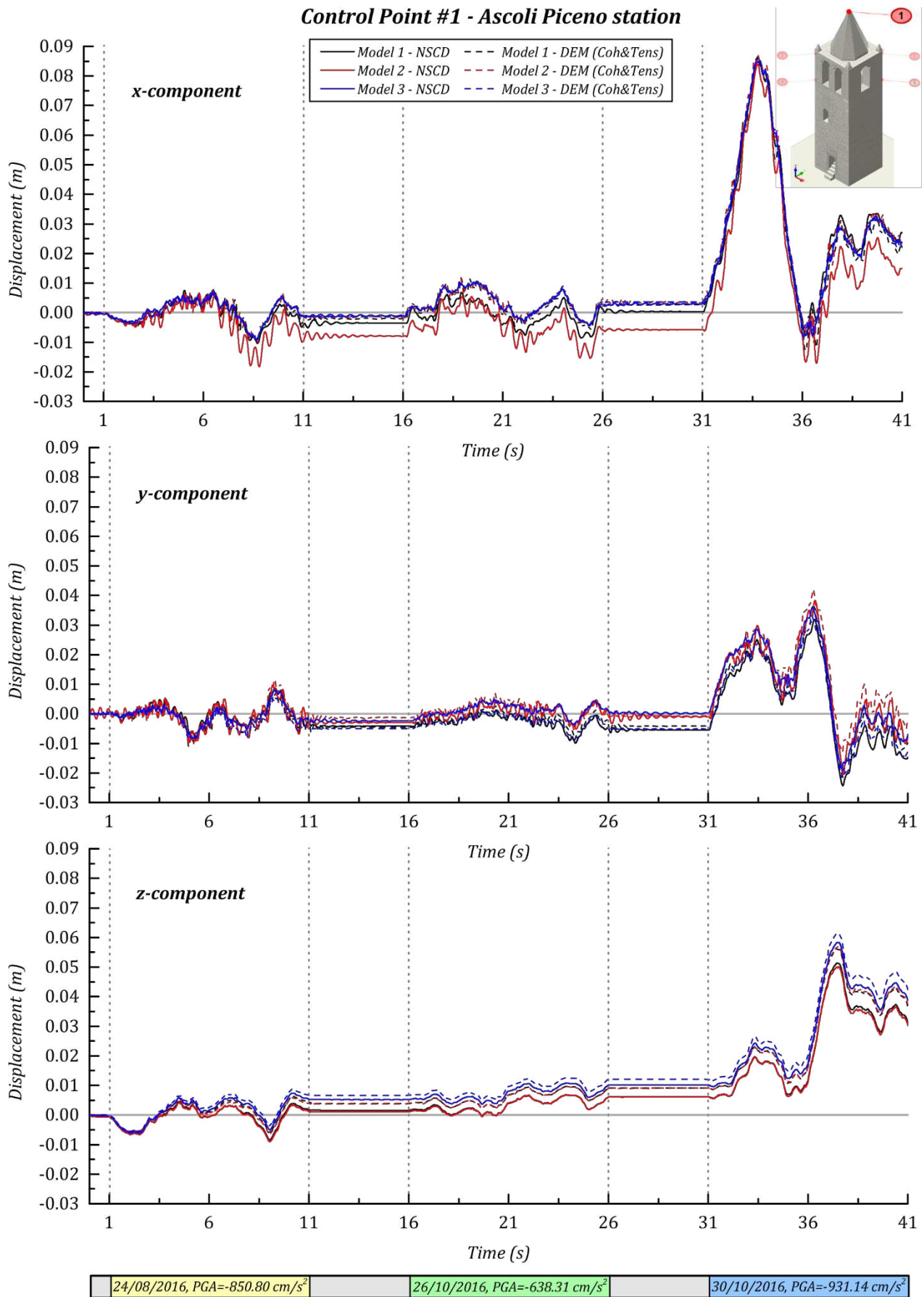
Figure 13 Displacements time histories of the control point #1 of the civic tower of Rotella (Ascoli Piceno, Italy) under the three main shocks recorded in the village during the Central Italy seismic sequence of 2016 for the three configurations of the models analysed using the both methods, NSCD and DEM

The control point #1 is plotted over time in Figure 13 and it exhibits, for every component, similar values for all the analyses, while this does not occur for the other control points. This is especially true for the x-component of the three models analysed with DEM. In contrast to this, the x-component of the model 2 with the NSCD method presents largest displacements from the mid of the first shock to the end of the sequence. Between the seconds 26 and 31 it is possible to figure out the difference between the two methods in terms of managing the contacts and how they achieve equilibrium of the residual displacements. In fact, the x-displacements from 3DEC require more seconds to reach the equilibrium state. The peaks displacements are reached at the 34 seconds with the greater values of the x-displacement near to ~0.086 m for the model 1 with NSCD and model 1 and 2 with DEM.

The displacements THs of control points #2 and #3 over time are drawn in Figure 14 and Figure 15 and of control points #4 and #5 in Figure 16 and Figure 17 respectively. The evolution of displacements for the control points #2 and #4 are similar in all numerical results. In particular, these control points present nearly coincident trend for each component x, y and z of displacements in the model 3 with both NSCD and DEM method. Instead, the model 2 introduces main differences for the x-displacements between the two methods used. This behaviour is more remarkable for the control point #2 than #4. Looking at x-displacements of model 2 for the control point #2, the difference of values between NSCD and DEM is equal to ~0.01 m for the residual values in the range 11-16 seconds, ~0.012 m in the range 26-31 seconds and ~0.018 m at the final step. For control point #4 of the same models 2, the difference of values of residual x-displacements is equal to ~0.005 m in the range 11-16 seconds, ~0.008 m in the range 26-31 seconds and ~0.014 m at the end. The peaks x-displacement present closer values at the 34 seconds, i.e. ~0.085 m for the both control points #2 and #4 in the model 3 with NSCD.

Moreover, the control points #3 and #5 show comparable displacements for each direction x, y and z among all computed results. The largest displacements obtained for the more detailed models 1 and 2 and especially for the x component. The peaks of the x-displacement are equal to 0.106 m for the control point #3 and 0.102 m for the point #5 from the model 1 with NSCD method at 34 seconds. Looking at the main displacements for the control point #3 and #5, it is visible that the higher values are from point #3 over time. In fact, it assumes residual x-displacement equal to 0.011 m in the range 11-16 seconds, 0.017 m in the range 26-31 seconds and m 0.055 m at the final second. For control point #5 the residual x-displacement is equal to 0.008 m in the range 11-16 seconds, 0.013 in the range 26-31 seconds and m 0.049 m at the last step.

Additionally, the larger displacements THs of control points #2 and #3, compared to #4 and #5, highlight the inherent vulnerability of the cell bell of the tower. These results are useful as guidelines for future reinforcement work to the seismic risk reduction of the structure, e.g. confinement of the masonry to limit the displacements over time.

Hence, with an overall look at the displacements THs, the amplifications of the progressive damage of the structure over time becomes evident due to the application of the main seismic actions in sequence. The effects of several seismic events on the masonry influence the dynamic behaviour and seismic resistance capability of the structure. These discrete nonlinear analyses allow to predict the cumulate damages of the tower, which is a major aspect to consider for the study of the ancient existing masonry structures.
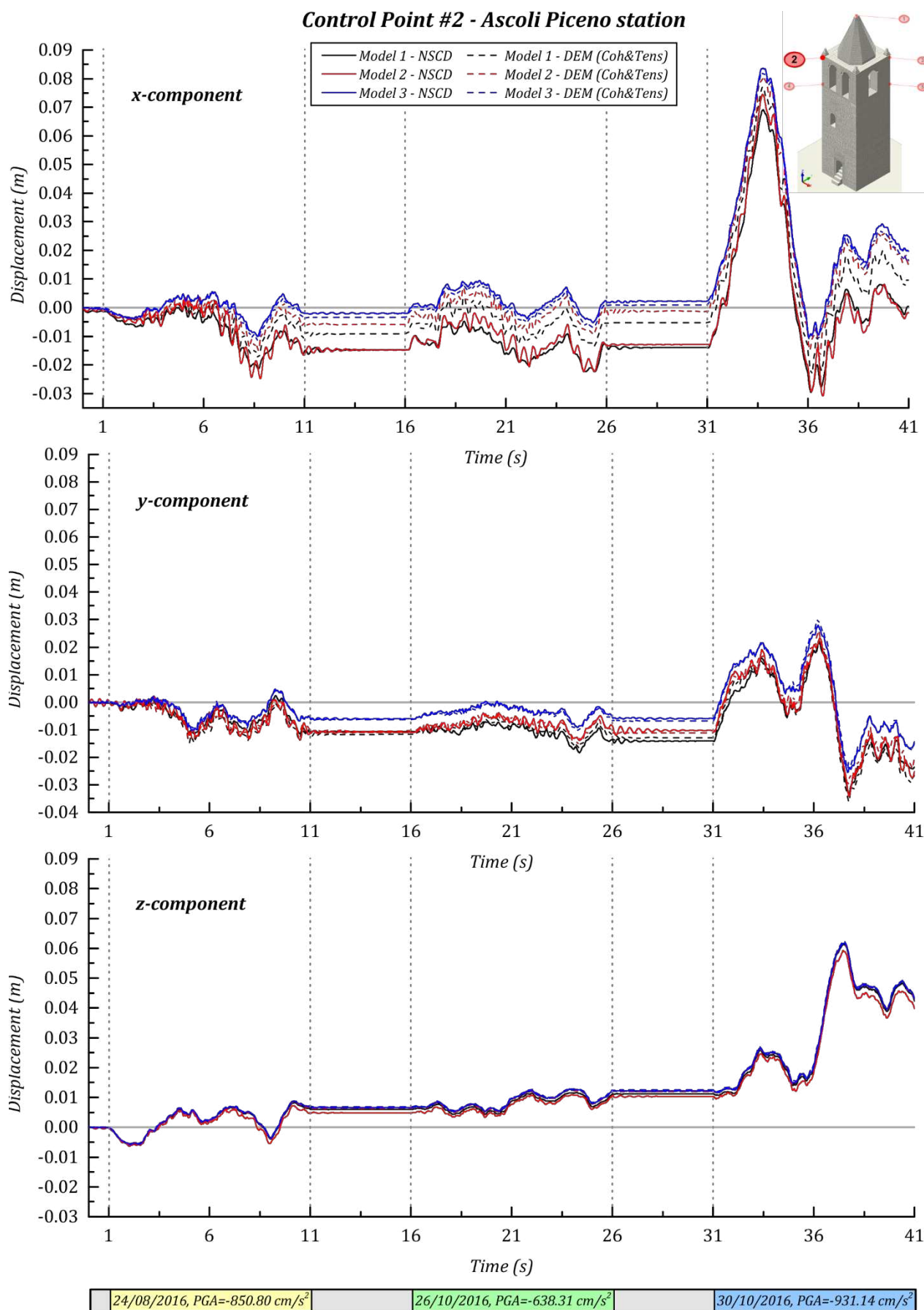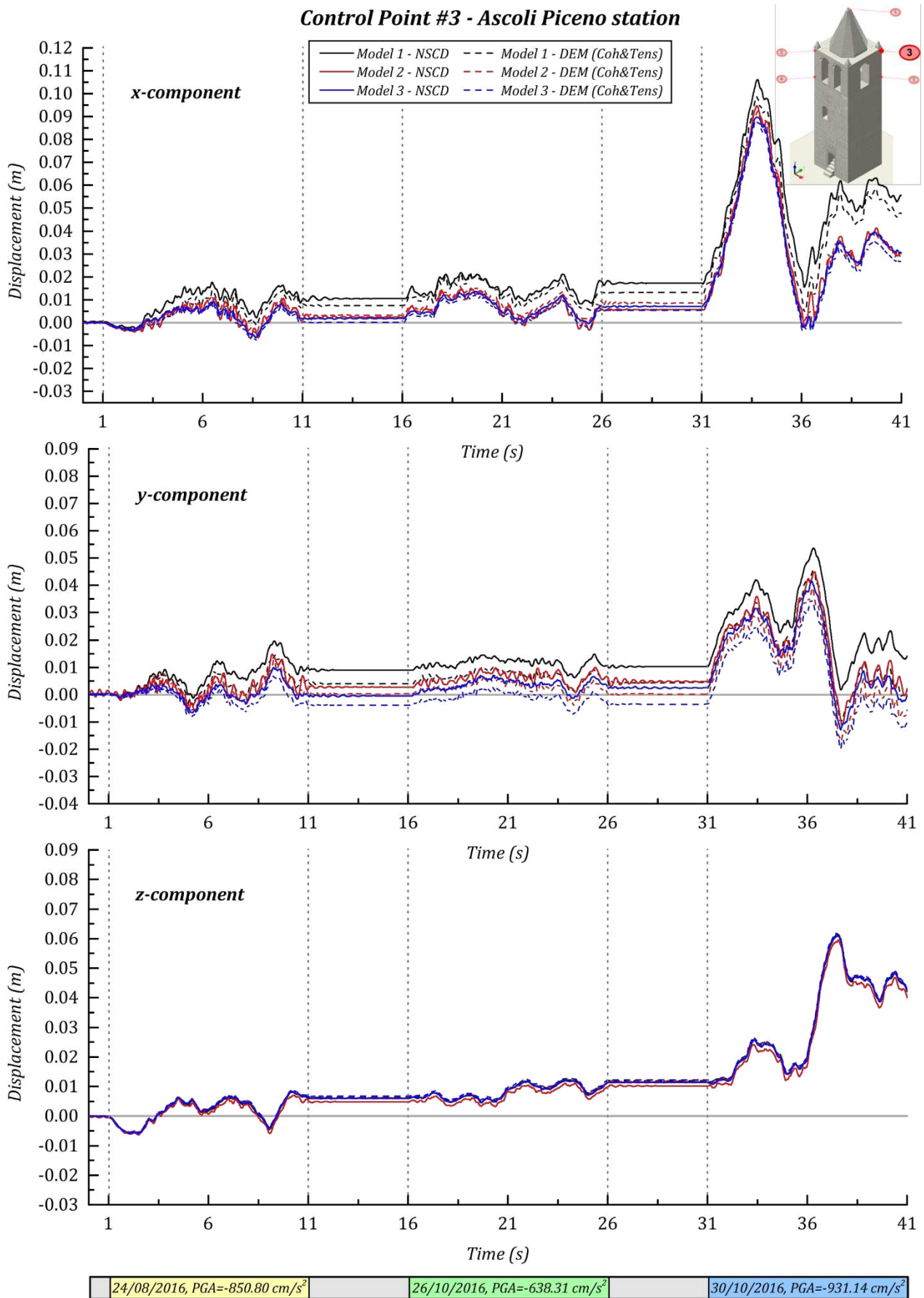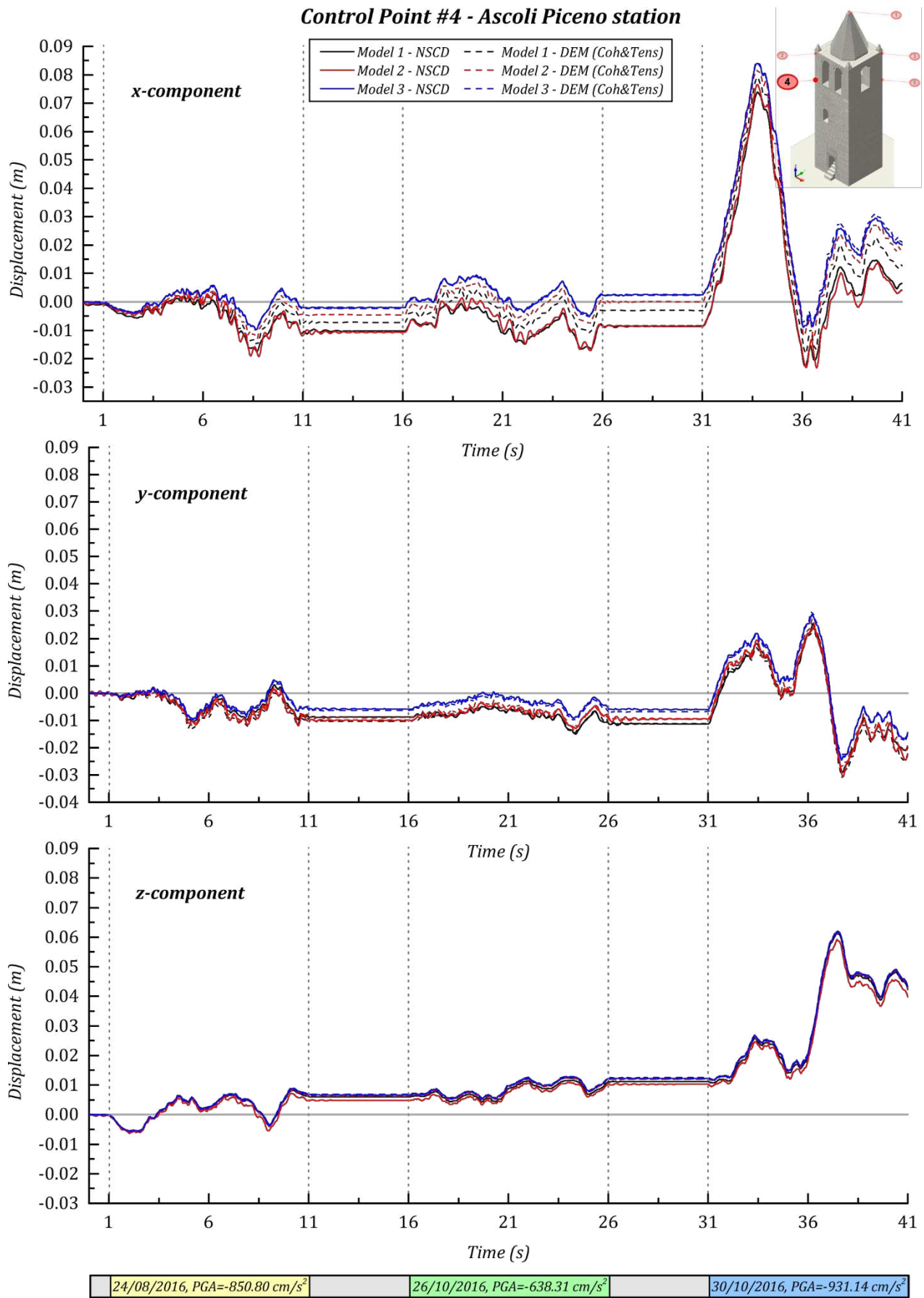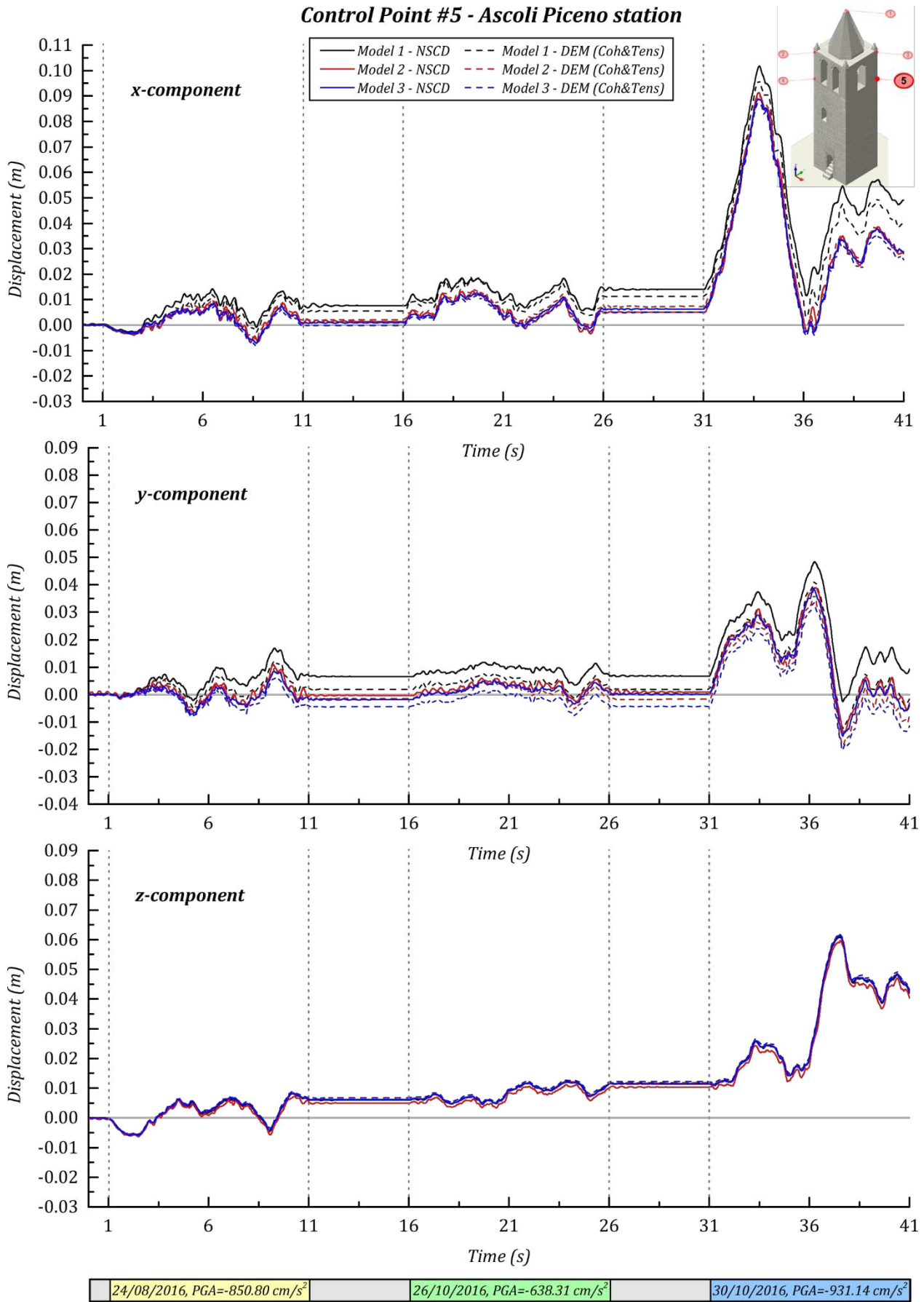
Control Point #2 - Ascoli Piceno station

x-component

Model 1 - NSCD — — — Model 1 - DEM (Coh&Tens)
Model 2 - NSCD — — — Model 2 - DEM (Coh&Tens)
Model 3 - NSCD — — — Model 3 - DEM (Coh&Tens)

y-component

z-component

| 24/08/2016, PGA=-850.80 cm/s² | 26/10/2016, PGA=-638.31 cm/s² | 30/10/2016, PGA=-931.14 cm/s² |

Figure 14 Displacements time histories of the control point #2 of the civic tower of Rotella (Ascoli Piceno, Italy) under the three main shocks recorded in the village during the Central Italy seismic sequence of 2016 for the three configurations of the models analysed using the both methods, NSCD and DEM

Figure 15 Displacements time histories of the control point #3 of the civic tower of Rotella (Ascoli Piceno, Italy) under the three main shocks recorded in the village during the Central Italy seismic sequence of 2016 for the three configurations of the models analysed using the both methods, NSCD and DEM

Figure 16 Displacements time histories of the control point #4 of the civic tower of Rotella (Ascoli Piceno, Italy) under the three main shocks recorded in the village during the Central Italy seismic sequence of 2016 for the three configurations of the models analysed using the both methods, NSCD and DEM

Figure 17 Displacements time histories of the control point #5 of the civic tower of Rotella (Ascoli Piceno, Italy) under the three main shocks recorded in the village during the Central Italy seismic sequence of 2016 for the three configurations of the models analysed using the both methods, NSCD and DEM

5.2 Survey of the displacements Time Histories for the nonlinear analyses carried out with the strong motions recorded in the station of the epicentres

The displacements THs with strong motions recorded in the epicentres of the Central Italy seismic sequence of 2016 are studied for both the NSCD and DEM method, with the aim to gain deeper insight to the nonlinear behaviour of the civic clock tower of Rotella.

Control points #1, #2 and #3, in Figure 18, Figure 19 and Figure 20 respectively, introduce the largest displacements observed during the simulations. Control points #1 and #3 describe the collapse of the upper part of the tower at 17 seconds, after the beginning of the second earthquakes of model 1 with both NSCD and DEM methods. The same behaviour of the control points #5, is reported in Figure 22. Control point #3 of the model 1 presents residual x-displacements of 0.21 m for the NSCD method and 0.17 m for DEM, both at 16 seconds. For the same model 1, the control point #5 has residual x-displacements of 0.17 m for the NSCD method and 0.15 m for DEM, both at 16 seconds. Control point #1 introduces the lowest values for the residual x-displacements near to 0.00 m for the NSCD method and equal to -0.06 m for DEM, both at 16 seconds. Thus, it is possible to understand the evolution of the collapse evolution began with the major dislocation of the masonry where control point #3 is placed.

Other collapses related to the control point #1 of models 2 and 3 in all the analyses appear at the beginning of the third seismic action. At the final step of the control point #2 and #4 there are collapses of model 3 when analysed using the NSCD method. Control point #2 presents larger displacements than point #4, e.g. at 38 seconds the peak x-displacement is equal to -0.56 m for #2 and to -0.4 m for point #4 of model 3 with DEM. Furthermore, control point #3 and #5 exhibit collapses for the model 3 analysed with NSCD method and model 2 and 3 with DEM. The displacements are higher for point #3 and the major peak displacement is in y direction at 35 and 37 seconds and it is equal to 0.60 m for the point # 3 and to 0.40 m for the point #5 of the model 2 with NSCD.

Moreover, further information on the dynamical behaviour of the structure is provided by the results of the sensitivity analyses carried out on Model 3 (the coarsest one) in Appendix 1 and Appendix 2. In these cases, it should be noted that the responses of the structure when the friction between the soil (considered as a rigid block) and the tower is varied turn out to be rather close one each other. This is an indication that the friction coefficient does not change significantly the trigger of the possible collapse. Since the early stages of heavy damage are uninfluenced by the variation of the friction coefficient at the base, it may be argued that the global behaviour of the structure is roughly independent from the mechanical properties assumed for the soil. As expected, the magnitude of displacements in the control points differs in line with the variation of the friction coefficient. The displacements assume indeed larger values when the friction coefficient is greater, because the slips become secondary when compared to the relative rotations, that are obviously responsible for larger displacements at the top nodes. Actually, the overturning mechanisms gradually prevail over sliding mechanisms, proportionally to the increase of the value of the friction coefficient. In addition, the sensitivity analyses reported in Appendix 1 highlight that the effects of varying friction coefficient at the interface between foundation and structure are far less important than those related to a variation of the friction coefficient between contiguous blocks belonging to the structure in elevation.
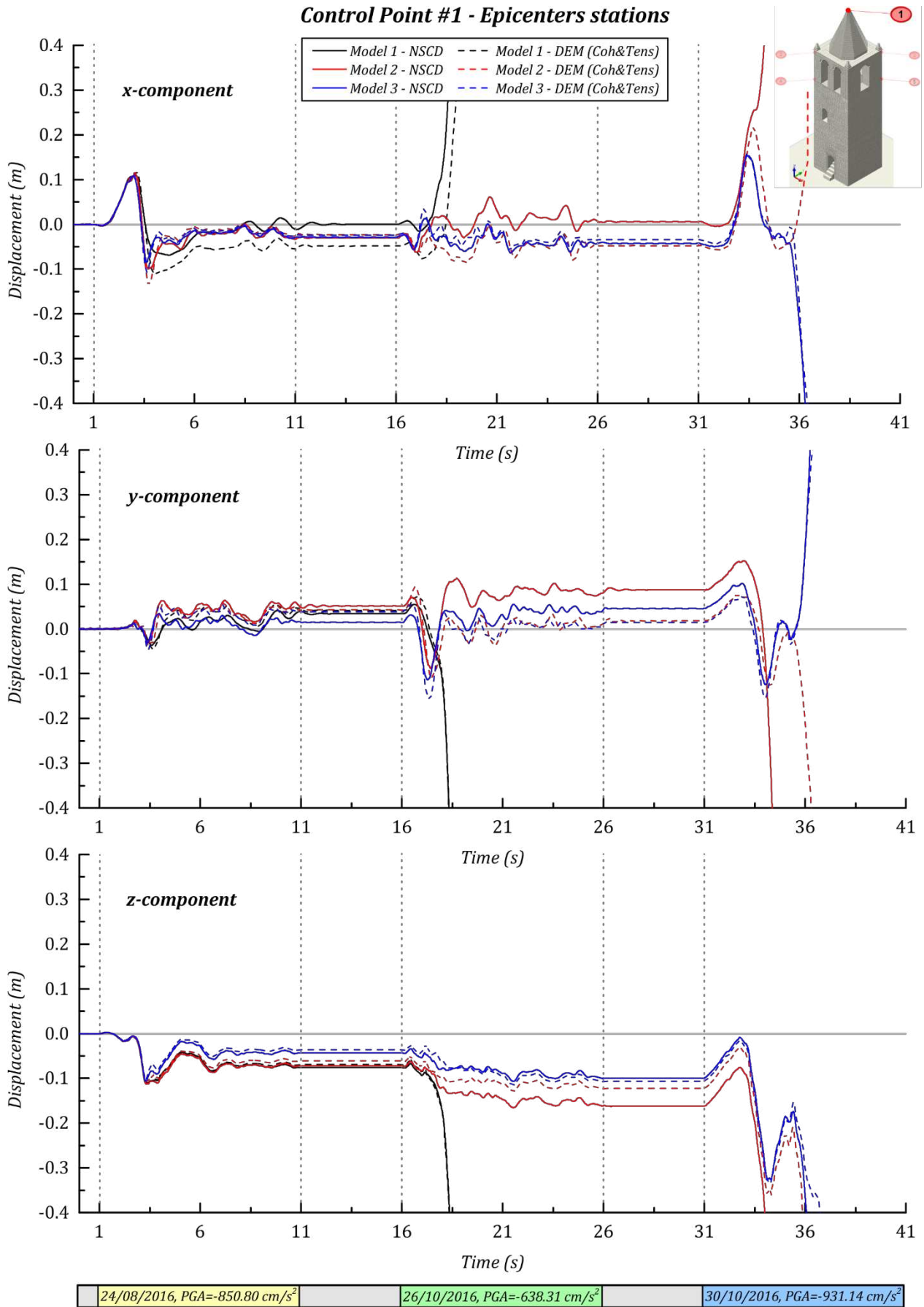
Figure 18 Displacements time histories of the control point #1 of the civic tower of Rotella (Ascoli Piceno, Italy) under the three main shocks recorded in the epicentres during the Central Italy seismic sequence of 2016 for the three configurations of the models analysed using the both methods, NSCD and DEM
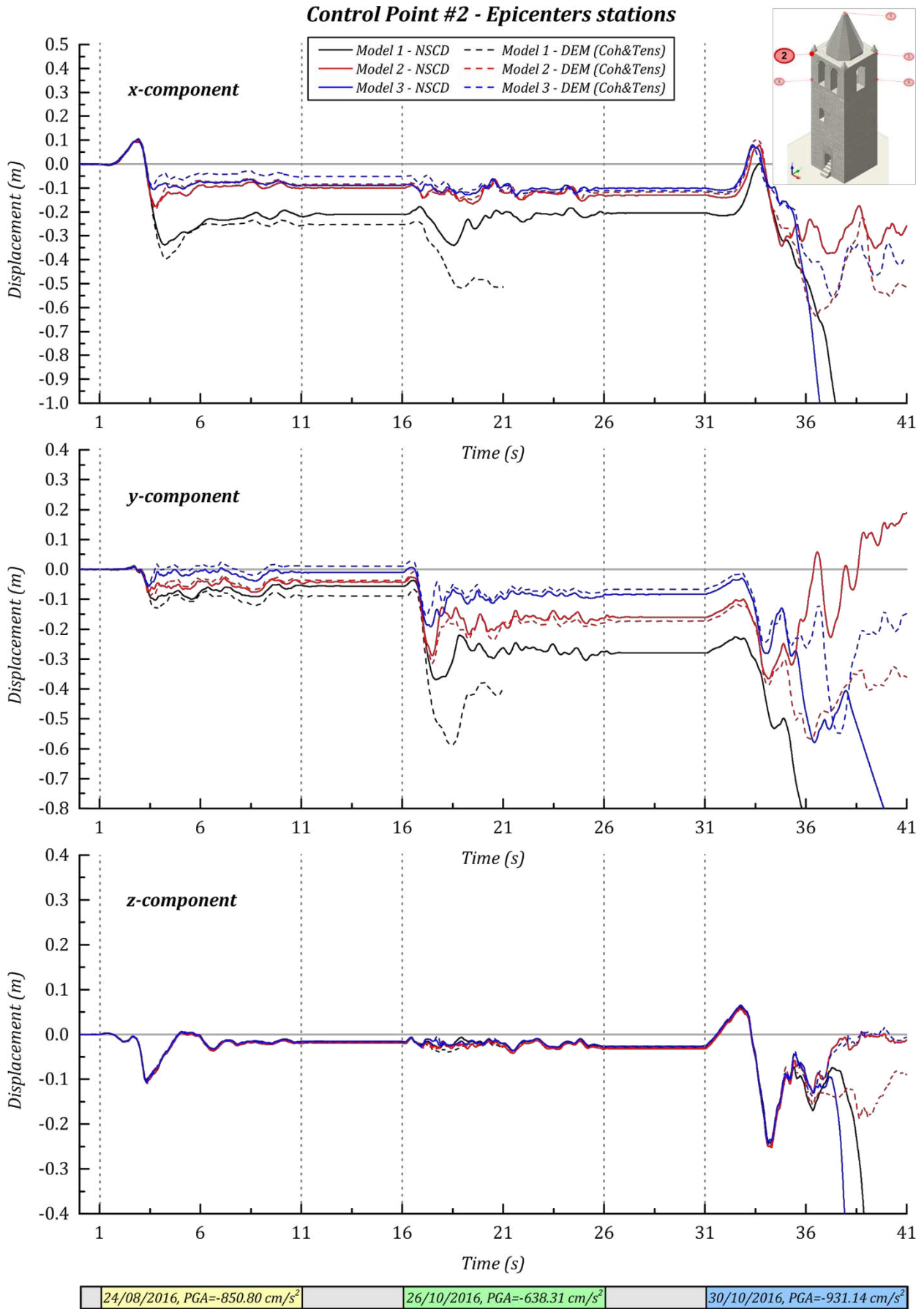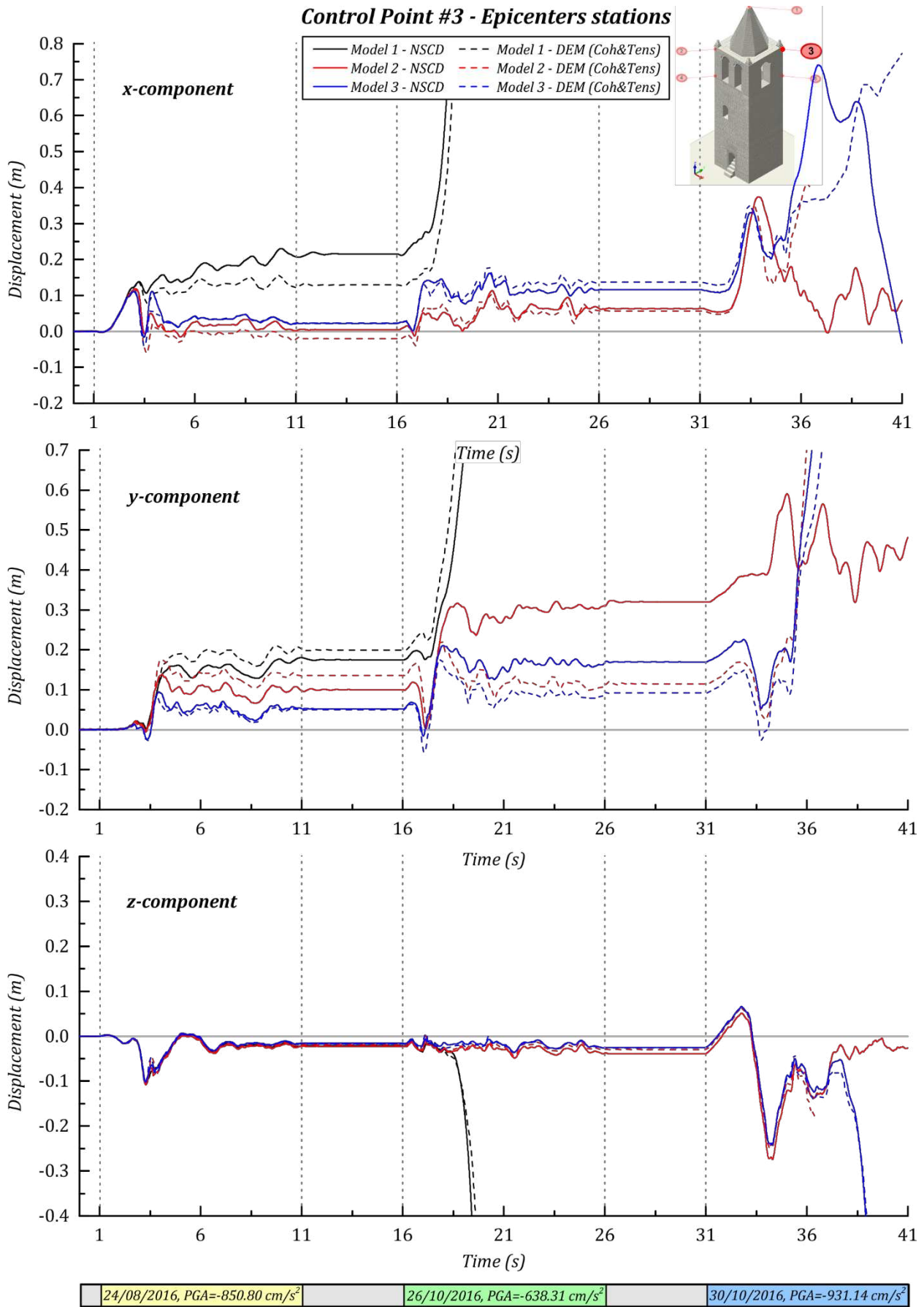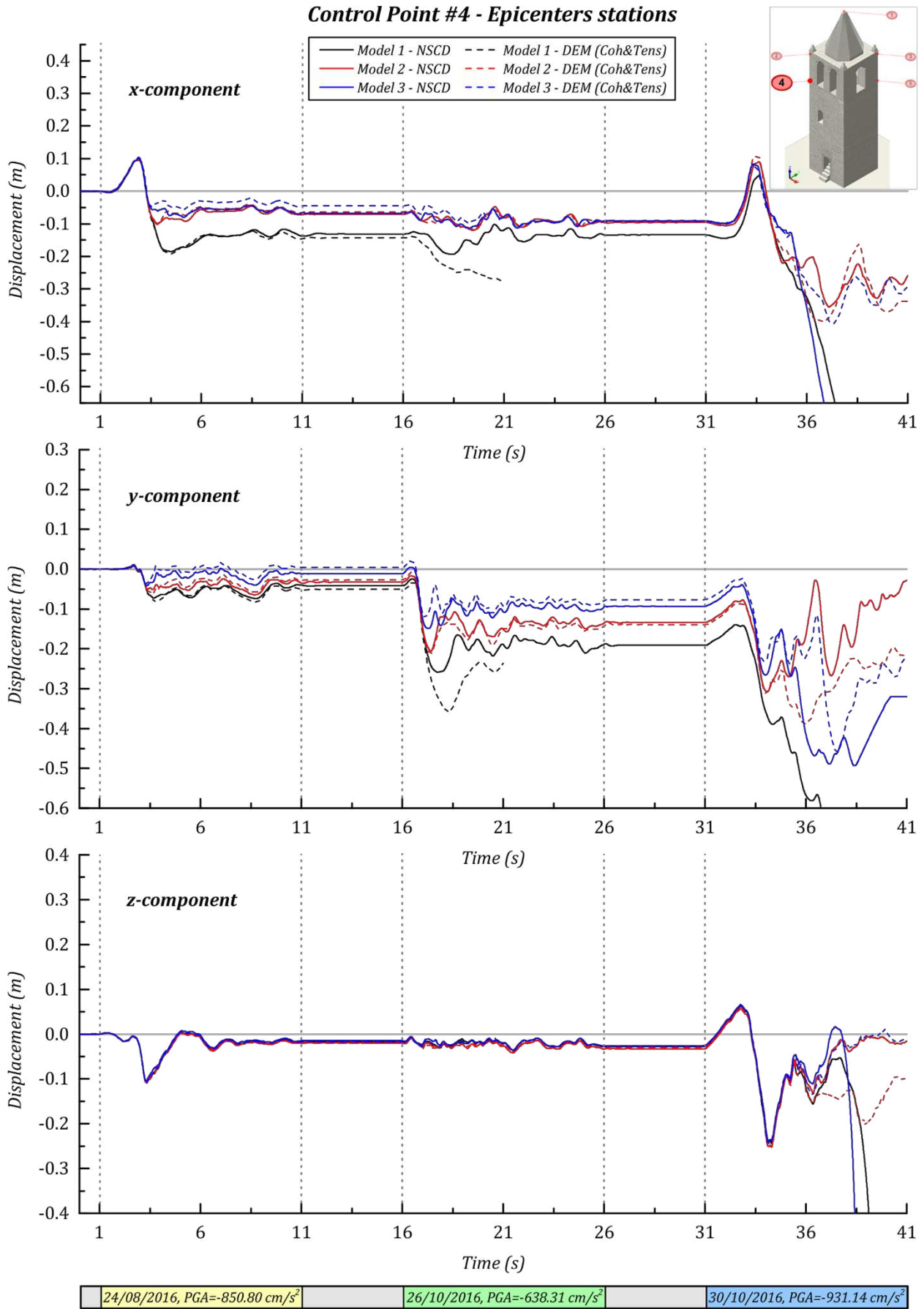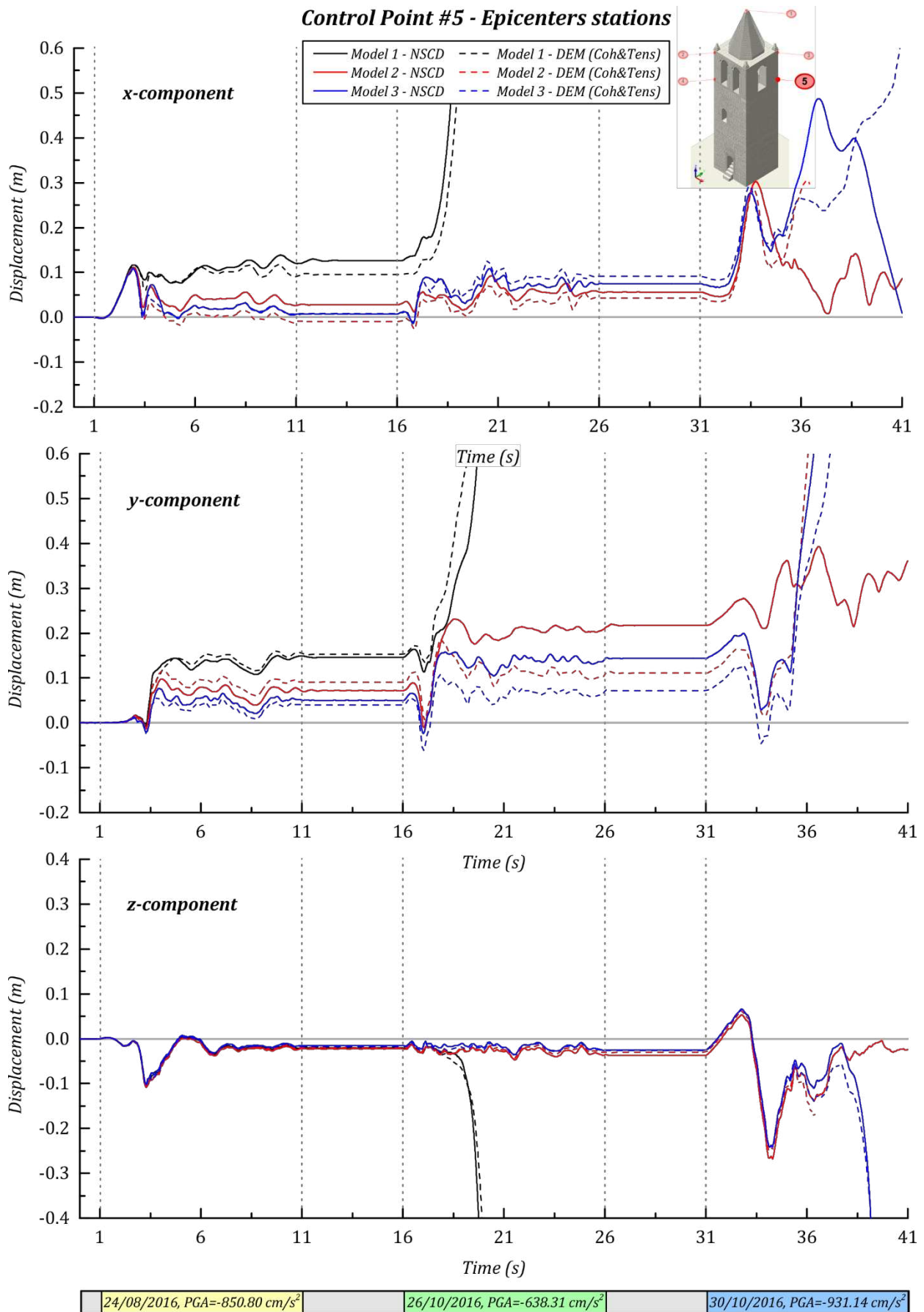
27

Figure 19 Displacements time histories of the control point #2 of the civic tower of Rotella (Ascoli Piceno, Italy) under the three main shocks recorded in the epicentres during the Central Italy seismic sequence of 2016 for the three configurations of the models analysed using the both methods, NSCD and DEM

Figure 20 Displacements time histories of the control point #3 of the civic tower of Rotella (Ascoli Piceno, Italy) under the three main shocks recorded in the epicentres during the Central Italy seismic sequence of 2016 for the three configurations of the models analysed using the both methods, NSCD and DEM

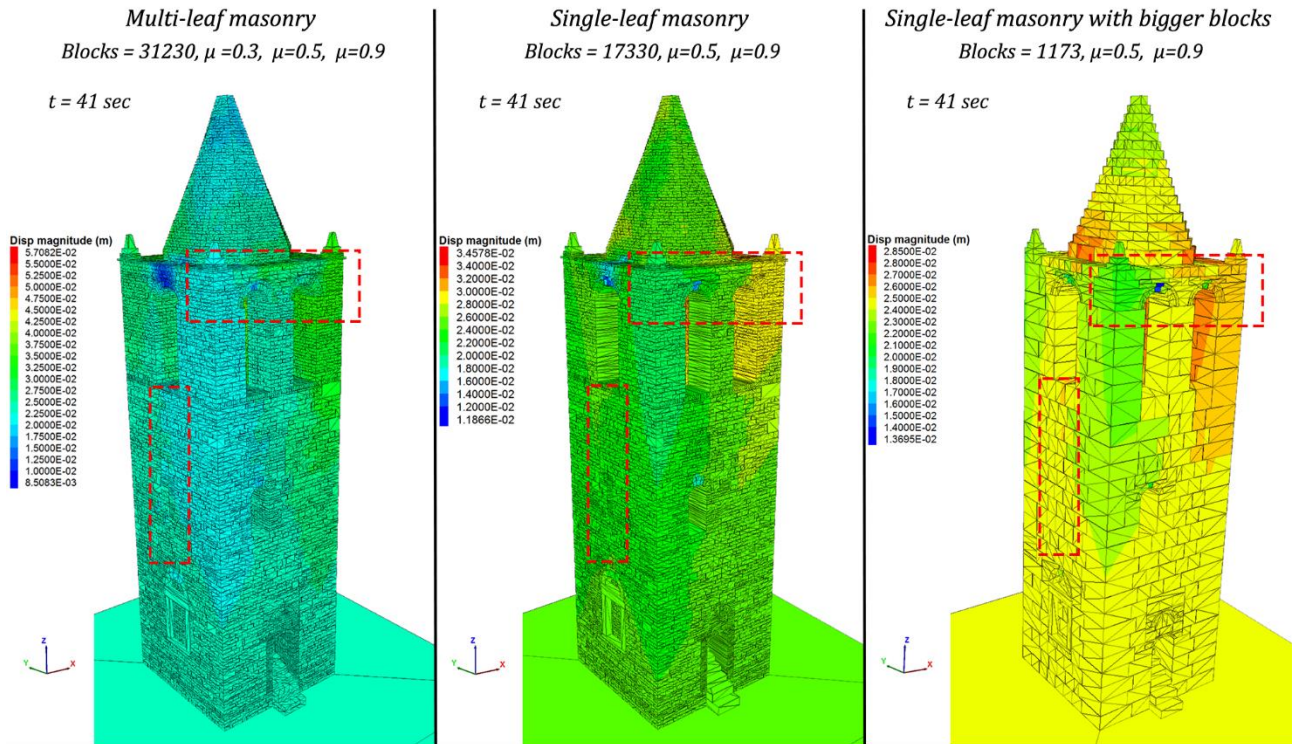Figure 21 Displacements time histories of the control point #4 of the civic tower of Rotella (Ascoli Piceno, Italy) under the three main shocks recorded in the epicentres during the Central Italy seismic sequence of 2016 for the three configurations of the models analysed using the both methods, NSCD and DEM

Figure 22 Displacements time histories of the control point #5 of the civic tower of Rotella (Ascoli Piceno, Italy) under the three main shocks recorded in the epicentres during the Central Italy seismic sequence of 2016 for the three configurations of the models analysed using the both methods, NSCD and DEM

31

5.3 Comparison of the damages from the numerical analyses and the real existing structure

The main results provided by nonlinear analyses, of the NSCD and DEM methods respectively, are reported in Figure 23 and Figure 24. These outcomes are due to the sequence applied, which matches the three major strong motions recorded near the location of the tower. The global behaviour of the models is similar for both the NSCD and DEM methods. Moreover, the activated failure mechanisms are comparable for different level of geometry details in the models 1, 2 and 3. To explore this issue further, the Figure 25 and Figure 26 display the results among the different cases.
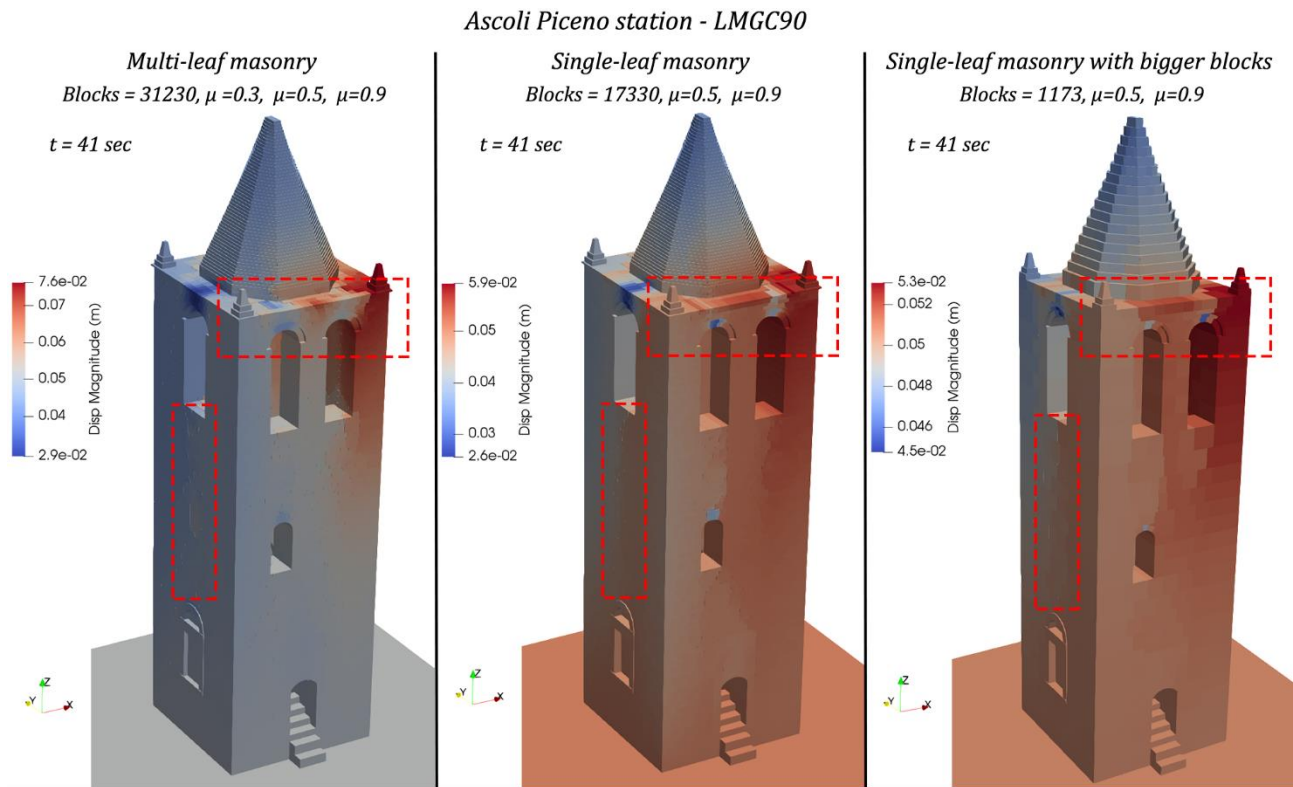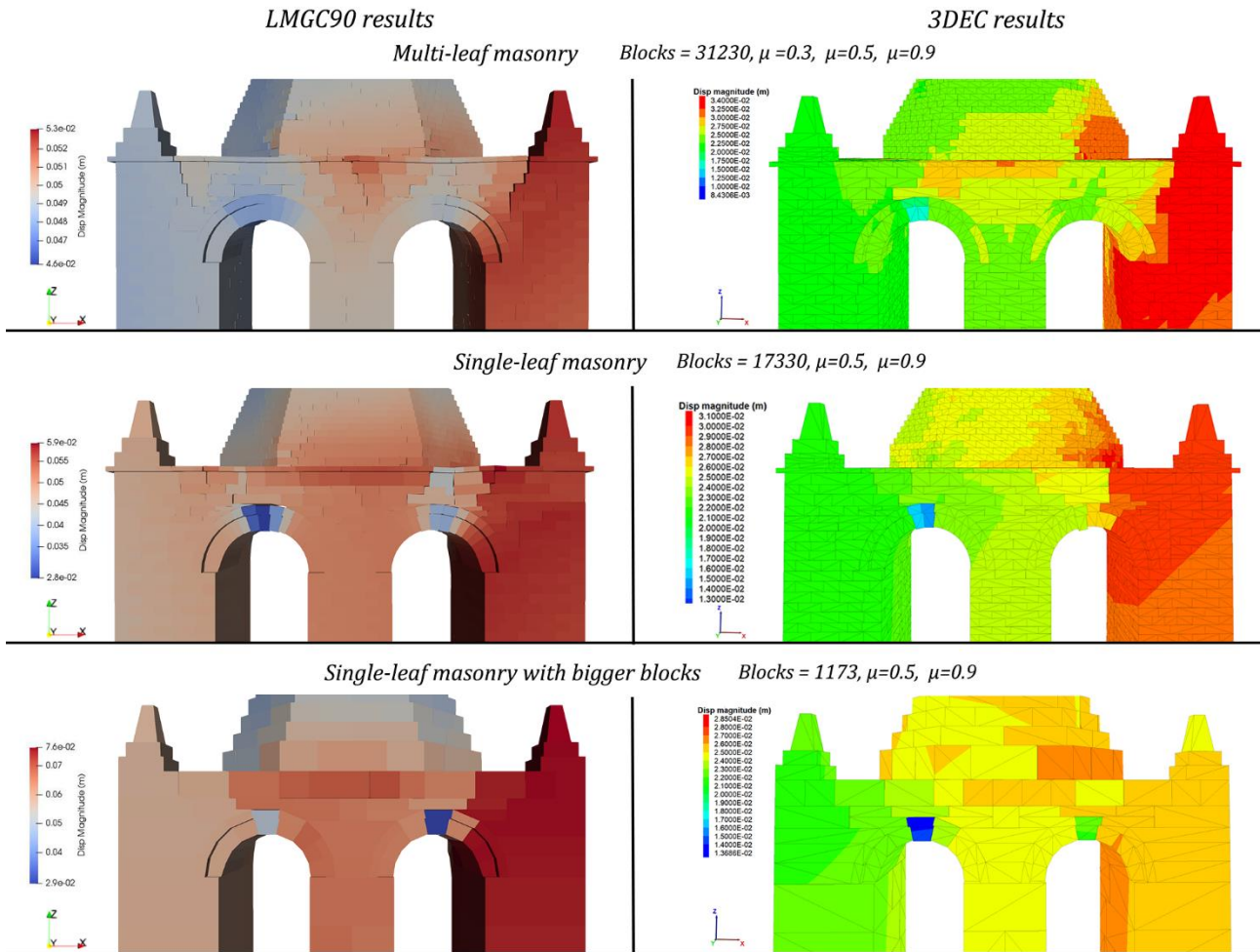

Figure 23 Numerical cumulative damages of the civic tower of Rotella (Ascoli Piceno, Italy) under the three main shocks recorded in the village during the Central Italy seismic sequence of 2016 for the three configurations of the models analysed using the NSCD method

Multi-leaf masonry
Blocks = 31230, μ =0.3, μ=0.5, μ=0.9

t = 41 sec

Single-leaf masonry
Blocks = 17330, μ=0.5, μ=0.9

t = 41 sec

Single-leaf masonry with bigger blocks
Blocks = 1173, μ=0.5, μ=0.9

t = 41 sec

Figure 24 Numerical cumulative damages of the civic tower of Rotella (Ascoli Piceno, Italy) under the three main shocks recorded in the village during the Central Italy seismic sequence of 2016 for the three configurations of the models analysed using DEM

The principal purpose of these analyses is the comparison of the numerical damages with the real ones. This is achieved by comparing the crack patterns of the civic clock tower of Rotella in Figure 5 with those on the numerical models of both codes. In particular, the failure mechanisms of the double-arched window of the South-West façade of the cell bell are reported in Figure 25. Furthermore, the vertical failures along the development of the South- East façade of the tower, are examined in Figure 26. The three different geometries lead to obtain three different interpretations of the damages. The more complex model with the multi-leaf masonry presents very similar behaviour to reality. The single-leaf masonry model introduces a behaviour that is close to reality but still not as accurate. The simpler model with single-leaf masonry and bigger blocks offers an approximate behaviour compared to the actual structure.
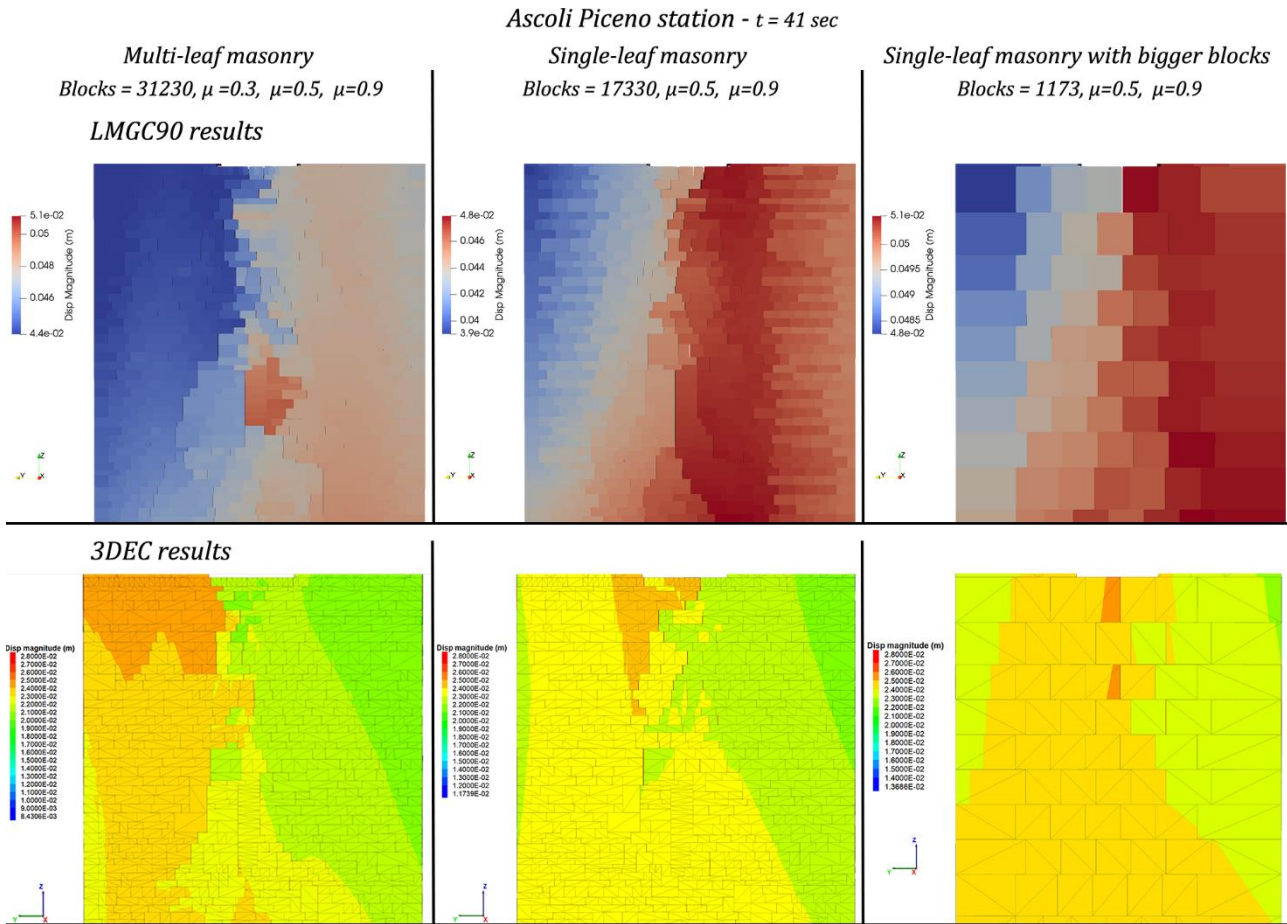
33

Figure 25 Numerical cumulative damages of the civic tower of Rotella (Ascoli Piceno, Italy) under the three main shocks recorded in the village during the Central Italy seismic sequence of 2016 for the three configurations of the models analysed using both the NSCD method and DEM

Moreover, the application of the strong motions recorded in the epicentres leads to the amplifications of the damages until the total collapses of the civic clock tower of Rotella, as reported in Figure 27, Figure 28, Figure 29 and Figure 30. This behaviour is stressed in the results for each quake applied in the sequence. In particular, in Figure 27 it is possible to evaluate how the damages caused by the initiation of the strongest shocks reproduce the final real damages shown in the results of the Ascoli Piceno recordings in Figure 23 and Figure 24. In fact, model 1 and 2 exhibit closer to reality damages at 2.8 seconds of the recordings of the epicentres, while for model 3 similar damages appear at 3.0 seconds. The comparison seems clearer with model 1 than the other ones.

The damages at a time equal to 16 seconds are plotted after the first shock of the sequence. The main failure mechanism is activated by the opening of the cylindrical hinges, alternated the intrados and extrados outline of the window arches at the cell bell. This behaviour is further developed in model 1, characterized by multi-leaf masonry, for both the NSCD and DEM methods (see Figure 28).

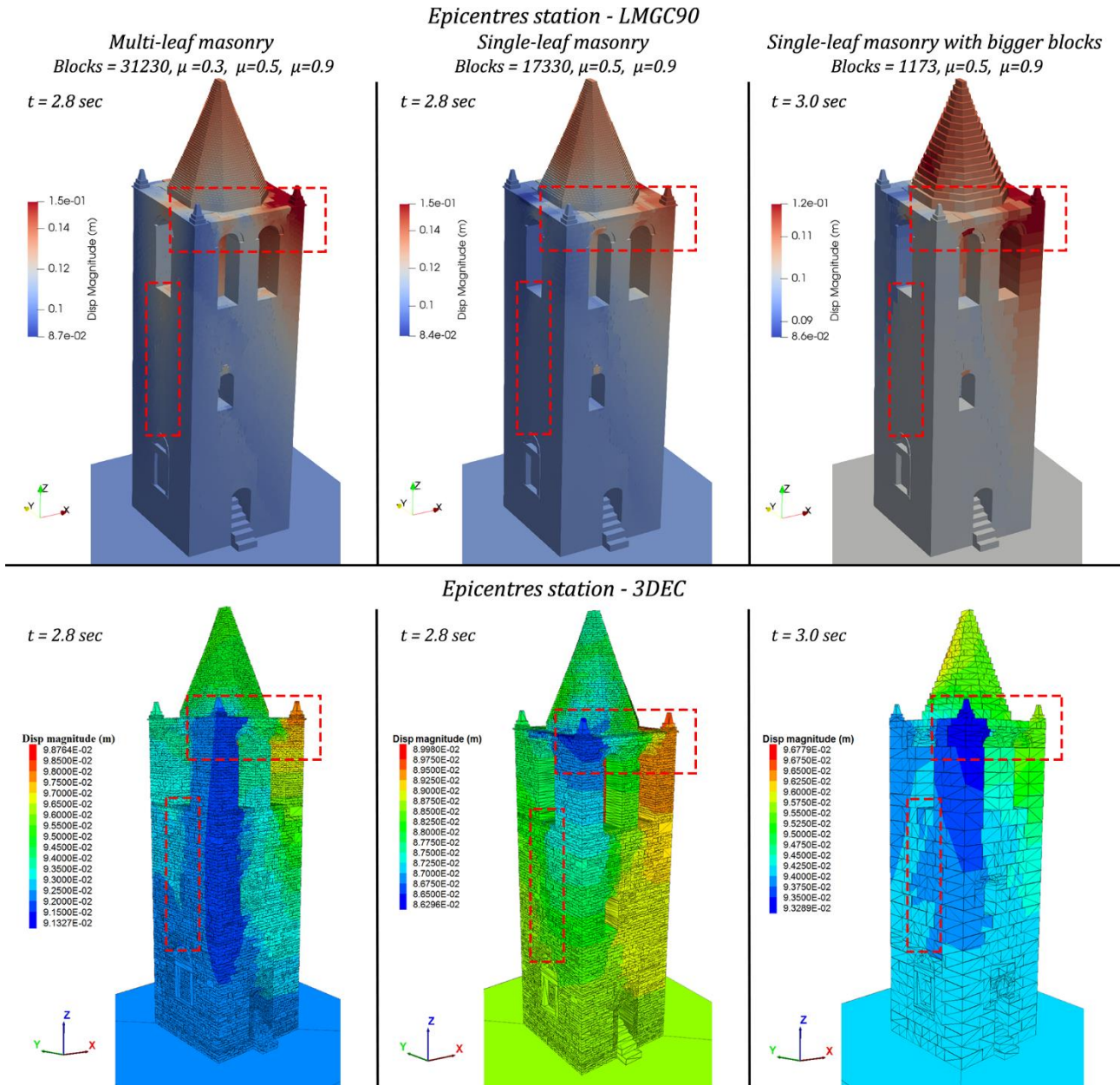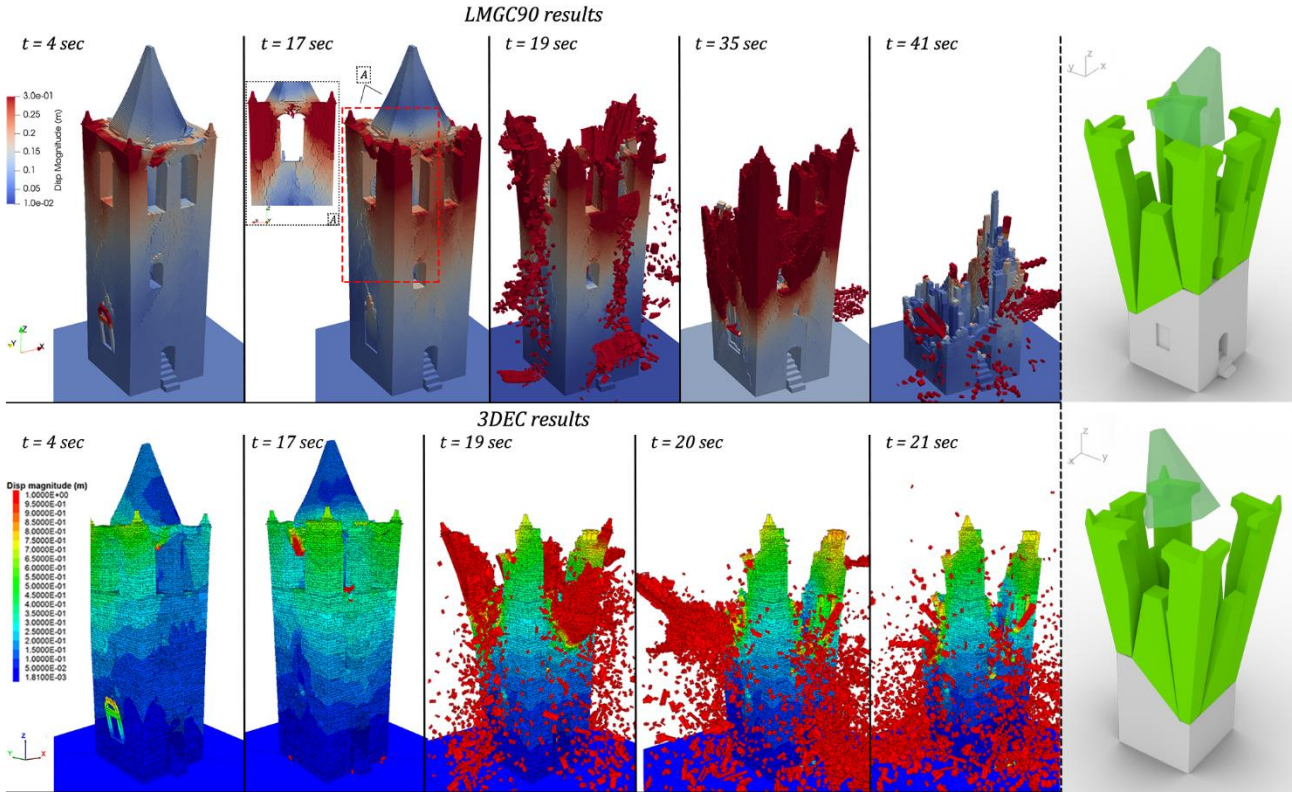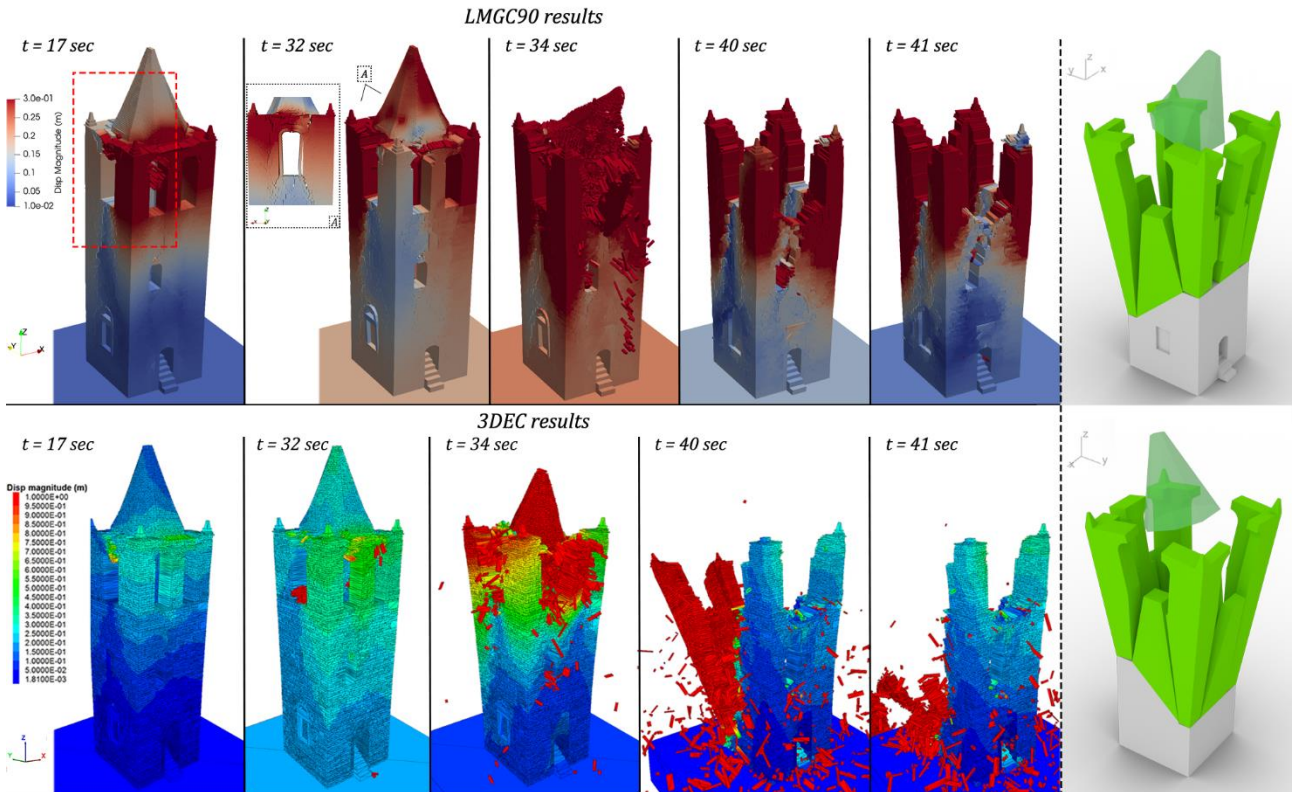*Figure 26 Numerical cumulative damages of the civic tower of Rotella (Ascoli Piceno, Italy) under the three main shocks recorded in the village during the Central Italy seismic sequence of 2016 for the three configurations of the models analysed using both the NSCD method and DEM*

The activations of damage mechanisms for model 2 and 3 are widely visible with both computational methods after the second main shock in the applied sequence. The combined presence of the opening of cylindrical hinges in the arched windows of the cell bell and the absence of confined and well-structured masonry along the vertical development of the structure, led to collapses of the tower. These failure mechanisms are characterized by the combination of diagonal cracking, rocking and vertical splitting of the walls. At the end, these behaviours are clearly visible for model 1 at 19 seconds with NSCD and DEM in Figure 28. For model 2 and 3, these activated mechanisms are respectively visible at 34 seconds and 36 seconds in Figure 29 and Figure 30.

At the end of the analyses at 41 seconds, the tower exhibits total collapses in all models and both methods (NSCD and DEM). The amplifications of the damages with the seismic actions of the epicentres in these results, compared to the analyses carried out with the recordings of the earthquakes near the location of the tower, become evident in this last step. It is important to stress the resultant cumulative damage of these analyses and to focus on this major feature, for the study of existing masonry of cultural heritage.

Figure 27 Numerical cumulative damages of the civic tower of Rotella (Ascoli Piceno, Italy) at 2.8 seconds and 3.0 seconds under the three main shocks recorded in the epicentres during the Central Italy seismic sequence of 2016 for the three configurations of the models analysed using both the NSCD method and DEM

Finally, different macro-models summarize the evolution of the failure modes of the tower in Figure 28, Figure 29 and Figure 30. The considered macro-elements are representative for this kind of isolated towers. Their main features concern the inclined crack pattern rising from the base and the vertical splitting. Furthermore, the configuration of the cell bell with arched window and the masonry weighty cover contribute to the evolution of such failure modes. Consequently, the portions of masonry involved in the activation of failure mechanisms are the same for all the models with both methods. However, the model 3 exhibits a different participation of the macro-elements over time due to the different interlocking of the masonry modelling.
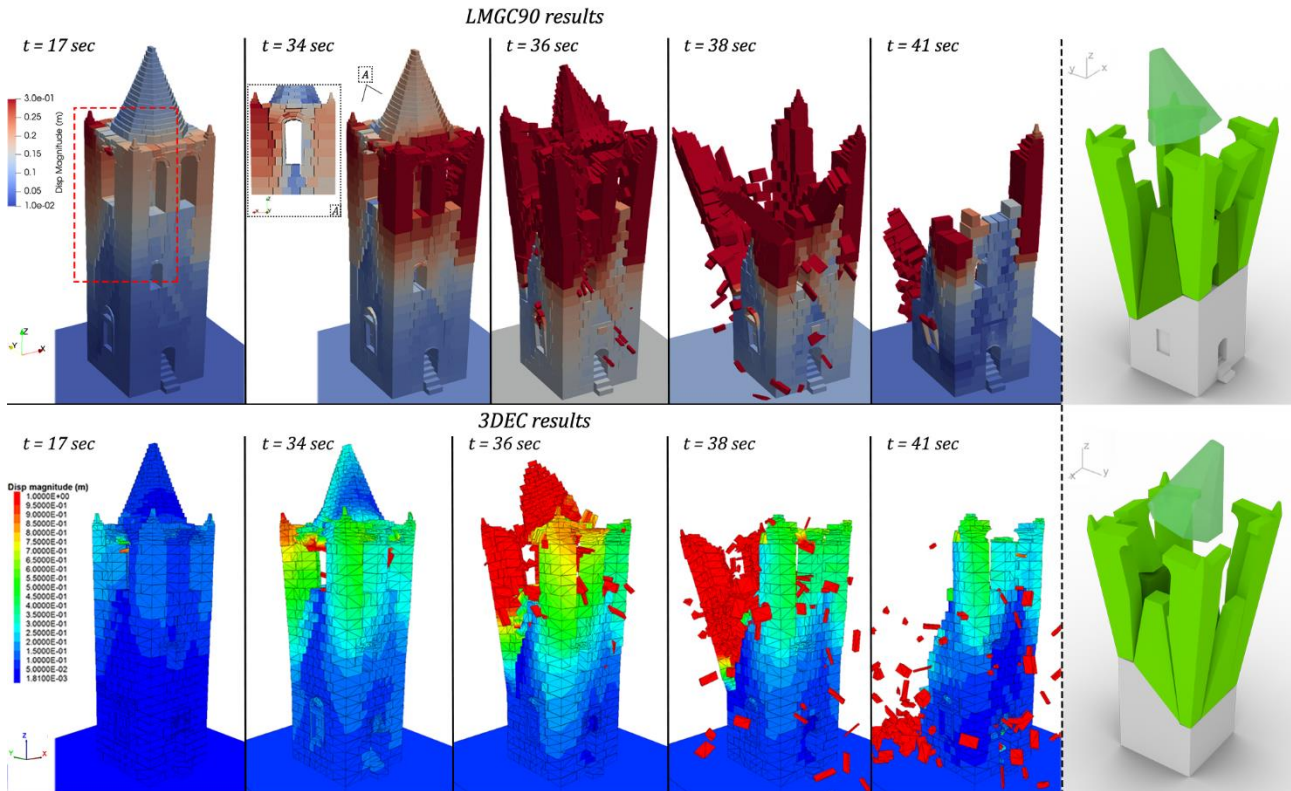
Figure 28 Numerical cumulative damages of the civic tower of Rotella (Ascoli Piceno, Italy) under the three main shocks recorded in the epicentres during the Central Italy seismic sequence of 2016 for the numerical model 1 with multi-leaf masonry analysed using both the NSCD method and DEM

Figure 29 Numerical cumulative damages of the civic tower of Rotella (Ascoli Piceno, Italy) under the three main shocks recorded in the epicentres during the Central Italy seismic sequence of 2016 for the numerical model 2 with single-leaf masonry analysed using both the NSCD method and DEM

Figure 30 Numerical cumulative damages of the civic tower of Rotella (Ascoli Piceno, Italy) under the three main shocks recorded in the epicentres during the Central Italy seismic sequence of 2016 for the numerical model 3 with single-leaf with bigger blocks masonry analysed using both the NSCD method and DEM
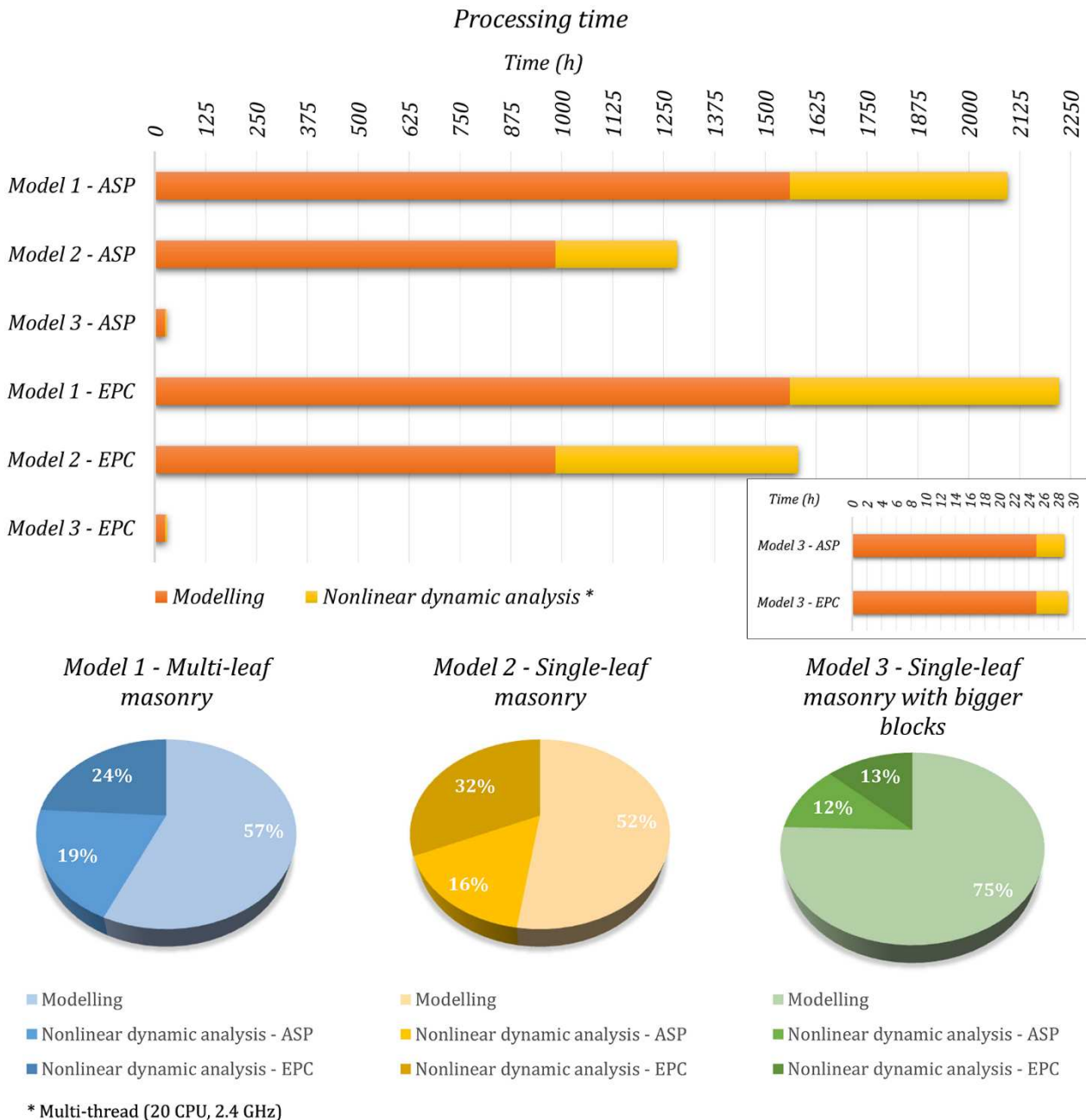
5.4   Considerations on the full processing

The evolution of the elapsed time for the whole process of modelling and computing of the nonlinear dynamic analyses of the civic tower of Rotella (Ascoli Piceno, Italy) for the three different level of details of discretization is reported in Figure 31. The time required for the modelling is an estimation of the time spent both for the design of the masonry pattern and the entire 3D structure. Obviously, for model 1 and 2 these stages are longer than for model 3 due to the detailed survey of the real masonry pattern from photographs and the largest number of blocks created.

Figure 31 Evolution of the elapsed time for the whole process of modelling and computing of the nonlinear dynamic analyses of the civic tower of Rotella (Ascoli Piceno, Italy) for the three different level of details of discretization

The computational time of the nonlinear dynamic analyses is an average of the processing time of both NSCD and DEM methods. The elapsed computational time of the analyses with widespread collapses (as for epicentres recording - EPC) is greater than the analyses with the reduced failures (as for recording near the location of the tower - ASP) because of the higher number of iterations of the solver in the codes.

The major elapsed time regards the analysis with the multi-leaf masonry model and real earthquakes epicentres (Model 1 – EPC), which is estimated equal to ~2222 hours. Instead, the model with the single-leaf masonry and larger blocks and earthquakes near the location of the tower (Model 3 – ASP) has a significantly lower processing time, which is estimated to ~30 hours.

Thus, the data plotted in Figure 31 allow to understand the impact of the different level of discretization in the whole processing time of the analysis. For the vulnerability assessment of existing masonry structures, these typologies of modelling must be selected carefully in view of both the accuracy of numerical results and the large processing time.

6 Conclusions

The numerical assessment of the civic clock tower of Rotella (Ascoli Piceno, Italy) is investigated by means of both NSCD and DEM methods. The development and the theory of these methods are examined in several studies in literature. The applications of both methods in other comparison studies regard the granular materials. The progress of computer science allowed the applications on large-scale structures. Thus, this work proposes the comparison of the non-smooth and smooth approaches for the investigation of large-scale historical masonry. They proved to be meaningful tools for the evaluation of the masonry vulnerabilities, despite their huge processing time. The possibility to consider large displacements and rotations of the bricks including complete detachment is a remarkable capability for these methods. On the other hand, the limitation of suitable packages for modelling increase the time to prepare the 3D structures in both methods. Furthermore, the comparison of the results from the two methods introduces similar failure mechanisms, typical for this kind of structure, and final collapses. An important difference of the results between the non-smooth and smooth methods is related to the presence of relevant bounces in DEM and the inelastic collisions in NSCD without bounces. Another difference in the numerical results is due to the effect of cohesion, which is taken into account in DEM and shows lower shifts compared to NSCD in which there is no cohesion. In addition, the explicit solution procedure in DEM is conditionally stable.

However, although the area of application of these discrete approaches appears theoretically large, their high computational requirement currently limits their employment to very relevant case studies and research works. Nevertheless, every masonry element is described in detail: blocks, mortar and interfaces. Thus, they could be implemented to gain in-depth insights on specific issues of the mechanics of masonry structures for very accurate response, and to provide reference solutions for more simplified approaches.

The numerical results underline that the modelling of the masonry influences the numerical results and the comparison with the existing structural damages caused by the seismic sequence that took place in Central Italy in 2016. In particular, the three different levels of detail for the discretization of the masonry provide deeper insight into the dynamical behaviour of the structure. Obviously, the analyses characterized by the model with the multi-leaf masonry led to detailed crack patterns and collapse mechanisms closer to reality. The two different single-leaf masonry models prove to be useful to predict the possible failure mechanisms of the structure with less details on the damages. Nonetheless, the simpler model with bigger blocks introduces correct damage mechanisms and faster analyses than the other ones.

Moreover, these results are relevant to ancient masonry investigation and future retrofitting works. The knowledge of the crack pattern is mandatory for the strengthening intervention, in particular when analyses with pre-assigned failure mechanisms are used. In fact, as demonstrated, the incidence of the z-component of the seismic input proved to be important. Lastly, the more complex and detailed model is the most appropriate for an accurate

prediction of future possible collapses mechanisms or to reconstruct existing damages. The simplest model is advised for faster results but at the cost of accuracy.

In conclusion, the main issue of the investigation of cumulative damage is well-developed in the nonlinear dynamic analyses of the tower. The numerical results prove the relevance of the use of main earthquakes in sequence for the vulnerability assessment of the existing structures. This strategy permits to recreate the real stress conditions of the cultural heritage in the seismic areas and offers an insight into the reduction of seismic resistance capacity of the masonry over time due to several sequences of earthquakes through the years.

A future research stream -which deserves dedicated analyses but is out-of-the scopes of the present paper- will be an extensive numerical investigation on the influence of the soil structure interaction at specific site conditions, which accounts also for a detailed determination of the soil mechanical properties, according to the approach proposed in [26], where however the masonry tower considered is roughly discretized and more emphasis is given to the soil modeling.

References

[1]   Roca P, Cervera M, Gariup G, Pela' L. Structural Analysis of Masonry Historical Constructions. Classical and Advanced Approaches. Arch Comput Methods Eng 2010;17:299–325. https://doi.org/10.1007/s11831-010-9046-1.

[2]   Brandonisio G, Lucibello G, Mele E, Luca A De. Damage and performance evaluation of masonry churches in the 2009 L'Aquila earthquake. Eng Fail Anal 2013;34:693–714. https://doi.org/10.1016/j.engfailanal.2013.01.021.

[3]   Hofer L, Zampieri P, Zanini MA, Faleschini F, Pellegrino C. Seismic damage survey and empirical fragility curves for churches after the August 24, 2016 Central Italy earthquake. Soil Dyn Earthq Eng 2018;111:98–109. https://doi.org/10.1016/j.soildyn.2018.02.013.

[4]   Sarhosis V, Milani G, Formisano A, Fabbrocino F. Evaluation of different approaches for the estimation of the seismic vulnerability of masonry towers. Bull Earthq Eng 2018;16:1511–45. https://doi.org/10.1007/s10518-017-0258-8.

[5]   Giordano A, Mele E, De Luca A. Modelling of historical masonry structures: comparison of different approaches through a case study. Eng Struct 2002;24:1057–69. https://doi.org/10.1016/S0141-0296(02)00033-0.

[6]   Roca P, Cervera M, Pelà L, Clemente R, Chiumenti M. Continuum FE models for the analysis of Mallorca Cathedral. Eng Struct 2013;46:653–70. https://doi.org/10.1016/j.engstruct.2012.08.005.

[7]   Betti M, Borghini A, Boschi S, Ciavattone A, Vignoli A. Comparative Seismic Risk Assessment of Basilica-type Churches. J Earthq Eng 2018;22:62–95. https://doi.org/10.1080/13632469.2017.1309602.

[8]   Rafiee A, Vinches M. Mechanical behaviour of a stone masonry bridge assessed using an implicit discrete element method. Eng Struct 2013;48:739–49. https://doi.org/10.1016/j.engstruct.2012.11.035.

[9]   Beatini V, Royer-Carfagni G, Tasora A. A non-smooth-contact-dynamics analysis of Brunelleschi's cupola: an octagonal vault or a circular dome? Meccanica 2019;54:525–47. https://doi.org/10.1007/s11012-018-00934-9.

[10]   Pulatsu B, Erdogmus E, Lourenço PB. Comparison of in-plane and out-of-plane failure modes of

masonry arch bridges using discontinuum analysis. Eng Struct 2019;178:24–36. https://doi.org/10.1016/j.engstruct.2018.10.016.

[11] Clementi F, Ferrante A, Giordano E, Dubois F, Lenci S. Damage assessment of ancient masonry churches stroked by the Central Italy earthquakes of 2016 by the non-smooth contact dynamics method. Bull Earthq Eng 2020;18. https://doi.org/10.1007/s10518-019-00613-4.

[12] Dubois F, Acary V, Jean M. The Contact Dynamics method: A nonsmooth story. Comptes Rendus Mécanique 2018;346:247–62. https://doi.org/10.1016/j.crme.2017.12.009.

[13] Chetouane B, Dubois F, Vinches M, Bohatier C. NSCD discrete element method for modelling masonry structures. Int J Numer Methods Eng 2005;64:65–94. https://doi.org/10.1002/nme.1358.

[14] Itasca Consulting Group Inc. 3DEC- 3D Distinct Element Code, Version 5.0, User's Manual. 2013. https://doi.org/10.1017/CBO9781107415324.004.

[15] Pulatsu B, Bretas EM, Lourenco PB. Discrete element modeling of masonry structures: Validation and application. Earthquakes Struct 2016;11:563–82. https://doi.org/10.12989/eas.2016.11.4.563.

[16] Cundall PA. A computer model for simulating progressive large-scale movements in blocky rock systems. Proocedings Symp. Int. Soc. Rock Mech. Nancy 2, 1971.

[17] Moreau JJ. Unilateral Contact and Dry Friction in Finite Freedom Dynamics. Nonsmooth Mech. Appl., Vienna: Springer Vienna; 1988, p. 1–82. https://doi.org/10.1007/978-3-7091-2624-0_1.

[18] Jean M. The non-smooth contact dynamics method. Comput Methods Appl Mech Eng 1999;177:235–57. https://doi.org/10.1016/S0045-7825(98)00383-1.

[19] Cundall PA, Strack ODL. A discrete numerical model for granular assemblies. Geotechnique 1979;29:47–65. https://doi.org/10.1680/geot.1979.29.1.47.

[20] CUNDALL, A. P. Distinct element models of rock and soil structure. Anal Comput Methods Eng Rock Mech 1987:129–63.

[21] Lemos J V. Discrete element modeling of masonry structures. Int J Archit Herit 2007. https://doi.org/10.1080/15583050601176868.

[22] Ministero delle infrastrutture e dei trasporti. Circolare 21 gennaio 2019 n. 7 C.S.LL.PP. Istruzioni per l'applicazione dell'aggiornamento delle "Norme Tecniche per le Costruzioni" di cui al D.M. 17/01/2018 (in Italian). Suppl Ord Alla GU n 35 Del 11/2/19 2019.

[23] Vasconcelos G, Lourenço PB. Experimental characterization of stone masonry in shear and compression. Constr Build Mater 2009;23:3337–45. https://doi.org/10.1016/j.conbuildmat.2009.06.045.

[24] Clementi F, Ferrante A, Ribilotta E, Milani G, Lenci S. On the dynamics of the civic clock tower of Rotella (Ascoli Piceno) severly damaged by the Central Italy seismic sequence of 2016. Atti del XVIII Convegno ANIDIS L'ingegneria Sismica Ital. Ascoli Piceno, 15-19 settembre 2019, Pisa: Pisa University Press; 2019. https://doi.org/10.1400/271235.

[25] Lourenco PB. Computational strategies for masonry structures. 1996. https://doi.org/ISBN 90-407-1221-2.

[26] de Silva F. Influence of soil-structure interaction on the site-specific seismic demand to masonry towers. Soil Dyn Earthq Eng 2020;131:106023. https://doi.org/https://doi.org/10.1016/j.soildyn.2019.106023.

[27] Pluijm, van der R. Material properties of masonry and its components under tension and shear. Proc. 6th Can. Mason. Symp. 15-17 June 1992, Saskatoon, Canada, University of Saskatchewan;

1992, p. 675–86.

[28]   Luzi L, Pacor F, Puglia R. Italian Accelerometric Archive v 2.3. Rome: 2017.
       https://doi.org/10.13127/ITACA.2.3.

[29]   Luzi L, Hailemikael S, Bindi D, Pacor F, Mele F, Sabetta F. ITACA (ITalian ACcelerometric Archive): A
       Web Portal for the Dissemination of Italian Strong-motion Data. Seismol Res Lett 2008;79:716–22.
       https://doi.org/10.1785/gssrl.79.5.716.

[30]   Pacor F, Paolucci R, Luzi L, Sabetta F, Spinelli A, Gorini A, et al. Overview of the Italian strong motion
       database ITACA 1.0. Bull Earthq Eng 2011;9:1723–39. https://doi.org/10.1007/s10518-011-9327-6.

7 Appendix 1

In the present Appendix 1 the results of the application of repeated accelerograms are reported as a function of the friction coefficient assumed between foundation and superstructure. In particular, from Figure 32 to Figure 36 the displacement histories for the five control nodes investigated are represented assuming as accelerogram that registered in the Ascoli Piceno station, whereas from Figure 37 to Figure 41 the same results are depicted assuming as accelerogram that of the epicenters of the different earthquakes (24/08/2016 yellow band, 26/10/2016 green band, 30/10/2016 light blue band). As it can be observed, the behavior is quite uninfluenced by the interaction, albeit simplified between the tower and the soil. A future research stream -which deserves dedicated analyses and is certainly out-of-the scopes of the present paper- will be an extensive numerical simulation campaign in order to have a deep insight into the role played by the interaction between the soil -with its own properties- and the superstructure, as reported in a very detailed manner by De Silva in [26], where the focus is given more to the soil rather than the masonry tower, which is modeled as a regular homogeneous structure with a low detail level. As a matter of fact, this is a very intriguing but challenging issue to investigate, belonging however to the soil dynamics research field. It is also worth noting that, at present, the codes here used for the NLDAs do not allow the user to properly model the soil by means of infinite elastic boundaries, still not available for DEM approaches. At this stage, it would be therefore impossible to establish a correct volume of soil with sound mechanical properties that should be modelled under the tower, even in the simplest case of a soil with elastic behaviour. In addition, the research carried out was based on the assumption of rigid blocks (even if there is in both codes the possibility to add their elastic deformability); as a consequence, the natural period of the tower in the modelling approach is equal to zero in LMGC90 and quite stiff for 3DEC, a feature that does not allow to consider the deformability of the soil as a meaningful parameter for the output results.
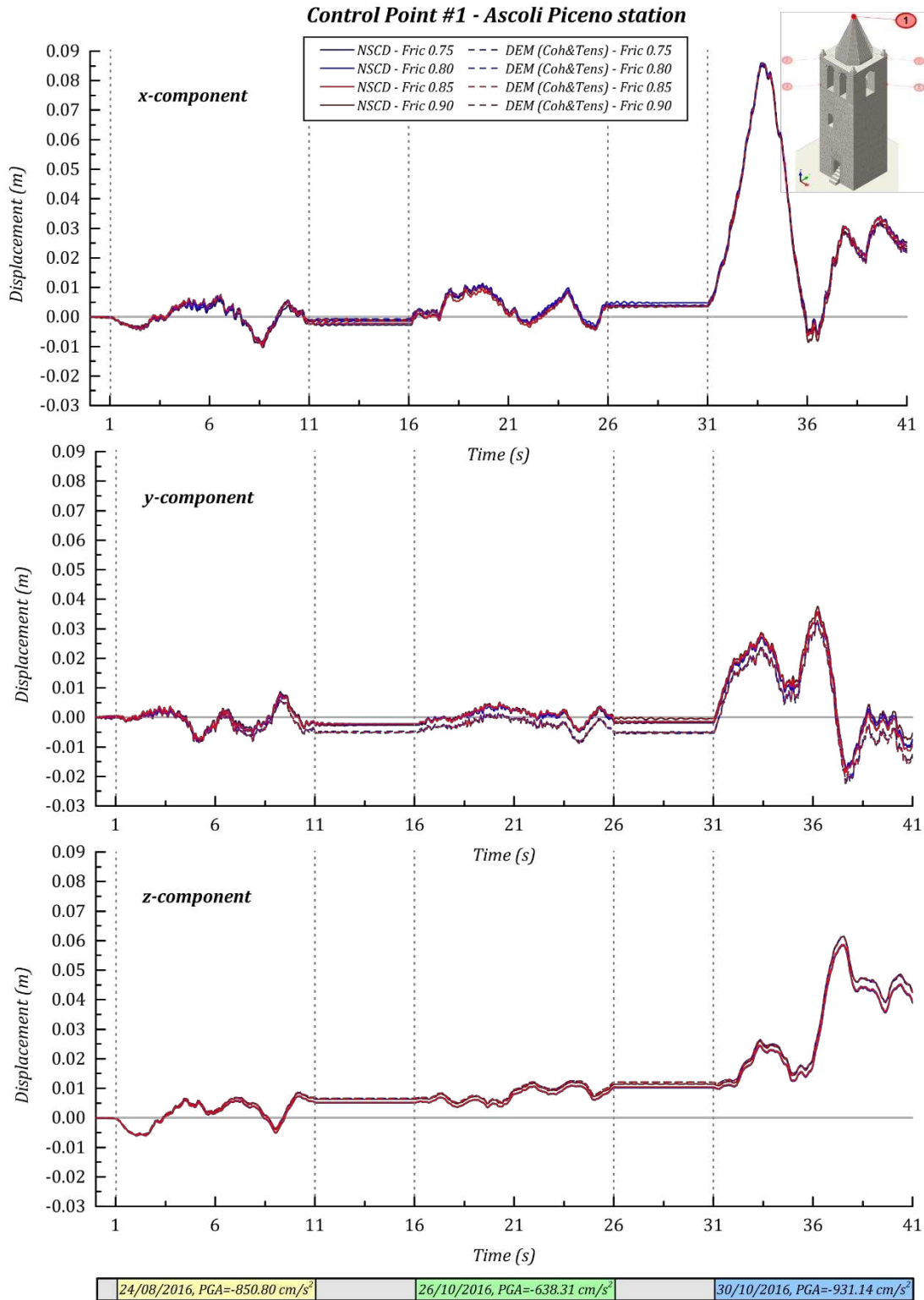
Figure 32 Displacements time histories of the control point #1 of the civic tower of Rotella (Ascoli Piceno, Italy) under the three main shocks recorded in Ascoli Piceno during the Central Italy seismic sequence of 2016 for the 4 friction coefficients assumed at the interface between superstructure and foundation. Ascoli Piceno station.
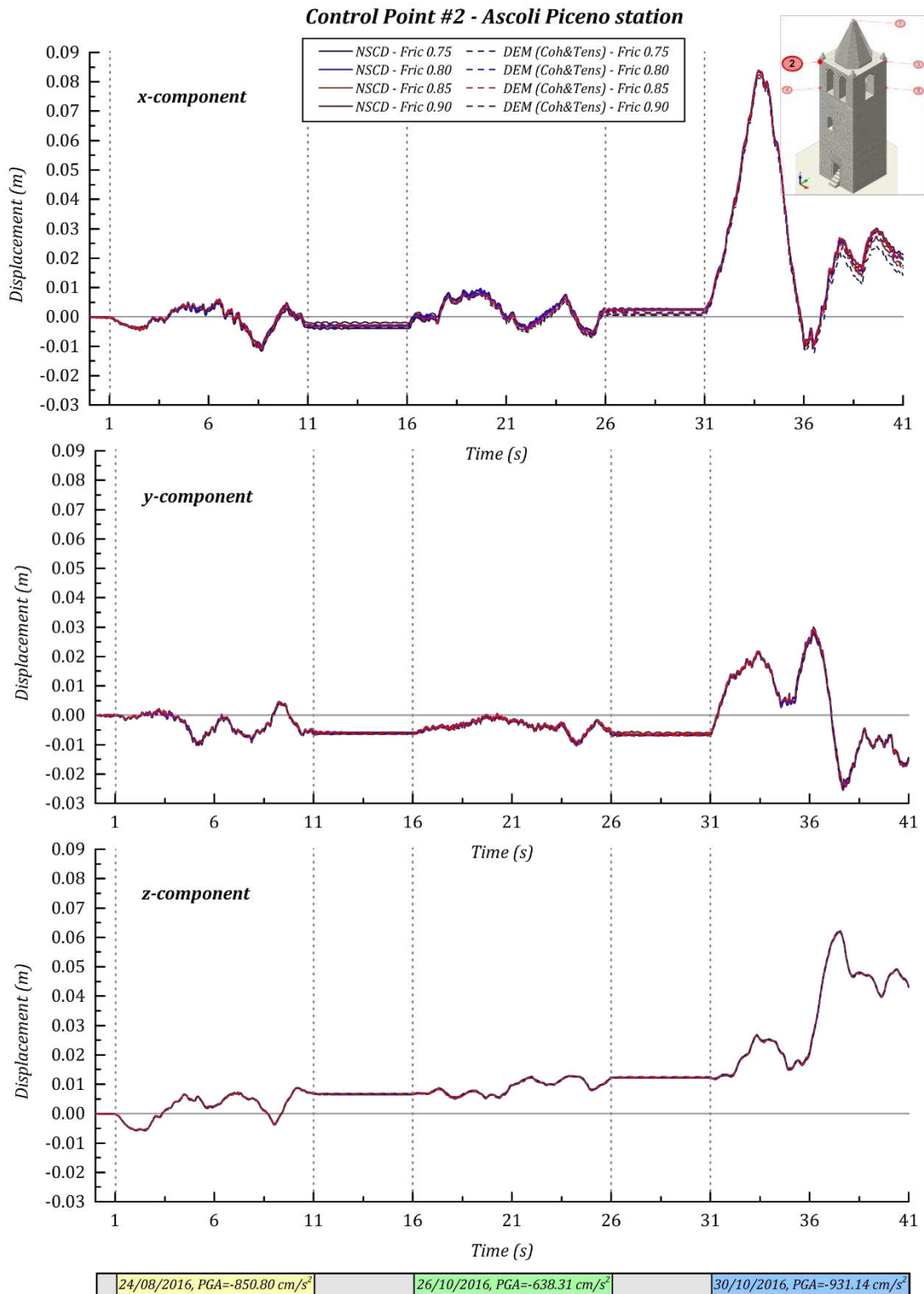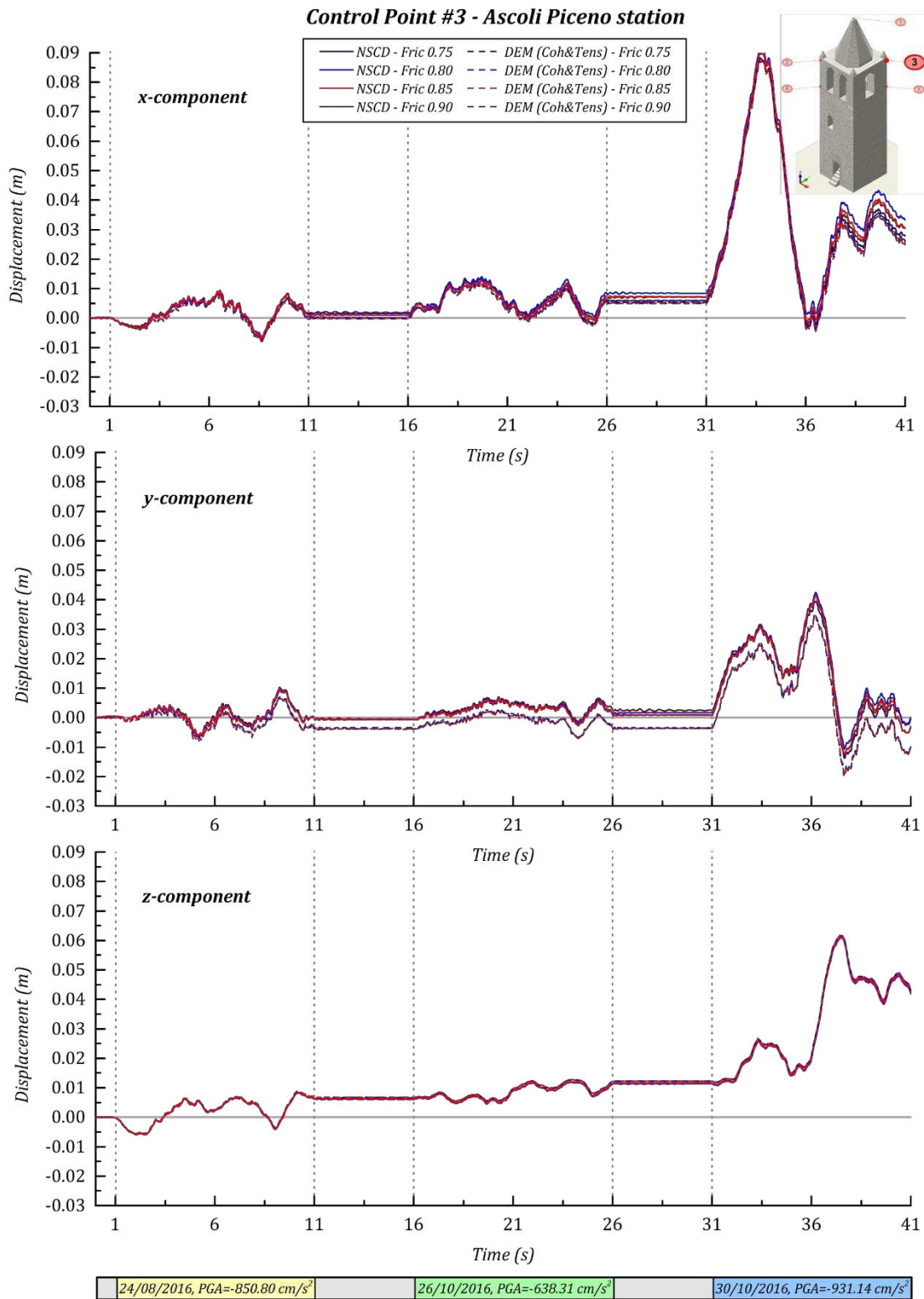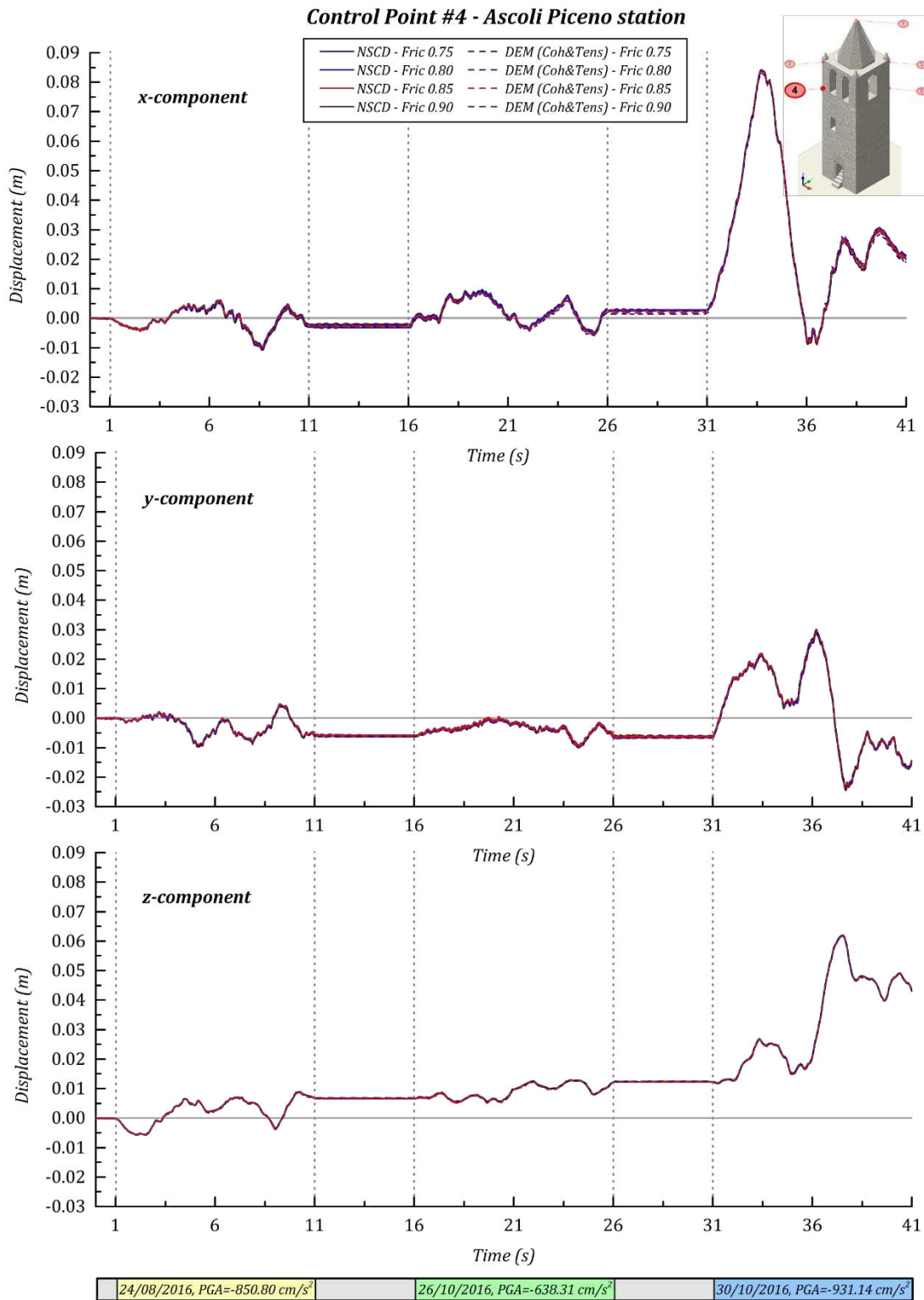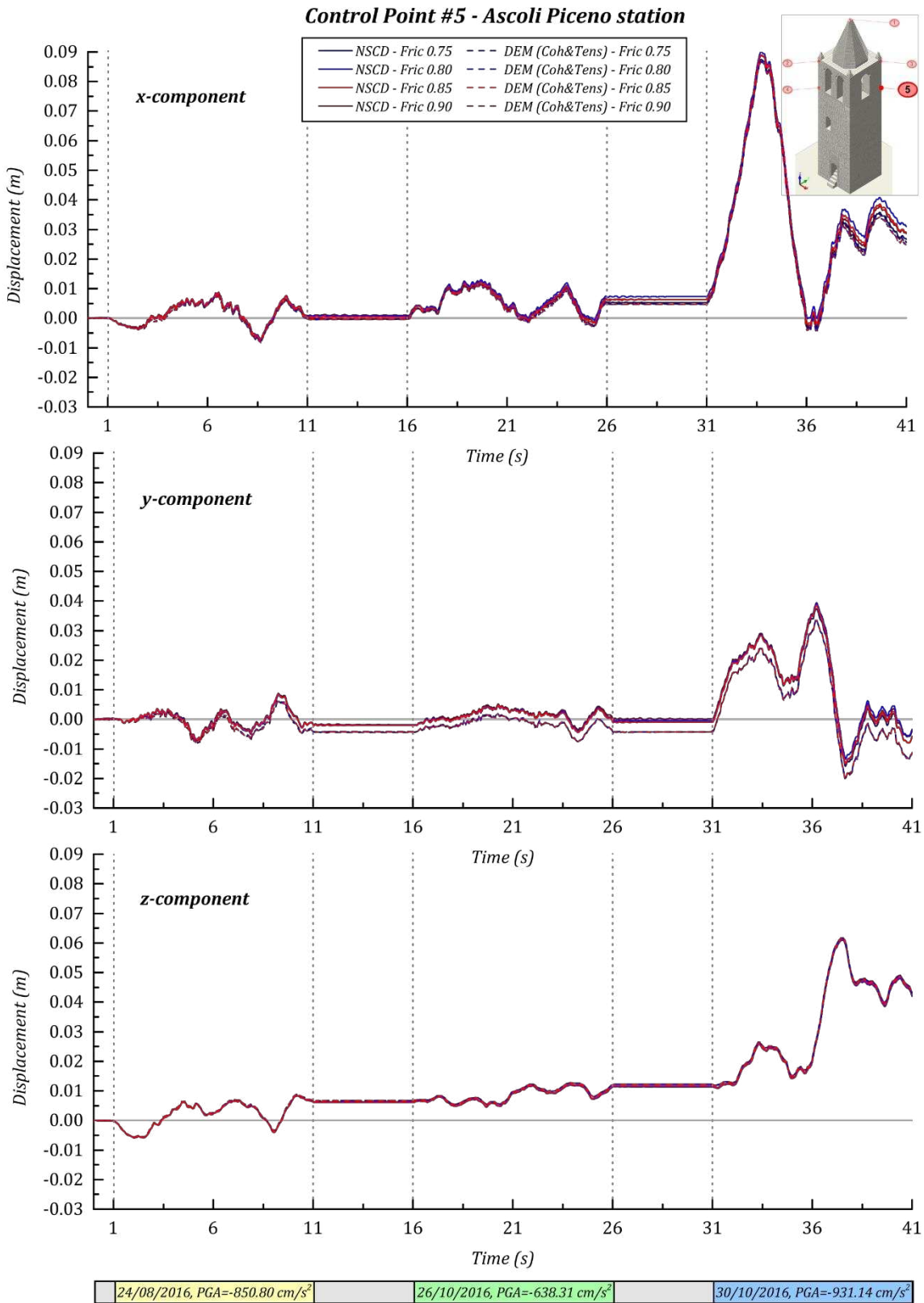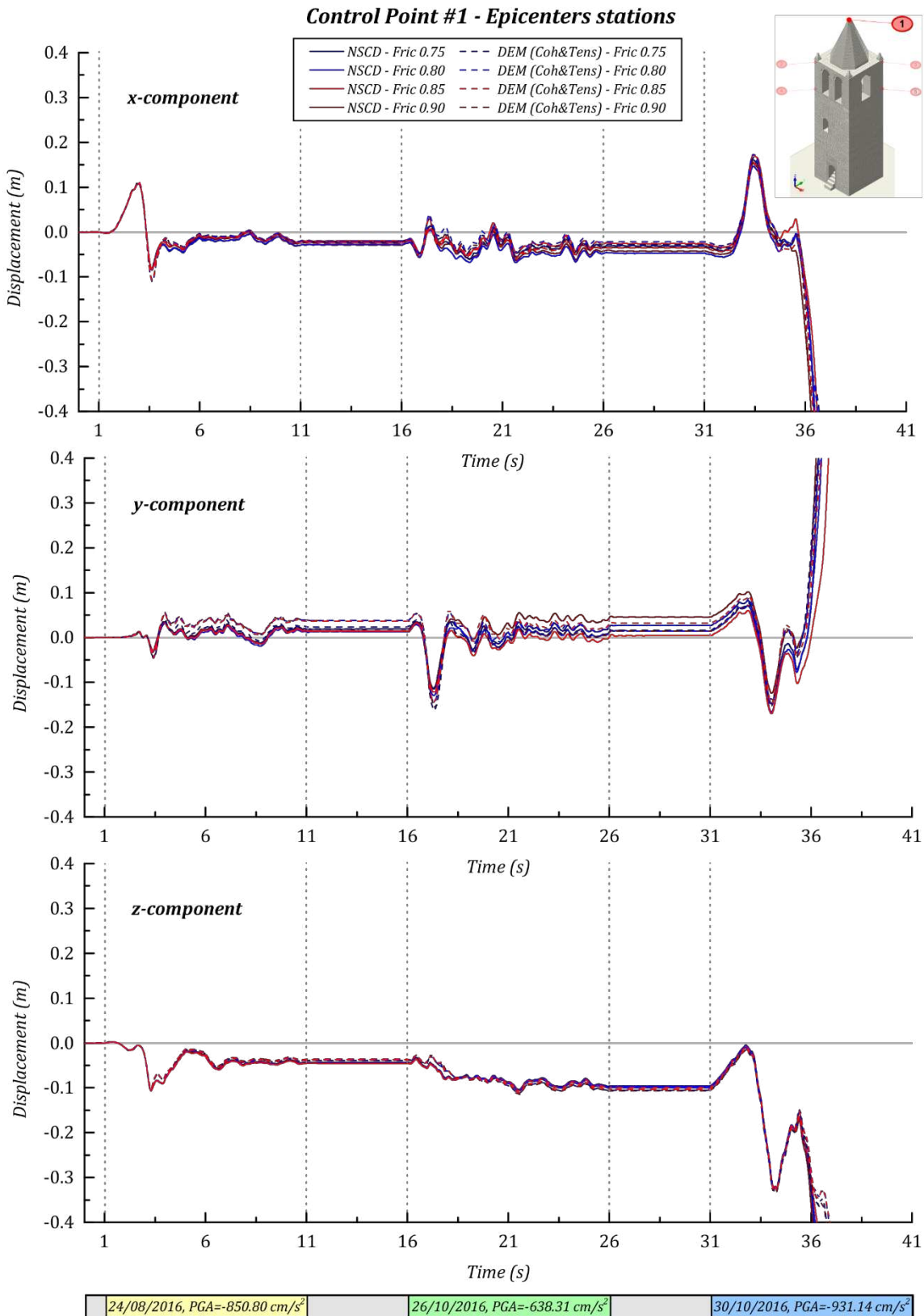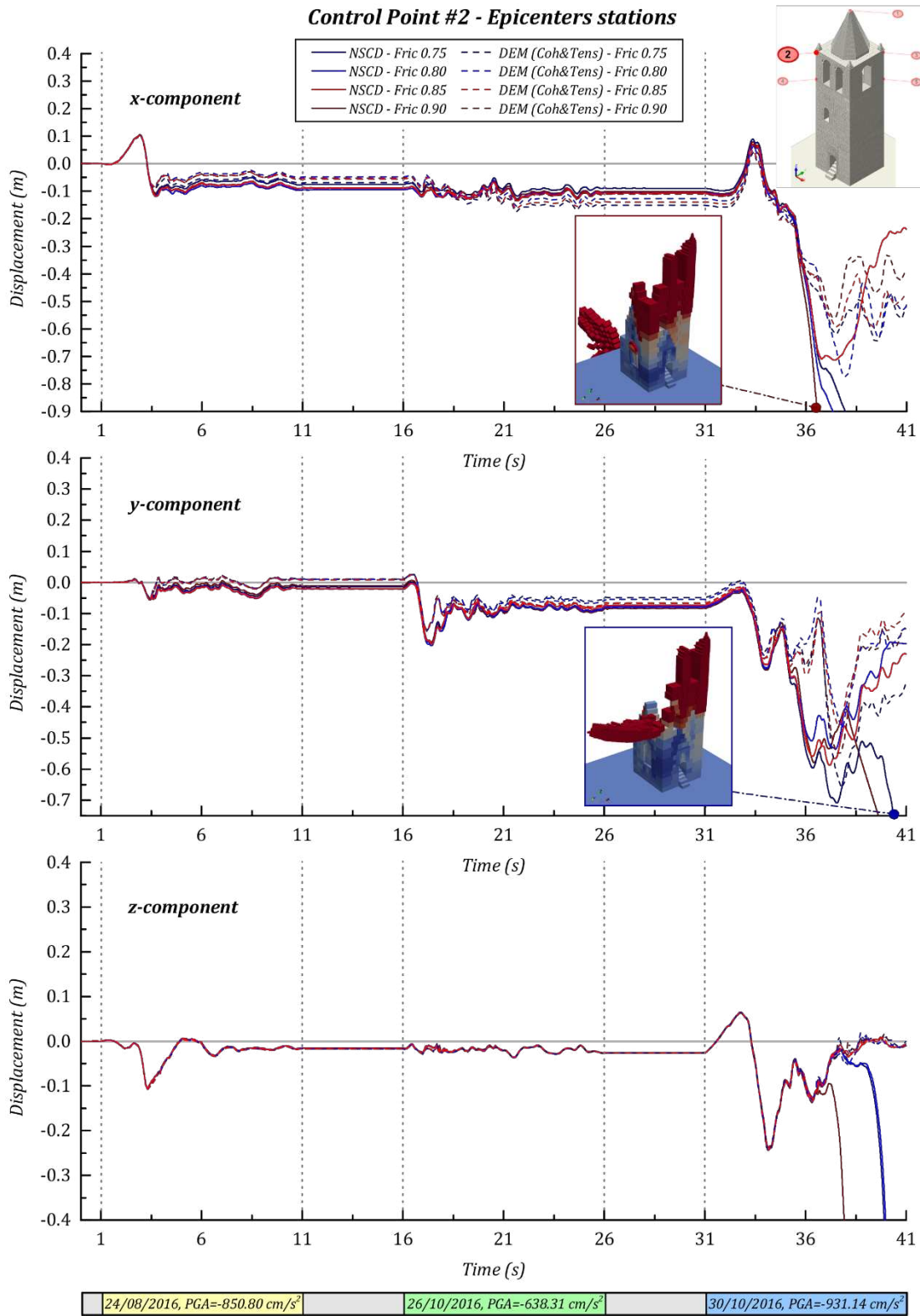
Figure 33 Displacements time histories of the control point #2 of the civic tower of Rotella (Ascoli Piceno, Italy) under the three main shocks recorded in Ascoli Piceno during the Central Italy seismic sequence of 2016 for the 4 friction coefficients assumed at the interface between superstructure and foundation. Ascoli Piceno station.
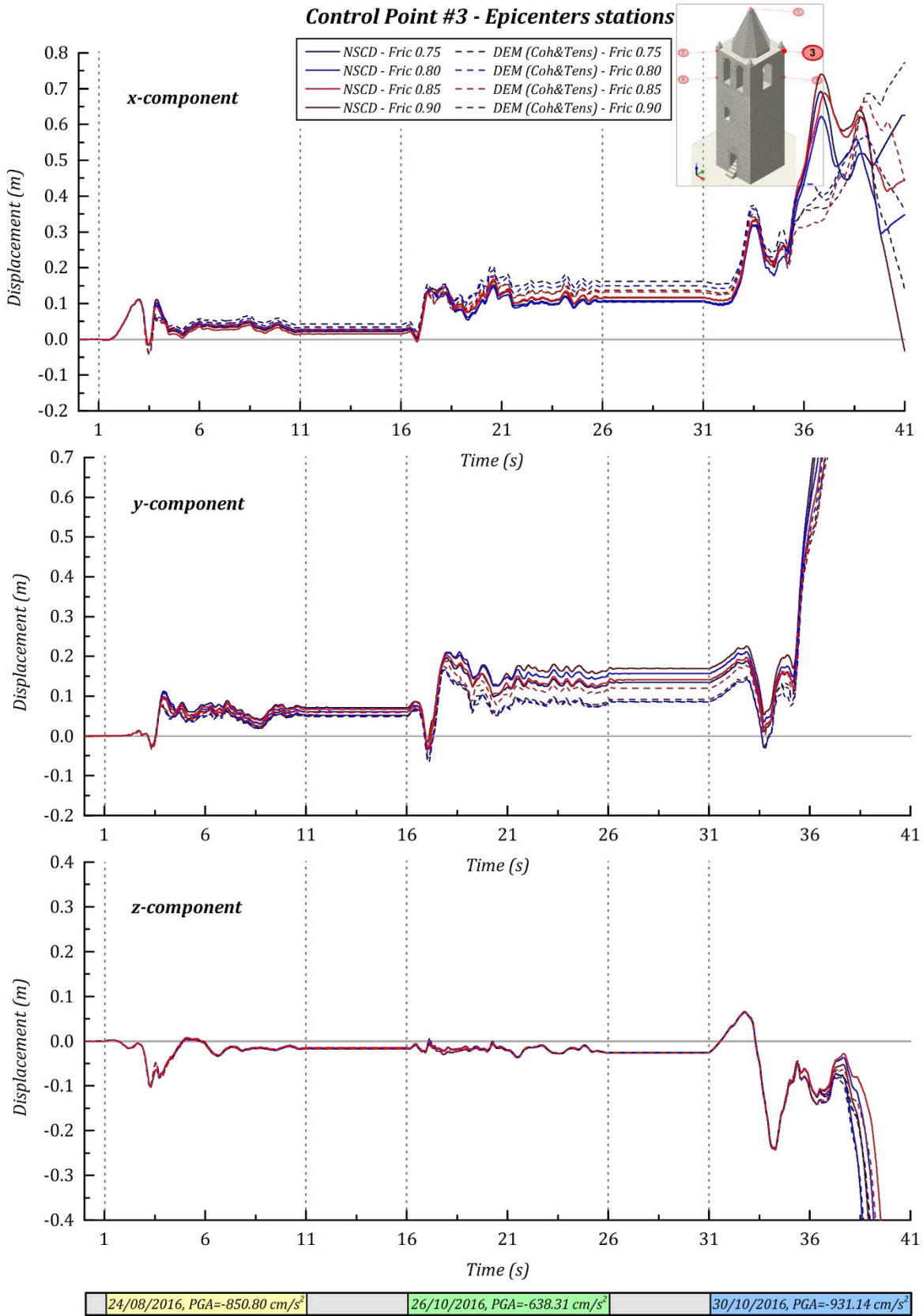
Figure 34 Displacements time histories of the control point #3 of the civic tower of Rotella (Ascoli Piceno, Italy) under the three main shocks recorded in Ascoli Piceno during the Central Italy seismic sequence of 2016 for the 4 friction coefficients assumed at the interface between superstructure and foundation. Ascoli Piceno station.

Figure 35 Displacements time histories of the control point #4 of the civic tower of Rotella (Ascoli Piceno, Italy) under the three main shocks recorded in Ascoli Piceno during the Central Italy seismic sequence of 2016 for the 4 friction coefficients assumed at the interface between superstructure and foundation. Ascoli Piceno station.
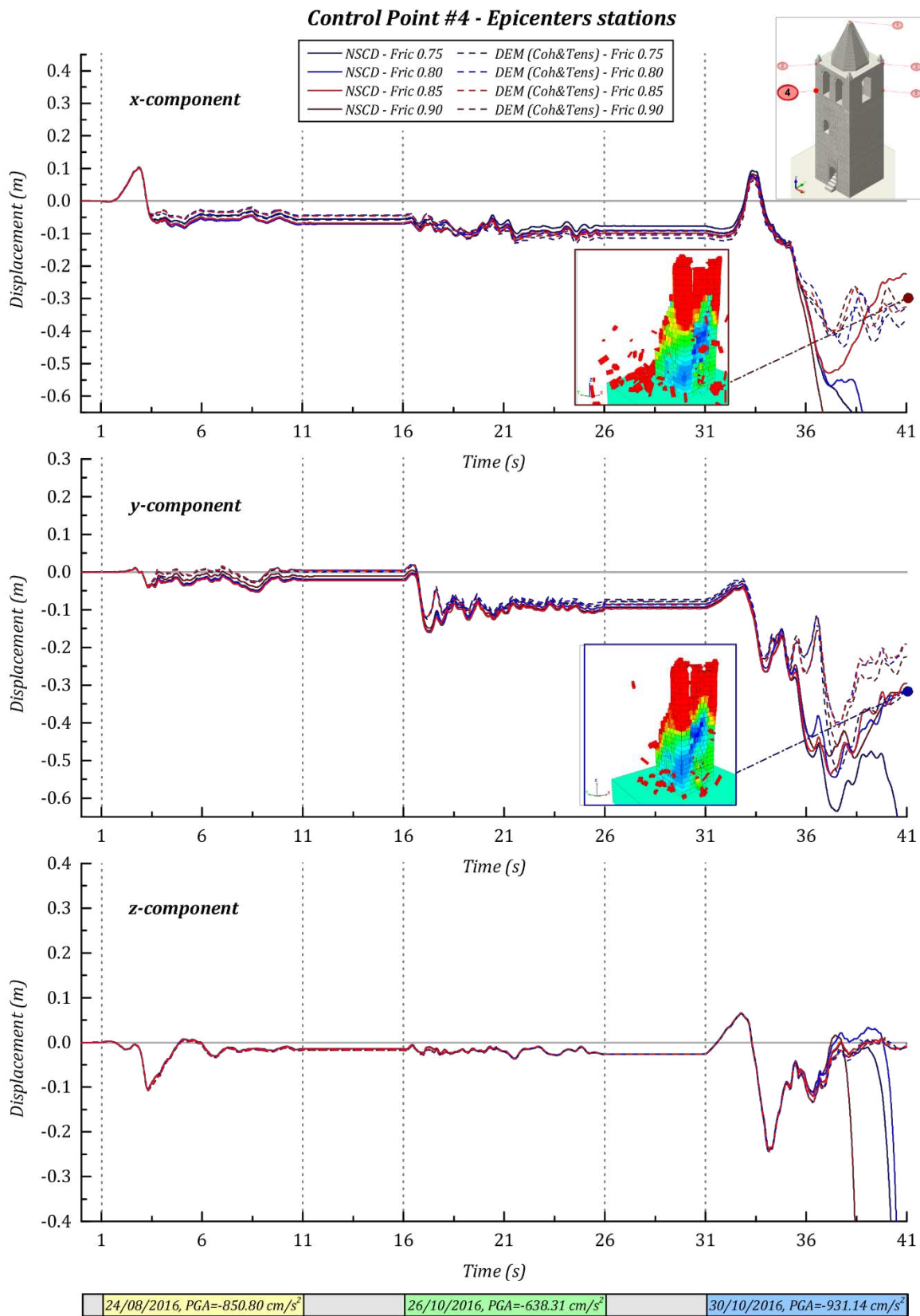
Figure 36 Displacements time histories of the control point #5 of the civic tower of Rotella (Ascoli Piceno, Italy) under the three main shocks recorded in Ascoli Piceno during the Central Italy seismic sequence of 2016 for the 4 friction coefficients assumed at the interface between superstructure and foundation. Ascoli Piceno station.

Figure 37 Displacements time histories of the control point #1 of the civic tower of Rotella (Ascoli Piceno, Italy) under the three main shocks recorded in the epicentres during the Central Italy seismic sequence of 2016 for the 4 friction coefficients assumed at the interface between superstructure and foundation.
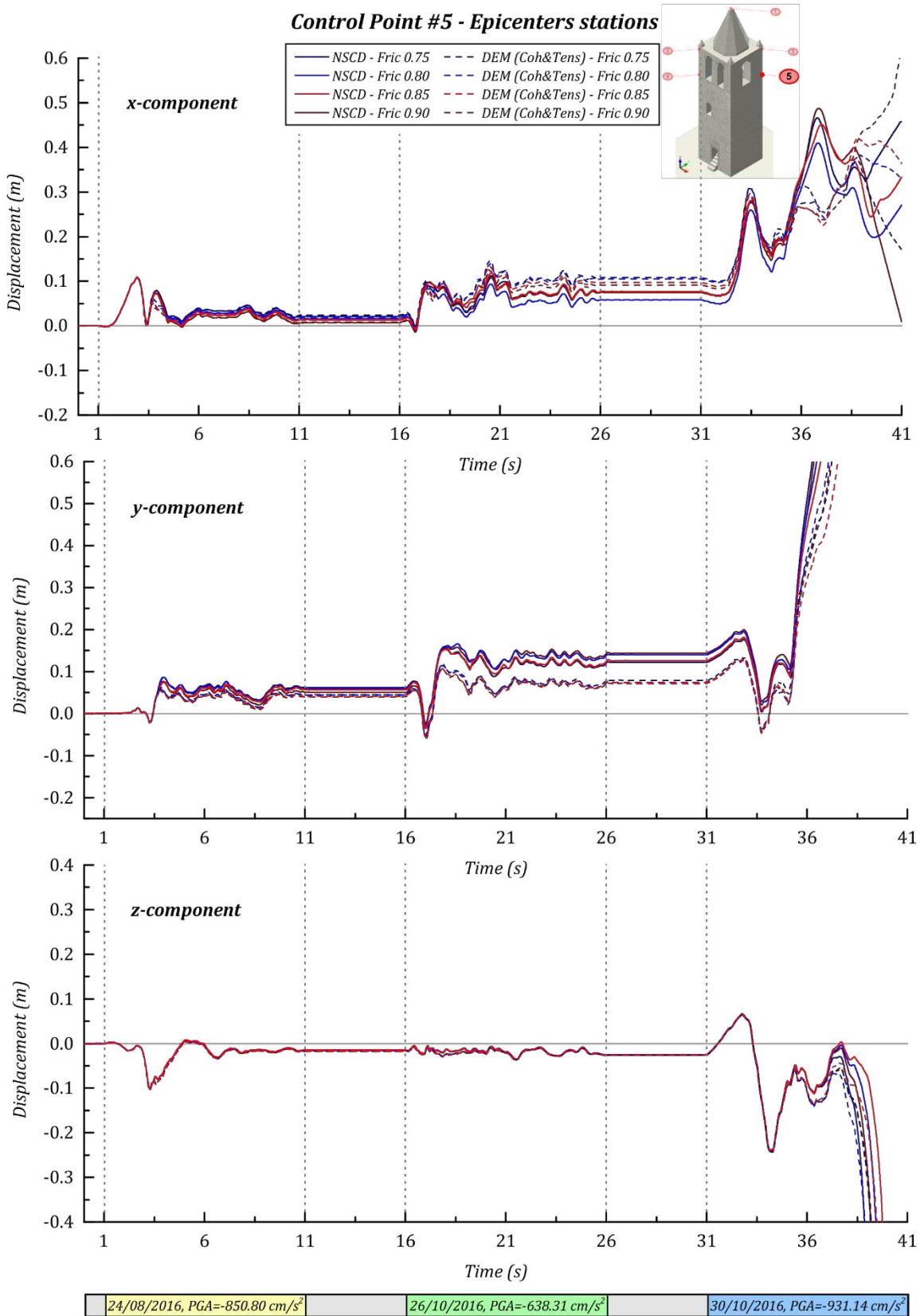
Figure 38 Displacements time histories of the control point #2 of the civic tower of Rotella (Ascoli Piceno, Italy) under the three main shocks recorded in the epicentres during the Central Italy seismic sequence of 2016 for the 4 friction coefficients assumed at the interface between superstructure and foundation.

Figure 39 Displacements time histories of the control point #3 of the civic tower of Rotella (Ascoli Piceno, Italy) under the three main shocks recorded in the epicentres during the Central Italy seismic sequence of 2016 for the 4 friction coefficients assumed at the interface between superstructure and foundation.

Figure 40 Displacements time histories of the control point #4 of the civic tower of Rotella (Ascoli Piceno, Italy) under the three main shocks recorded in the epicentres during the Central Italy seismic sequence of 2016 for the 4 friction coefficients assumed at the interface between superstructure and foundation.
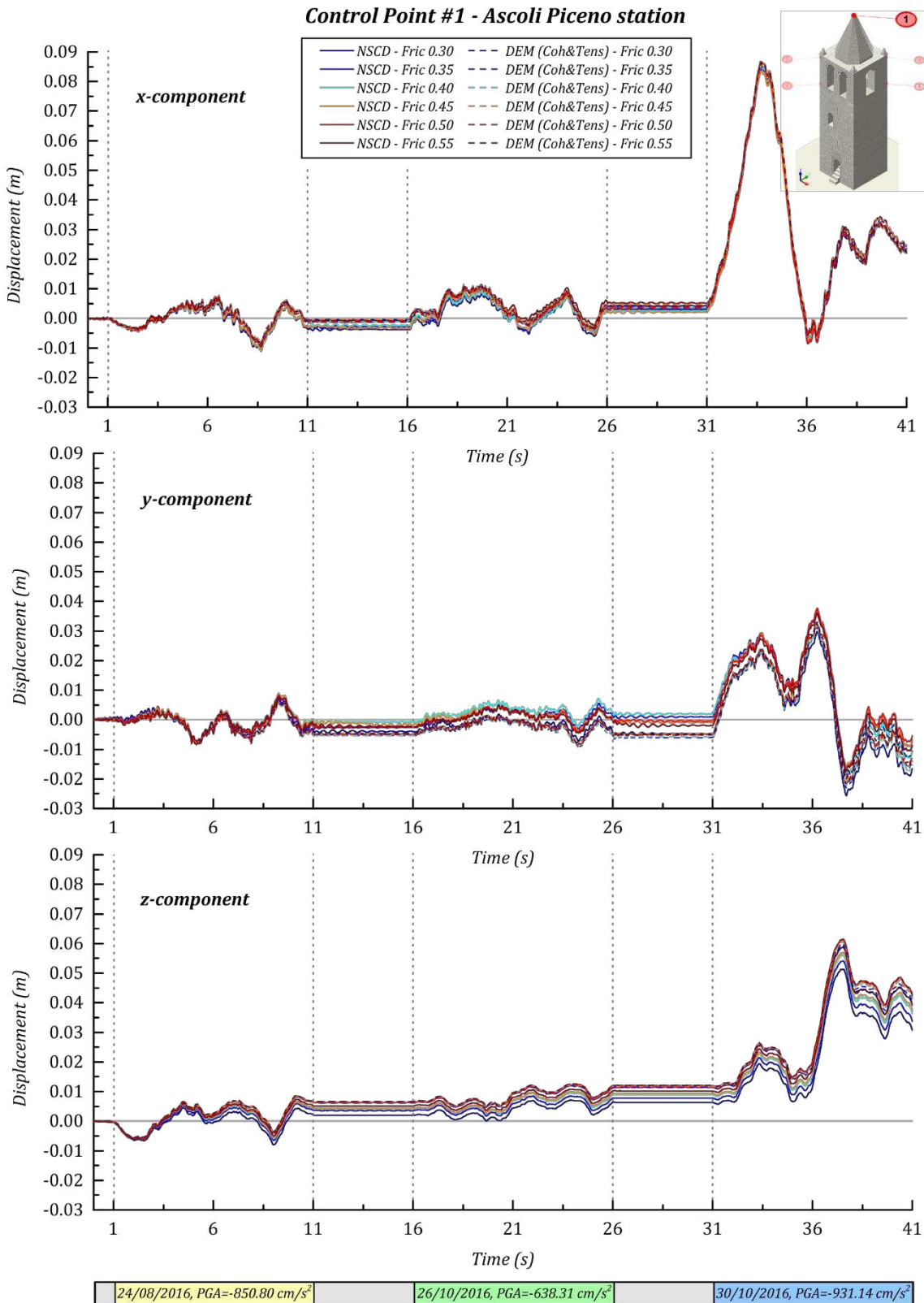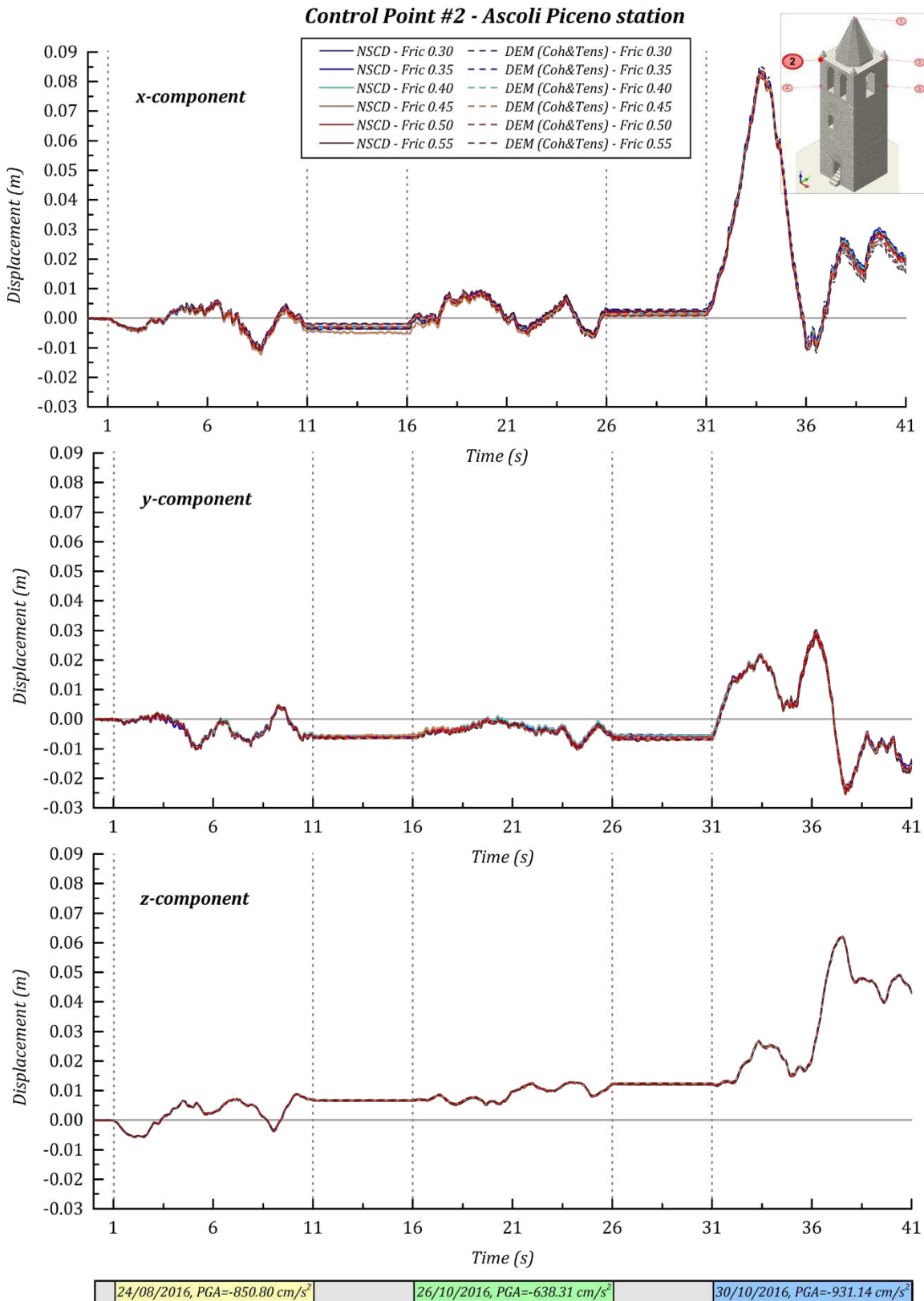
Figure 41 Displacements time histories of the control point #5 of the civic tower of Rotella (Ascoli Piceno, Italy) under the three main shocks recorded in the epicentres during the Central Italy seismic sequence of 2016 for the 4 friction coefficients assumed at the interface between superstructure and foundation.

8 Appendix 2

In the present Appendix 2 the results of the application of repeated accelerograms are reported as a function of the friction coefficient assumed between the blocks belonging to the superstructure. In particular, from Figure 42 to Figure 46 the displacement histories for the five control nodes investigated are represented assuming as accelerogram that registered in the Ascoli Piceno station, whereas from Figure 47 to Figure 51 the same results are depicted assuming as accelerogram that of the epicenters of the different earthquakes (24/08/2016 yellow band, 26/10/2016 green band, 30/10/2016 light blue band). As it can be observed, the behavior seems more influenced by such parameter rather than that assumed for the interface between soil and tower.

Figure 42 Displacements time histories of the control point #1 of the civic tower of Rotella (Ascoli Piceno, Italy) under the three main shocks recorded in Ascoli Piceno during the Central Italy seismic sequence of 2016 for the 6 friction coefficients assumed at the interface between contiguous blocks.
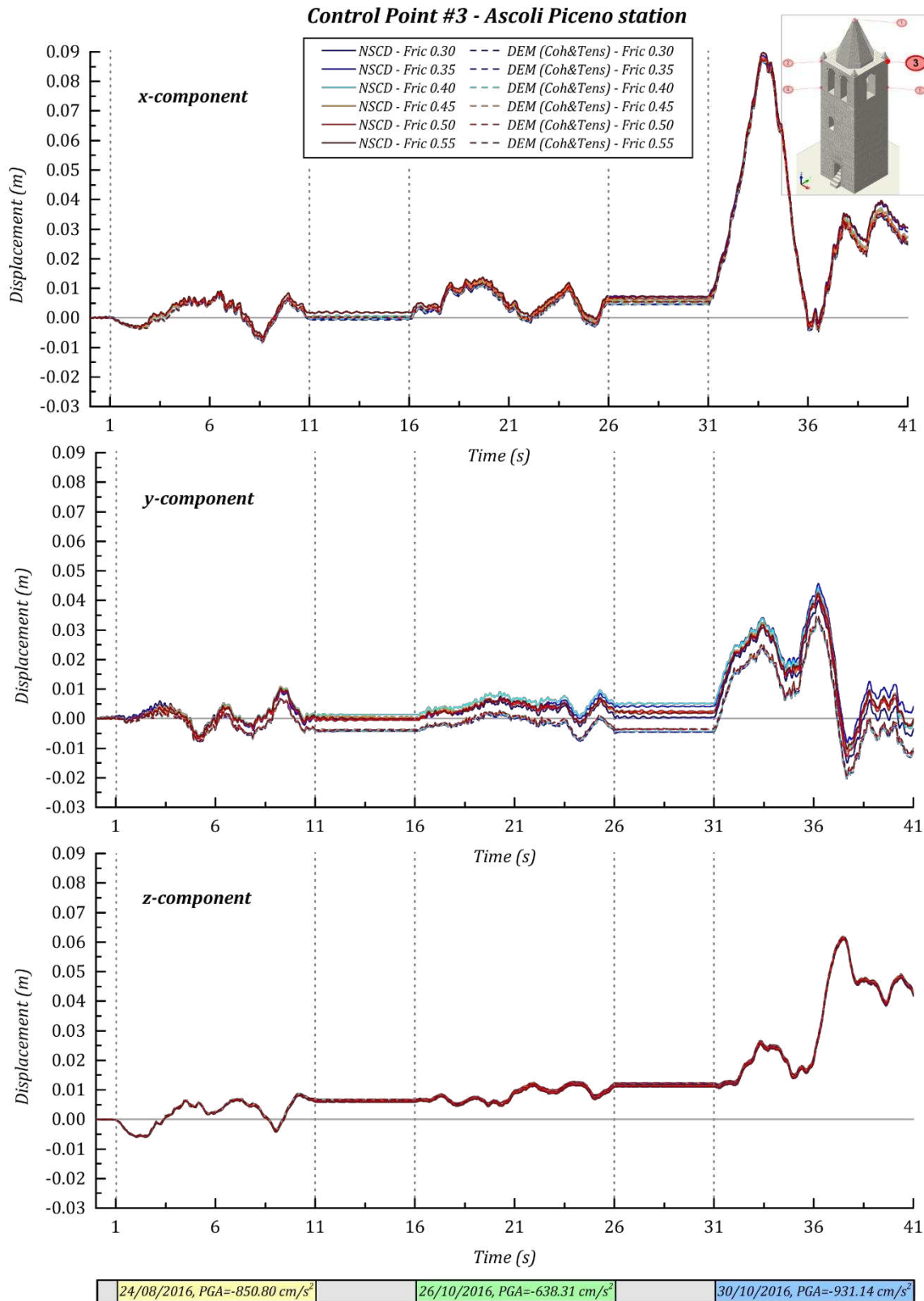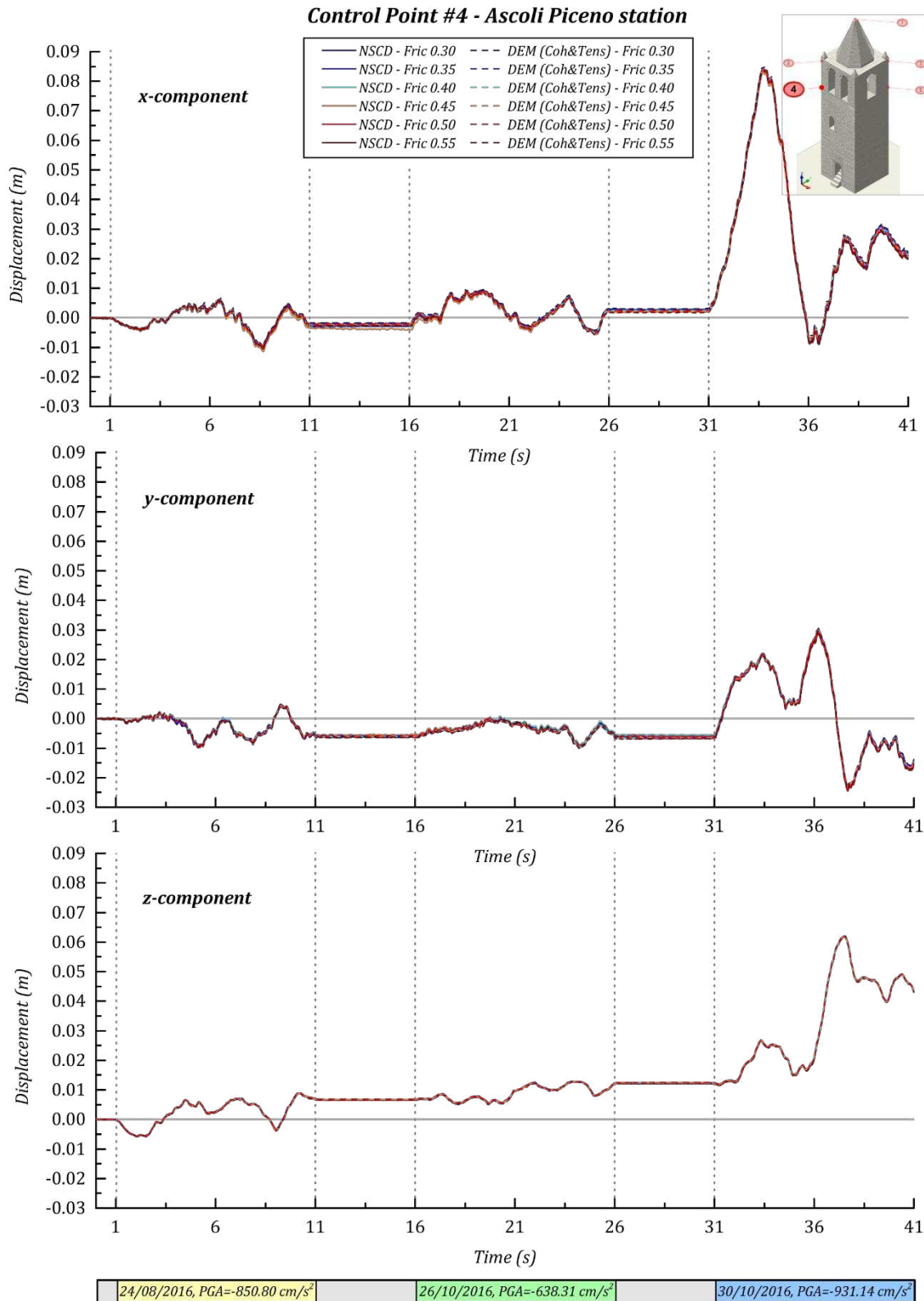
Figure 43 Displacements time histories of the control point #2 of the civic tower of Rotella (Ascoli Piceno, Italy) under the three main shocks recorded in Ascoli Piceno during the Central Italy seismic sequence of 2016 for the 6 friction coefficients assumed at the interface between contiguous blocks.
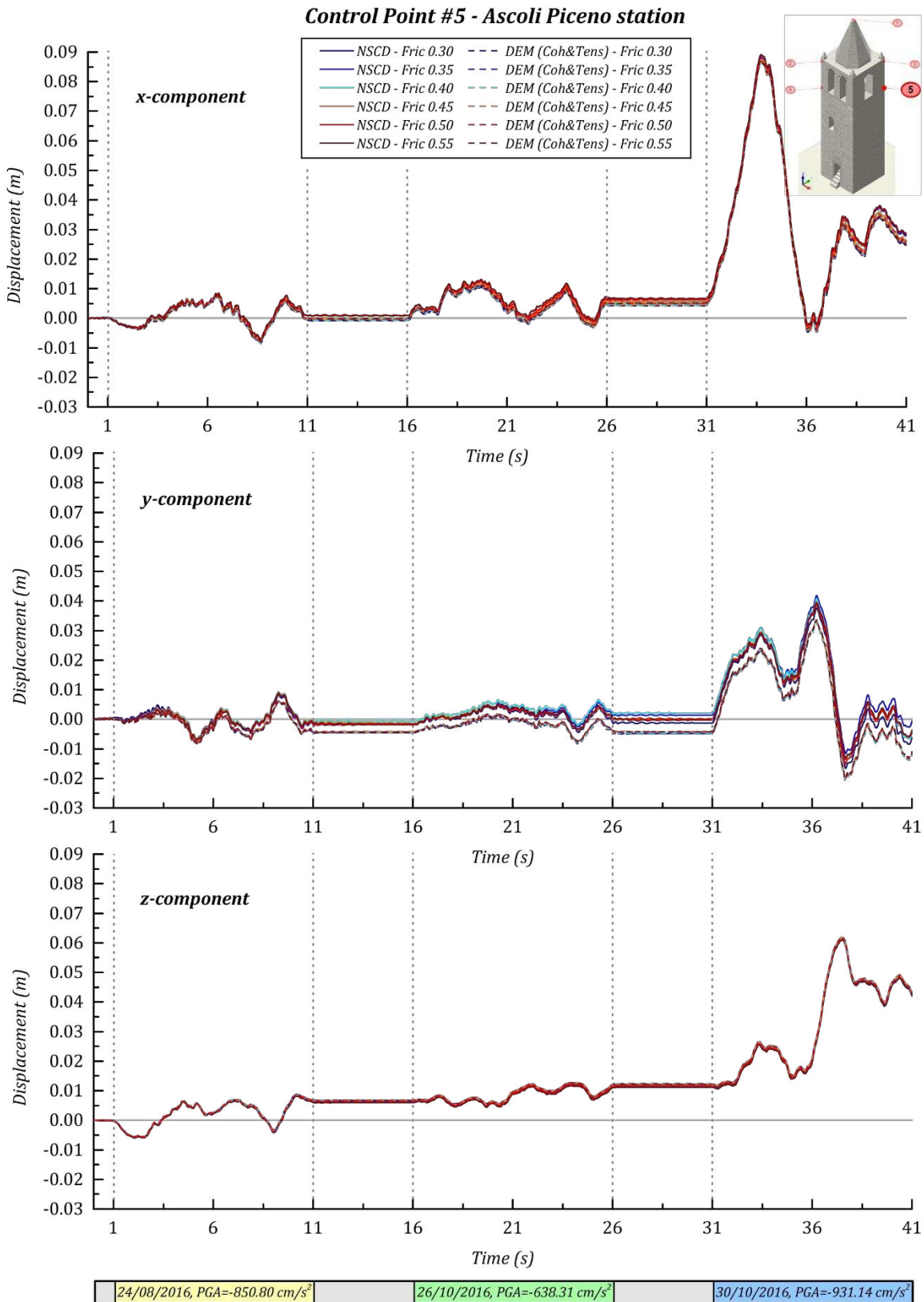
Figure 44 Displacements time histories of the control point #3 of the civic tower of Rotella (Ascoli Piceno, Italy) under the three main shocks recorded in Ascoli Piceno during the Central Italy seismic sequence of 2016 for the 6 friction coefficients assumed at the interface between contiguous blocks.

Figure 45 Displacements time histories of the control point #4 of the civic tower of Rotella (Ascoli Piceno, Italy) under the three main shocks recorded in Ascoli Piceno during the Central Italy seismic sequence of 2016 for the 6 friction coefficients assumed at the interface between contiguous blocks.
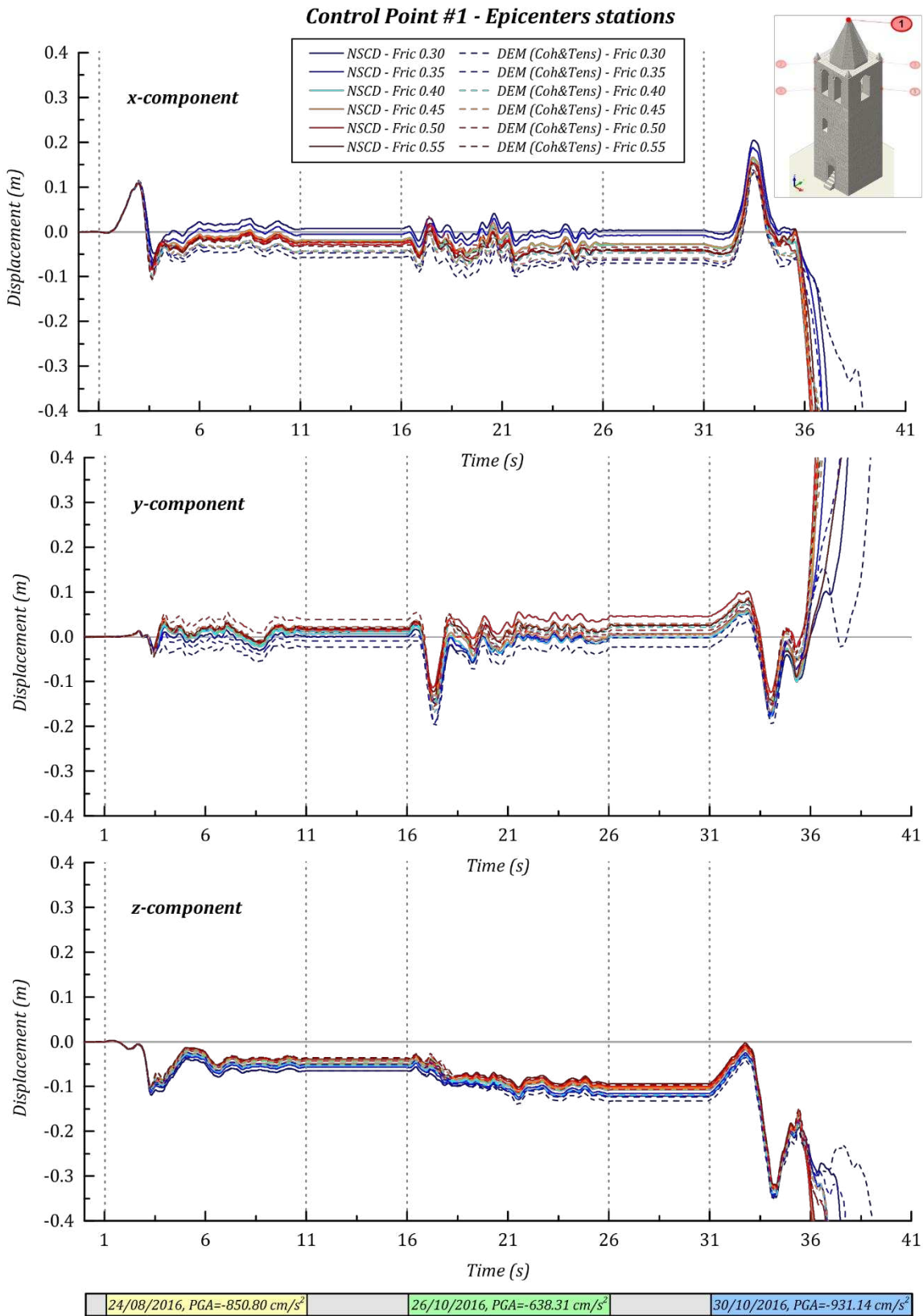
Figure 46 Displacements time histories of the control point #5 of the civic tower of Rotella (Ascoli Piceno, Italy) under the three main shocks recorded in Ascoli Piceno during the Central Italy seismic sequence of 2016 for the 6 friction coefficients assumed at the interface between contiguous blocks.

Figure 47 Displacements time histories of the control point #1 of the civic tower of Rotella (Ascoli Piceno, Italy) under the three main shocks recorded in the epicentres during the Central Italy seismic sequence of 2016 for the 6 friction coefficients assumed at the interface between contiguous blocks.
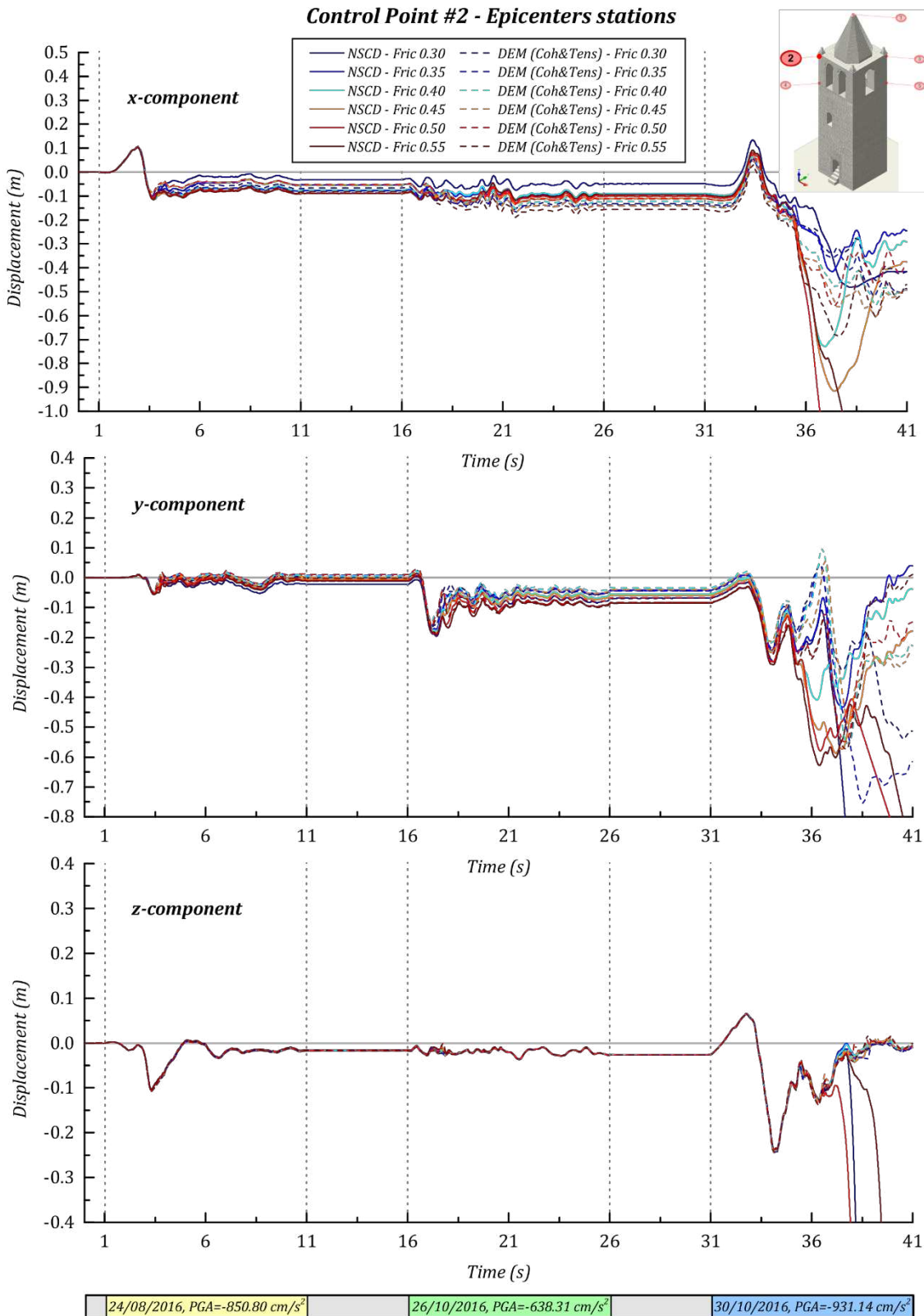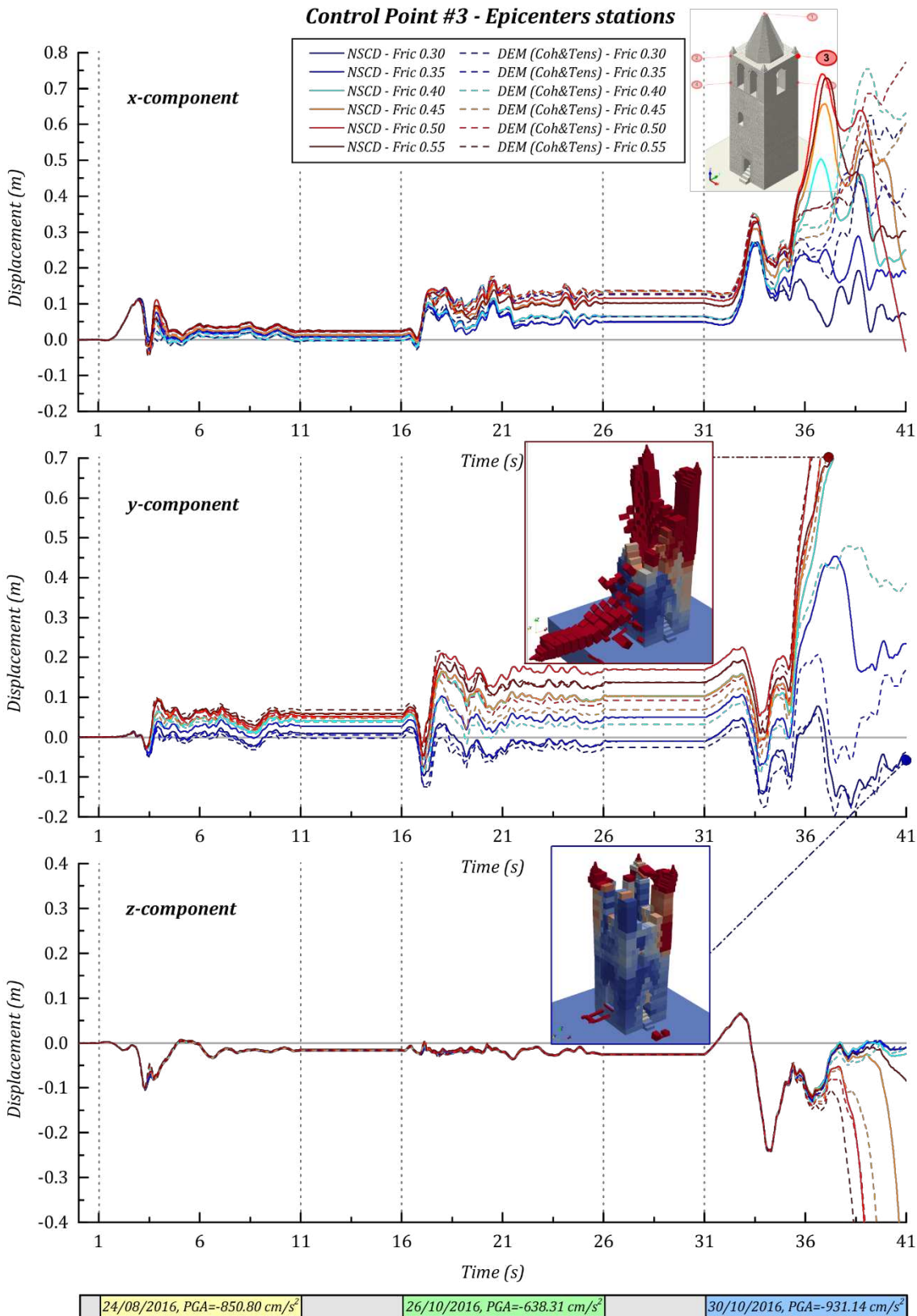
Figure 48 Displacements time histories of the control point #2 of the civic tower of Rotella (Ascoli Piceno, Italy) under the three main shocks recorded in the epicentres during the Central Italy seismic sequence of 2016 for the 6 friction coefficients assumed at the interface between contiguous blocks.

Figure 49 Displacements time histories of the control point #3 of the civic tower of Rotella (Ascoli Piceno, Italy) under the three main shocks recorded in the epicentres during the Central Italy seismic sequence of 2016 for the 6 friction coefficients assumed at the interface between contiguous blocks.
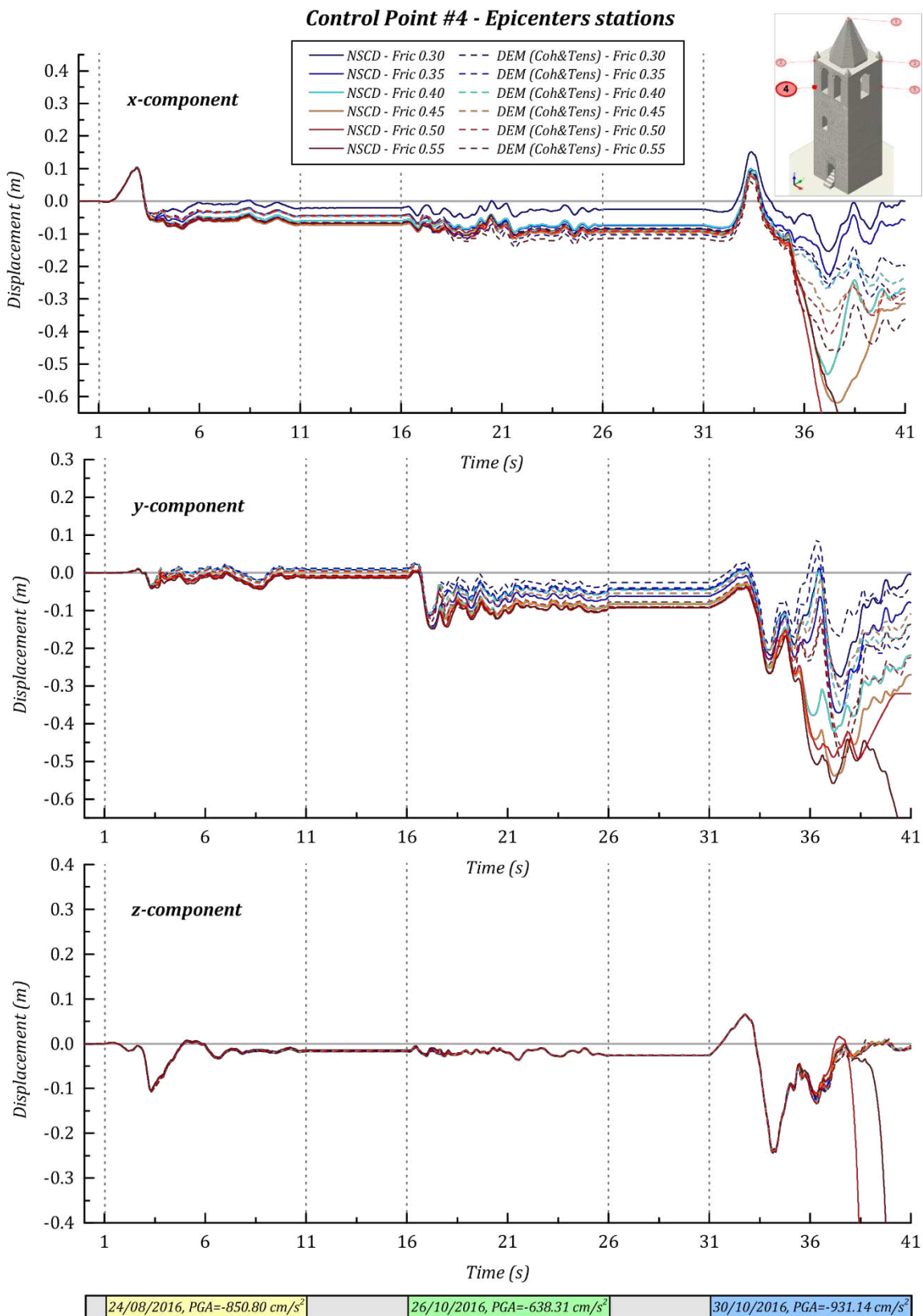
Figure 50 Displacements time histories of the control point #4 of the civic tower of Rotella (Ascoli Piceno, Italy) under the three main shocks recorded in the epicentres during the Central Italy seismic sequence of 2016 for the 6 friction coefficients assumed at the interface between contiguous blocks.
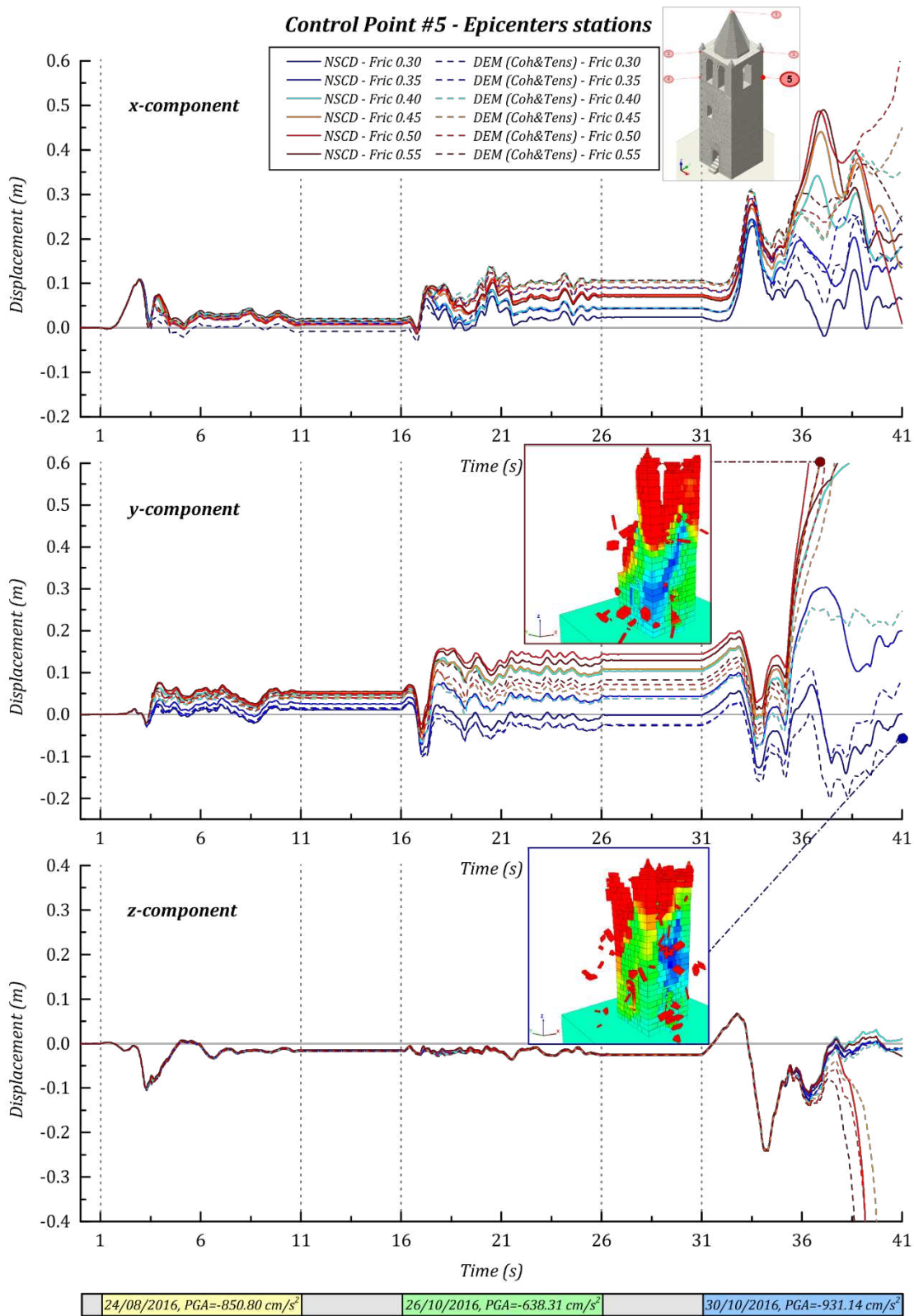
Figure 51 Displacements time histories of the control point #5 of the civic tower of Rotella (Ascoli Piceno, Italy) under the three main shocks recorded in the epicentres during the Central Italy seismic sequence of 2016 for the 6 friction coefficients assumed at the interface between contiguous blocks.